

UNIVERSITY OF CINCINNATI

Date: 19-Apr-2010

I, Ratandeep Kukreja ,

hereby submit this original work as part of the requirements for the degree of:

Doctor of Philosophy

in Materials Science

It is entitled:

SYNTHESIS OF THIN FILMS IN BORON-CARBON-NITROGEN TERNARY

SYSTEM BY MICROWAVE PLASMA ENHANCED CHEMICAL VAPOR

DEPOSITION

Student Signature: Ratandeep Kukreja

This work and its defense approved by:

Committee Chair: Raj Singh, ScD
Raj Singh, ScD

SYNTHESIS OF THIN FILMS IN BORON-CARBON-NITROGEN TERNARY
SYSTEM BY MICROWAVE PLASMA ENHANCED CHEMICAL VAPOR
DEPOSITION

A dissertation submitted to the

Division of Graduate Studies and Research of the
University of Cincinnati

In partial fulfillment of the requirements
of the degree of

DOCTORATE OF PHILOSOPHY (Ph.D.)

In the Department of Chemical and Materials Engineering
of the College of Engineering

2010

By

RATANDEEP SINGH KUKREJA

B.E., College of Engineering Pune, 2000

Dissertation Committee:
Dr. Raj N. Singh (committee Chair)
Dr. Relva C. Buchanan
Dr. Rodney Roseman
Dr. Vesselin Shanov

ABSTRACT

The Boron Carbon Nitrogen (B-C-N) ternary system includes materials with exceptional properties such as wide band gap, excellent thermal conductivity, high bulk modulus, extreme hardness and transparency in the optical and UV range that find application in most fields ranging from micro-electronics, bio-sensors, and cutting tools to materials for space age technology. Interesting materials that belong to the B-C-N ternary system include Carbon nano-tubes, Boron Carbide, Boron Carbon Nitride (B-CN), hexagonal Boron Nitride (*h*-BN), cubic Boron Nitride (*c*-BN), Diamond and beta Carbon Nitride (β -C₃N₄). Synthesis of these materials requires precisely controlled and energetically favorable conditions.

Chemical vapor deposition is widely used technique for deposition of thin films of ceramics, metals and metal-organic compounds. Microwave plasma enhanced chemical vapor deposition (MPECVD) is especially interesting because of its ability to deposit materials that are meta-stable under the deposition conditions, for e.g. diamond. In the present study, attempt has been made to synthesize beta-carbon nitride (β -C₃N₄) and cubic-Boron Nitride (*c*-BN) thin films by MPECVD. Also included is the investigation of dependence of residual stress and thermal conductivity of the diamond thin films, deposited by MPECVD, on substrate pre-treatment and deposition temperature.

Si incorporated CN_x thin films are synthesized and characterized while attempting to deposit β -C₃N₄ thin films on Si substrates using Methane (CH₄), Nitrogen (N₂), and Hydrogen (H₂). It is shown that the composition and morphology of Si incorporated CN_x thin film can be tailored by controlling the sequence of introduction of the precursor

gases in the plasma chamber. Greater than 100 μm size hexagonal crystals of N-Si-C are deposited when Nitrogen precursor is introduced first while agglomerates of nano-meter range graphitic needles of C-Si-N are deposited when Carbon precursor is introduced first in the deposition chamber.

Hexagonal – BN thin films are successfully deposited using Diborane (B_2H_6) (5% in H_2), Ammonia (NH_3) and H_2 as precursor gases in the conventional MPECVD mode with and without the negative DC bias. The quality of *h*-BN in the films improved with pressure and when NH_3 used as the first precursor gas in the deposition chamber.

c-BN thin films are successfully deposited using Boron-Trifluoride (BF_3) (10% in Argon (Ar)), N_2 , H_2 , Ar and Helium (He) gases in the electron cyclotron resonance (ECR) mode of the MPECVD system with negative DC bias. Up-to 66% *c*-BN in the films is achieved under deposition conditions of lower gas flow rates and higher deposition pressures than that reported in the literature for film deposited by ECR-MPECVD. It is shown that the percentage *c*-BN in the films correlates with the deposition pressure, BF_3/H_2 ratio and, negative DC bias during nucleation and growth.

Diamond thin films are deposited using 60%Ar, 39% H_2 and, 1% CH_4 at 600 $^\circ\text{C}$, 700 $^\circ\text{C}$ and 800 $^\circ\text{C}$ substrate temperatures, measured by an IR pyrometer, on Si substrates pre-treated with 3-6nm diamond sol and 20-40 μm diamond slurry. Raman spectroscopy, FTIR, X-Ray diffraction (XRD) and, photo-thermal reflectivity methods are used to characterize the thin films. Residual stresses observed for the diamond thin films deposited in this study are tensile in nature and increased with deposition temperature. Better quality diamond films with lower residual stresses are obtained for films deposited on Si substrate pre-treated with 3-6nm diamond sol. Preliminary results on thermal

conductivity, k , suggest that k is directly dependent on the deposition temperature and independent of substrate pre-treatment signifying that the nano-seeding technique can be used to replace conventional surface activation technique for diamond seeding where needed.

ACKNOWLEDGEMENTS

A Doctorate in Philosophy is a journey, for me it has been a long one. Walking alone would have been an impossible task. Fortunately I was blessed with the company of highly supportive and kind friends and mentors who became my family away from home and helped me reach this point in my life where I can finally express my gratitude and appreciation for them.

First and foremost I would like to express my deepest gratitude to my advisor Dr. Raj N. Singh for accepting me under his tutelage and for providing me with guidance, support and motivation throughout my graduate studies.

My special and sincere thanks to Dr. Vesselin Shanov for always being there for me. His sincere concern and the ability to understand my problems, personal and academic, were enough to keep me motivated in my low times.

Sincere appreciation and gratitude are also to Dr. Relva C. Buchanan, and Dr. Rodney Roseman for their participation in my committee and their valuable insights and suggestions.

Special thanks to Dr. Vijay K. Vasudevan for being ever willing to spare time for a supportive talk.

I would like to thank Dr. Thomas Mantei and Dr. Douglas Kohls for supporting me as a Graduate Assistant at Advanced Material Characterization Center for three years.

It is said that in friendship “no thanks and no sorry”. And therefore I just want to say that without all my dear friends I would not be I. My most sincere and deepest appreciation goes to all my dear friends and colleagues who were always there at each

and every step during the long span of my Ph.D.: My group members Dr. Rahul Ramamurti, Dr. Samantaray, Dr. Indrajit Dutta, Dr. Shailendra Singh Parihar, Dr. Li Guo, Dr. Vidhya Sagar Jayaseelan, Dr. Nirmal Govindraju, Dr. Sandeep Chavan, Sandeep Singh, and Michael Rottmayer. My friends who were always ready for a technical discussion: Amrinder Singh Gill, Dr. Madhuranjan, Dr. Amit Katiyar, Dr. Santosh Yadav Katiyar, Akshay Aashirgade, and Song. My friends who made life more fun in Cincinnati: Abhilasha Singh, Kalyan Bemalkhedkar, Pranay Desai, Jaspreet Singh, Guneet Singh, Shubham Basu, Sushant Anand, Saurabh Anand, Jasman Kaur, and Sandeep Dosanjh. My deep appreciation also goes towards all my dear friends from undergraduate school in India for their constant support and motivation.

I would like to express my special thanks and un-diminishing appreciation for Pratima Dayal, Rashmi Dayal and, uncle and aunty (Maheshwar and Neena Dayal) for their love, support and belief in me.

I appreciate the support provided by the dedicated, enthusiastic and lively staff members of the Chemical and Materials Engineering Department.

The support given by the research grants (CMS-0210351 and ECCS-0853789) from the National Science Foundation is acknowledged tremendously, without which surviving would have been a difficult task.

This dissertation is dedicated to

My Parents, My Brothers And Their Families For Their Love, Care, Endurance

And Trust In Me, Throughout The Past Years.

TABLE OF CONTENT

Abstract	i
Acknowledgments	iv
Table of content	vii
Index of figures	x
Index of tables	xiv

Part I:

Microwave Plasma Enhanced Chemical Vapor Deposition System

Chapter 1: Introduction	1
1.1: Plasma Enhanced Chemical Vapor Deposition (PECVD)	3
1.2: Microwave Plasma CVD	5
1.3: Electron Cyclotron Resonance	7
1.4: Growth Mechanism	8
Chapter 2: Features of the ECR-MPECVD System	11
2.1: The ECR-MPECVD System	11
2.2: Optical Emission Spectroscopy	16
2.3: Quadrupole Mass Spectroscopy	19

Part II:

MPECVD for Synthesis of Beta-Carbon Nitride Thin Films

Chapter 1: Introduction	25
Chapter 2: Literature Review	29
2.1: Structure of Carbon Nitride	29
2.2: Properties of Carbon Nitride	31
2.3: Applications of Carbon Nitride Thin Films	32
2.4: Synthesis	32
2.5: Characterization	48

2.6: Summary of Literature Review on Beta-Carbon Nitride	52
2.7: Suggestions for Future Research	53
Chapter 3: Objectives and Research Plan	54
Chapter 4: Experimental	56
4.1: Substrate Preparation	56
4.2: Deposition Conditions	57
4.3: Characterization Techniques	58
Chapter 5: Results and Discussions of CN _x Thin Films Deposited by MPECVD	60
5.1: Effect of Nitrogen Addition to Diamond Thin Film Deposition Conditions	60
5.2: Synthesis of CN _x Thin Films	63
Chapter 6: Conclusions and Recommendations for Future Work	74

Part III:

Deposition of Cubic Boron Nitride Thin Films by MPECVD

Chapter 1: Introduction	76
Chapter 2: Literature Review	78
2.1: Structure of Boron Nitride	78
2.2: Properties and Applications of Cubic Boron Nitride	80
2.3: Synthesis of <i>c</i> -BN	81
2.4: Microwave Plasma Enhanced Chemical Vapor Deposition	86
Chapter 3: Objective and Research Plan	90
Chapter 4: Experimental	91
4.1: The Deposition System	93
4.2: Substrate Preparation	96
4.3: Deposition Conditions	97
4.4: Characterization Techniques	99
Chapter 5: Results and Discussions of Boron Nitride Thin Films Deposited by MPECVD	101
5.1: Hexagonal Boron Nitride Thin Films	103

5.2: Cubic Boron Nitride Thin Films	106
5.2.1: <i>c</i> -BN Thin Films Deposited by MPECVD	107
5.2.2: <i>c</i> -BN Thin Films Deposited by ECR-MPECVD	109
Chapter 6: Conclusions and Recommendations for Future Work	115

Part IV:

Effect of Substrate Pre-treatment and Deposition Temperature on the Structure, Residual Stresses and Thermal conductivity of Diamond Thin Films

Chapter 1: Introduction	117
Chapter 2: Literature Review	120
Chapter 3: Objectives and Research Plan	124
Chapter 4: Experimental	126
Chapter 5: Results and Discussions	128
5.1: Surface Morphology of Diamond Thin Films	130
5.2: FTIR Spectroscopy for Hydrogen Absorption	133
5.3: Diamond Quality and Yield by Raman Spectroscopy	136
5.4: Residual Stress by Raman Spectroscopy	142
5.5: Crystallite Size by X-Ray Diffraction	144
5.6: Stress Measurement and Analysis	148
5.7: Thermal Conductivity Measurement by Photothermal Reflectivity Method	154
Chapter 6: Conclusions	159

Part V:

Conclusions And Recommendations For Future Work

Conclusions	161
Recommendations For Future Work	163
References	164

INDEX OF FIGURES

Part I

Figure 2.1:	Schematic of electron cyclotron resonance microwave plasma enhanced chemical vapor deposition (ECR-MPECVD) system used in this study.	12
Figure 2.2:	Energy levels involved in typical OES experiments	16
Figure 2.3:	Schematic of OES setup used as a plasma diagnostic tool in MPECVD.	19
Figure 2.4:	(a) Static mode spectra of QMS showing partial pressures of various ions/radicals identified by their mass/charge ratio for Ar+H ₂ +CH ₄ +NH ₄ plasma. (b) Dynamic mode of QMS showing variation of partial pressure of the plasma species identified in the static mode with time.	21
Figure 2.5:	Schematic of quadrupole mass spectrometer.	22
Figure 2.6:	Stability areas of ions with different masses as a function of U and V .	24

Part II

Figure 2.1:	Crystal structure of β -C ₃ N ₄ with C and N atoms as white and grey respectively [10, 37, 38]	29
Figure 2.2:	Ball and stick models of C ₃ N ₄ phases. For the defect zinc-blende (a) and cubic (d) the carbon and nitrogen atoms are white and grey respectively. The α structure (b) and the graphite phase (c) both consist of two layers. The upper layer shows the C atoms in white and the N atoms in light grey. In the lower layer, the C and N atoms are dark grey and black respectively.	30
Figure 2.3:	Stability phase diagram of pCN [1]	32
Figure 2.4:	Schematic of typical MPECVD setup for synthesis of CN _x films	37
Figure 2.5:	Setup for RF pulsed modulation assisted Pulsed Laser Deposition of CN _x film [2].	39

Figure 2.6:	Comparison of X-ray diffraction peaks of CN_x films deposited on Pt and Si substrate [3].	43
Figure 2.7:	Typical SEM image of Hexagonal crystalline Si-C-N film [4]	46
Figure 2.8:	XPS spectrum of Si-C-N crystal showing C (1s) and N (1s) core level spectra [37]	48
Figure 5.1	SEM micrographs showing changes observed in the morphology of diamond thin films with increase in Nitrogen addition to the diamond deposition conditions	61
Figure 5.2:	XRD data showing effect of increasing N_2 in 1% CH_4+H_2 plasma on quality of diamond thin films.	62
Figure 5.3:	Effect of variation of process parameters on the type and morphology of CN_x thin films. (a) The two morphologies observed, (b-f) effect of increasing (b) CH_4 , (c) H_2 , (d) substrate temperature, (e) microwave power and (f) deposition pressure.	64
Figure 5.4:	Effect of sequence of introduction of precursor gases and deposition pressure on the morphology of the CN_x thin films.	66
Figure 5.5.	SEM micrographs show that the spheroids are agglomerates of nanometer sized needles while the RLCs have a well defined crystalline morphology.	67
Figure 5.6:	Raman spectra for N-C-Si crystals (RLCs) and C-Si-N agglomerated needles (spheroids).	68
Figure 5.7	OES spectra of methane, hydrogen and nitrogen plasma.	70
Figure 5.8:	Static mode QMS spectra of methane, nitrogen and hydrogen plasma showing different species formed and their partial pressures within the plasma.	72

Part III

Figure 2.1	Structure of various allotropes of BN: (a) hexagonal (<i>h</i> -BN), (b) wurzetic (<i>w</i> -BN), (c) rhombohedral (<i>r</i> -BN) and, (d) cubic (<i>c</i> -BN)	79
Figure 4.1:	Schematic of original and modified MPECVD deposition chamber with quartz feed through	92
Figure 4.2:	Bias cable constructed with K-type thermocouple wire, glass fiber	94

threads and domestic Aluminum foil.

Figure 4.3:	Schematic of the flexible DC bias in use for the two modes of MPECVD system.	95
Figure 5.1:	Raman spectra for h-BN thin films deposited at different pressures. (a) films deposited with B ₂ H ₆ gas as the first precursor gas to be introduced in the deposition chamber, (b) films deposited with NH ₃ gas as the first precursor gas to be introduced in the deposition chamber	104
Figure 5.2:	FTIR transmission spectra of BN thin films synthesized with increasing negative DC bias	107
Figure 5.3:	Transmission FTIR spectra of BN thin films with varying % <i>c</i> -BN. A maximum of 66 percent <i>c</i> -BN was achieved in the films	109
Figure 5.4:	(a) Transmission FTIR spectra of BN thin film showing both h-BN and <i>c</i> -BN peaks. (b) Transmission FTIR spectra from (a) converted to Absorbance spectra using the equation in the Figure, and (c) Deconvoluted and fitted spectra of the Absorbance FTIR spectrum in (b). Equation in (c) is used to calculate % <i>c</i> -BN in the film using the <i>c</i> -BN and <i>h</i> -BN deconvoluted peaks. Using the equation % <i>c</i> -BN in the spectrum shown above is 13.9%	110
Figure 5.5:	Correlation between process parameters and the % <i>c</i> -BN observed in the films by FTIR. (a) Effect of increasing nucleation voltage on % <i>c</i> -BN in the thin films, (b) Effect of nucleation and growth currents on % <i>c</i> -BN in the thin films, (c) effect of variation in BF ₃ /H ₂ ratio on % <i>c</i> -BN in the thin films, and (d) variation of % <i>c</i> -BN in the thin films with growth time.	111

Part IV

Figure 5.1:	SEM micrographs of diamond thin films deposited at 800, 700 and 600°C. (a-c) Diamond thin films on Si substrate pre-treated with 3-6nm diamond sol, and (d-f) diamond thin films on Si substrate pre-treated with 20-40µm diamond slurry. Inset on the left top corner shows the average grain size of the thin films.	132
Figure 5.2:	Typical FTIR spectrum observed for the diamond thin films deposited at 700°C.	133

Figure 5.3:	C-H stretch region of the FTIR spectrum for diamond thin film grown at 700°C fitted using PeakFit software.	134
Figure 5.4:	Effect of deposition temperature and substrate pre-treatment on the hydrogen absorption in diamond thin films	135
Figure 5.5:	Raman spectra of diamond films deposited at different temperatures, from (a) films on Si pre-treated with 20-40µm diamond slurry, and (b) films on Si pre-treated with 3-6nm diamond sol	138
Figure 5.6:	Raman spectra for 600°C diamond thin film on Si pre-treated with 20-40µm diamond slurry fitted with Peak Fit software.	139
Figure 5.7:	Variation of FWHM of diamond peaks from Raman spectroscopy with deposition temperature and substrate pre-treatment.	140
Figure 5.8:	Effect of deposition temperature and Si substrate pre-treatment on diamond yield estimated from Raman spectra of the thin films	141
Figure 5.9:	Effect of deposition temperature and Si substrate pre-treatment on residual stress in the diamond thin films calculated from the Raman spectra.	144
Figure 5.10:	Effect of deposition temperature on crystal structure of the diamond thin films. For clarity purposes the patterns are shifted to the right in increments of 1° 2θ, and up in increments of 2000 counts. Patterns (a), (c) and (e) represents diamond thin films on Si substrate pre-treated with 20-40µ diamond slurry and deposited at 800, 700 and 600°C respectively. Patters (b), (d) and (f) represent diamond thin films on Si substrate pre-treated with 3-6nm diamond sol and deposited at 800, 700 and 600°C respectively.	145
Figure 5.11:	Typical diamond (111) diffraction peak, fitted with Voigt Area using Peak Fit Software. The peak in the figure is from XRD pattern of diamond thin film deposited at 700°C on Si substrate pre-treated with 20-40µ diamond slurry.	147
Figure 5.12	Schematic of the Photothermal Reflectivity system used for measurement of thermal conductivity of diamond thin films.	155
Figure 5.13:	Phase profile plot of a 20 µm thick diamond film on silicon.	157

INDEX OF TABLES

Part I

Table 1.1	Pressure Ranges for different CVD techniques [5]	3
-----------	--	---

Part II

Table 2.1:	Comparison of some of the techniques used for the synthesis of CN_x films.	36
Table 2.2:	Comparison of different techniques of Nitrogen addition in PLD of CN_x films.	40
Table 2.3:	Different substrates investigated for deposition of Carbon Nitride thin films.	42
Table 2.4:	XPS peaks of different carbon nitride and silicon phases	49
Table 2.5:	Some of the overlapping peaks (calculated) of α - and β - C_3N_4 [6, 7].	50
Table 2.6:	FTIR peaks assigned to various phases of carbon nitride and silicon nitride.	51
Table 2.7:	characteristic Raman peaks for β - C_3N_4 and β - Si_3N_4 [7, 8].	52
Table 4.1:	Process parameters for N_2 addition in 1% CH_4 + H_2 plasma used for diamond deposition by MPECVD	58
Table 4.2:	Process parameters for the synthesis of CN_x thin films by MPECVD	58
Table 5.1:	Effect of first precursor gas and pressure on the morphology of the CN_x thin films deposited.	65
Table 5.2:	Quantitative EDS data observed for Spheroids and RLCs.	67
Table 5.3:	Observed OES peaks and their excitation source for hydrogen, methane and nitrogen plasma	71

Part III

Table 2.1:	Comparison of various properties of BN with those of other semiconductors [9]	80
Table 4.1:	Deposition conditions for synthesis of h-BN thin films	97
Table 4.2:	Deposition conditions for the study of effect of D.C. bias	98

Table 4.3: Deposition parameters for synthesis of *c*-BN using BF₃ and N₂ by ECR-MPECVD 99

Table 4.4: Characteristic FTIR and Raman shifts peaks for *c*-BN and *h*-BN 100

Part IV

Table 4.1: Process parameters used for diamond thin film deposition by MPECVD 127

Table 5.1: Characteristic vibration frequencies observed in FTIR spectra of the diamond thin films [1, 2]. 135

Table 5.2: Residual tensile stresses in diamond thin films on Si substrates pre-treated with 3-6nm diamond sol and 20-40µm diamond slurry and deposited at different temperatures. 144

Table 5.3: $I_{(220)}/I_{(111)}$ ratio for diamond thin films deposited at different temperatures and substrate pre-treatment in comparison with standard diamond powder. 146

Table 5.4: Crystallite size measured from XRD patterns of the thin films using Equation 5.3. 148

Table 5.5: A summary of calculated and experimental residual stresses for diamond thin film on Si substrates pre-treated with 3-6nm diamond sol or 20-40µm diamond slurry and deposited at different temperature. 151

PART I
THE MICROWAVE PLASMA ENHANCED CHEMICAL VAPOR
DEPOSITION SYSTEM

CHAPTER 1
INTRODUCTION

Chemical vapor deposition is a technique that uses homogeneous and/or heterogeneous reactions between volatile precursors to deposit solid material on substrates. The precursor gases are so chosen that the chemical reaction between the gases or decomposition of the gases results in a solid product that is deposited on the substrate. Some volatile products may also be produced that get removed by constant pumping of the deposition chamber.

The advantages of chemical vapor deposition technique include synthesis of uniform, pure, adherent and reproducible films, control of rate of deposition, ability to deposit films on sites that are difficult to reach by other techniques, low deposition temperatures and the ability to deposit materials that are metastable, under the deposition conditions, e.g. diamond [1]. The disadvantages include chemical hazards caused by toxic, flammable, corrosive, and explosive gases, and the complexity in optimizing the deposition conditions because of the large number of variables involved.

CVD techniques are widely used in semiconductor and coating industry for deposition of monocrystalline, polycrystalline, amorphous and epitaxial thin films of IV, IV-IV, III-V, II-VI, metals, dielectrics and superconductors [2]. Most commonly the technique is used for the

deposition of thin films on substrates. In recent years its use has expanded to deposition of nano-rods, nano-wire, nano-tubes and other nano-morphologies of various elements and compounds including carbon, silicon, SnO, and *h*-BN to name a few [12-17].

Wide fields of application for the technique include thin film coatings of Silicon oxide, aluminum nitride, silicon carbide, and various high-k dielectric materials for semiconductor industry, hard coatings of Tungsten Carbide, Diamond and other materials for application in the tooling industry, and of synthesis of special materials like carbon nano-tubes, nano-rods and nano-spheres for applications in the space and bio-medical industry.

Amongst the many types of CVD techniques available today, the following are widely used [2]:

1. CVD – Thermally activated / pyrolytic CVD – the technique employs thermal energy (resistance heating, RF heating, infrared heating etc,) for activating the CVD process. The technique works in a wide range of pressure conditions from atmospheric to ultralow pressure conditions.
2. MOCVD – Metalorganic CVD – the technique is used for deposition of III-V and II-VI materials using metalorganic gases or liquids. MOCVD is mostly used for epitaxial growth thin films taking advantage of the availability of pure metalorganic precursors.
3. PCVD – Photo CVD – Uses light for either local heating of the substrate or for causing a photochemical reaction that helps in increasing the reaction rate of the precursor gases.
4. PECVD – Plasma enhanced CVD – Plasma is the fourth state of matter in which the elements are ionized or dissociated and therefore highly excited. The excited state of

the precursor gases in PECVD helps in enhancing the growth rate and allows deposition at lower temperatures than in other CVD techniques.

5. ALE – Atomic layer epitaxy – In this technique the films are grown one monolayer at a time. Each monolayer is deposited by sequential supply of reactant gases on to the substrate surface. The technique is used for deposition of II-VI and III-V materials, elemental semiconductors, oxides, nitrides and sulphides.

Table 1.1 Pressure Ranges for different CVD techniques [2].

Technique	Pressure (Torr)
Thermal CVD	$10^{-5} - 760$
MOCVD	$10 - 760$
PCVD	$10 - 760$
PECVD	$10^{-3} - 760$
ALE	$10^{-2} - 760$

Table 1.1 gives the pressure ranges of some of the CVD techniques mentioned above. Among all the CVD techniques PECVD gives better growth rates at lower deposition temperatures, and is known for the deposition of metastable materials like diamond. The technique was therefore exploited in this research for the synthesis of thin films in boron-carbon-nitrogen ternary system. The technique is discussed in more detail in the proceeding section.

1.1 Plasma Enhanced Chemical Vapor Deposition (PECVD)

Plasma, the fourth state of matter or the ionized state of matter, contains an equal number of free negative charges (electrons and negative ions), positive ions and radicals in a pool of neutral gas. These charged particles can be manipulated (accelerated/decelerated,

dispersed, concentrated, directed, circulated, etc.) by applying various combinations of electrical and magnetic fields to the plasma. Ionization of a gas such as argon, helium, hydrogen etc, is established by exciting the electrons of the gas with enough energy to free them from the atoms. With an electron missing the atoms are left with a net positive charge converting them into positive ions. The free electrons move much faster than the atoms and ions, and in the process interact with them to cause further ionization. Typically 10 – 25eV of energy is required to produce ionization.

In PECVD, also known as plasma assisted CVD (PACVD), the chemical reactions of the CVD process are enhanced by plasma with the consequence that deposition of thin films can be achieved at temperatures that are much lower compared to other non-plasma CVD techniques. Two types of plasma arrangements can be used in PECVD processes [1, 3]

- Remote PECVD – The substrate in this arrangement is not directly immersed into the plasma and hence the physical effects like ion bombardment are minimized and substrate temperatures as low as room temperature can be achieved during deposition. The precursors may be introduced into the plasma or just over the substrate depending on the type of film being deposited.
- PECVD – The substrate in normal PECVD is immersed into the plasma. The physical effects like ion bombardment are exploited in this technique for deposition of metastable materials.

Some of the advantages of PECVD are [1, 3]:

- Unique capability to support non equilibrium reactions for metastable materials (e.g., diamond) deposition.

- Ability to maintain low substrate temperatures during deposition helps in making possible processing of passivation layer deposition on IC chips, for e.g., with Aluminum interconnects that require lower deposition temperatures.
- High energy content of the active species in the plasma helps in overcoming most activation energy barrier thus achieving high growth and etch rates.
- Very high electron temperature makes possible easy generation of very high-energy species like N_2^+ .
- Anisotropic, fast and high resolution (high aspect ratio) etching is possible by use of ultrahigh vacuum PECVD.
- Ease of control over certain properties of the film like composition, residual stress and grain size.

1.2 Microwave Plasma CVD [4-6]:

Microwave excitation is one of the most commonly used technique for ionization. Other techniques include radio-frequency (RF) parallel-plate, inductive and DC arc excitation to name a few. An ionization ratio (density of ions / density of neutral atoms) of up to three orders of magnitude higher as compared with RF excitation can be achieved by microwaves. The most commonly used microwave frequency for applications in thin film deposition is 2.45 GHz with a wavelength of about 122mm.

In a microwave plasma deposition reactor, process gases are introduced near the plasma source, into the reactor chamber, which contains the substrate to be coated. Microwaves are transferred from the microwave power head to the reactor chamber via a symmetric plasma coupler and through a quartz window (transparent to microwaves). Inside the reaction chamber

the microwaves are absorbed by the process gas electrons. These electrons with extra energy from the microwaves get ejected causing ionization of the atom. When enough atoms are ionized plasma is produced.

Ionization by microwave induced plasma differs from other types of plasma in that the plasma is produced by direct transfer of microwave energy to the electrons. RF and other types of plasma forming techniques use lower frequencies that transfer a large portion of their energies to ions. The ions thus generated are high in energy and can cause damage to the substrate and/or the growing thin film. In microwave plasma, ions are not subjected to a high DC electric field nor are they accelerated by the extremely high frequency electric field due mainly to their higher weight in comparison to electrons. An ion hardly moves during the half-period of the 2.45GHz electric field of the microwaves before the force of the field reverses. The ions in microwave plasma are therefore much lower in energy and cause less damage that helps in deposition of thin films at lower temperatures.

The reactor chamber of a MPECVD is designed so that it becomes an integral part of an electromagnetic cavity in which the microwave electric field profiles are such that the discharge is reproducibly produced at the same location. Typically the substrate to be coated is placed within this cavity and immersed in the plasma. Once plasma is formed, ions, electrons and radicals within the plasma react with each other and neutral atoms to form new species or cause dissociation of the precursor gases in the reaction chamber. These new species/dissociated ions then contribute to the deposition of thin films.

1.3 Electron Cyclotron Resonance [7]

When plasma generated by alternating electric field such as a microwave is exposed to a static perpendicular magnetic field, electrons from the plasma energized by the electric field interact with the magnetic field and gyrate in a helical motion following right hand rule. The electrons in the plasma get accelerated by the alternating electric field first in one direction and then in the other. Under the influence of the perpendicular magnetic field at a particular electric field frequency, the electrons are turned around just in time for the alternating electric field to accelerate the electrons in the opposite direction. In this condition the electrons get accelerated in both directions of the electric field thus maximizing the transfer of energy from the microwave source to the electrons/plasma achieving resonant energy transfer.

Under high pressure conditions the large number of electron-atom collisions that occur due to smaller mean-free-path of the electrons at those pressures, break the orbits of the electron into random walk instead of a smooth gyration resulting in minimum resonance. As pressure is decreased mean-free-path of the electrons increases allowing smooth gyrations that cause a rapid gain in resonance strength of the plasma. At high resonance strength the interactions that occur produce ionization, dissociation, and excitation of ions/molecules that is much greater than that achieved by microwave alone.

Resonance of electrons is dependent on the pressure in the reactor chamber, frequency of the alternating electric field and the strength of the static magnetic field. In this study the microwave source is of 2.45 GHz, and the strength of magnetic field at which resonance occurs is approximately 875 Gauss. Recommended typical pressure range for a strong resonance is between 5×10^{-3} Torr to 1×10^{-4} Torr.

1.4 Growth mechanism [2]

Thin film deposition in a chemical vapor deposition system is a result of sets of phenomenon taking place in the gas phase and at the surface of the substrate. The phenomenon can be divided into the following parts:

Gas – phase phenomena: It consists of homogenous reactions that occur in the gas phase resulting in formation of new radicals/species that accelerate the deposition of the thin films. Another aspect of the gas-phase phenomenon is the diffusion of reactants to the substrate surface. The diffusion process is greatly affected by the deposition pressure and temperature.

Surface Phenomena: There are a number of things happening on the substrate surface during deposition. It starts with adsorption of the reactant species on the surface. The adsorbed species then take part in heterogeneous chemical reactions resulting in bonding of the film with the substrate, substrate element diffusion in the growing film, and growth of the film. Migration of the depositing radicals on the surface helps in growth and crystal orientation of the film. The migration phenomenon is greatly affected by the deposition temperature. Lattice incorporation, very similar to migration, is another phenomenon that occurs at the surface during deposition of the thin films.

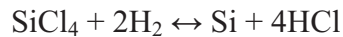
Gas-Phase Phenomena: This gas-phase phenomena is the third set of phenomena that includes desorption of reaction by-products from the surface. Desorption is followed by diffusion of the by-products into the main gas stream being pumped out from the reaction chamber.

Some of the chemical reactions that result in deposition of thin films in a CVD reactor include

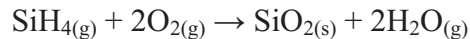
1. Pyrolysis: The thermal decomposition of a compound. For e.g.,



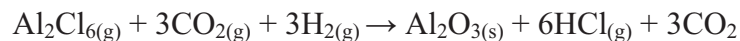
2. Reduction: The reduction reaction can be explained as a decomposition reaction supported by another reactant which helps to remove one or more reaction product. Si is homoepitaxially deposited using $\text{SiCl}_4 + \text{H}_2$, in which hydrogen serves as both reducing agent and carrier gas. The reaction is:



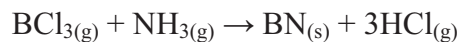
3. Oxidation: It's a reaction in which vapor-phase substances react with oxygen or other oxides to form solid oxide films. An example of such a reaction is the deposition of silicon oxide thin film from SiH_4 by the following reaction:



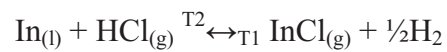
4. Hydrolysis: gaseous compounds in this reaction combine with externally or in situ formed water to form a solid thin film generally an oxide. Deposition of Alumina by the following reaction is a typical example of hydrolysis:



5. Nitridation: Reaction between gaseous reactants and ammonia (NH_3), nitrogen, hydrazine (N_2H_4) or other nitrogen containing compounds that result in the deposition of thin nitride films. A typical example is the formation of BN from BCl_3 and ammonia by the reaction:



6. Chemical transport: It involves the transport of relatively non-volatile solid precursor source by a transport agent which reacts with the solid to make a volatile species. The volatile species is transported to where the substrate is placed at which point it undergoes the reverse chemical reaction depositing the non-volatile solid on the substrate. Chemical transport reaction is usually achieved by shifting the reaction equilibrium of the reaction at the source and the substrate by adjusting temperature of the source and substrate. For e.g.:



$$T_1 > T_2$$

Along with the reaction types mentioned above some of the other types of reactions that occur in a CVD are catalysis, photolysis, disproportionation and a number of combined reactions. In the present study nitridation and reduction reactions are used for the synthesis of Beta carbon nitride, hexagonal boron nitride, cubic boron nitride and diamond thin films.

CHAPTER 2

FEATURES OF THE ECR-MPECVD SYSTEM

2.1 The ECR-MPECVD System

The ECR-MPECVD system used in this study for the deposition of thin films in B-C-N system is an ASTEX microwave magnetized plasma source type CVD system. Figure 2.1 shows a schematic of the CVD system, modified from its original state to accommodate plasma diagnostic equipment and toxic gases employed for the deposition of the thin films in this study.

The microwave power head can generate up to 1500 watts of power. An automatic tuner, Smart Match, is used to control the reflected power. The symmetric plasma coupler is used to couple the microwaves from the wave guide with the plasma. The microwaves are transmitted from the coupler to the reaction chamber through a quartz window which is transparent to the microwaves and vacuum-seals the plasma chamber.

The CVD reactor consists of two double walled water cooled chambers with 4.5” and 5” (top and bottom respectively) internal diameters. The cold chamber walls are protected against cooling water supply failure by water cooled dummy load attached next to the microwave generator. The dummy load acts as an interlock and turns off the power supply to the magnetron in an instance of cooling water supply failure. The top chamber is called the ECR chamber while the bottom chamber is called the downstream plasma chamber. Both the top and bottom chambers consist of viewing ports and loading doors.

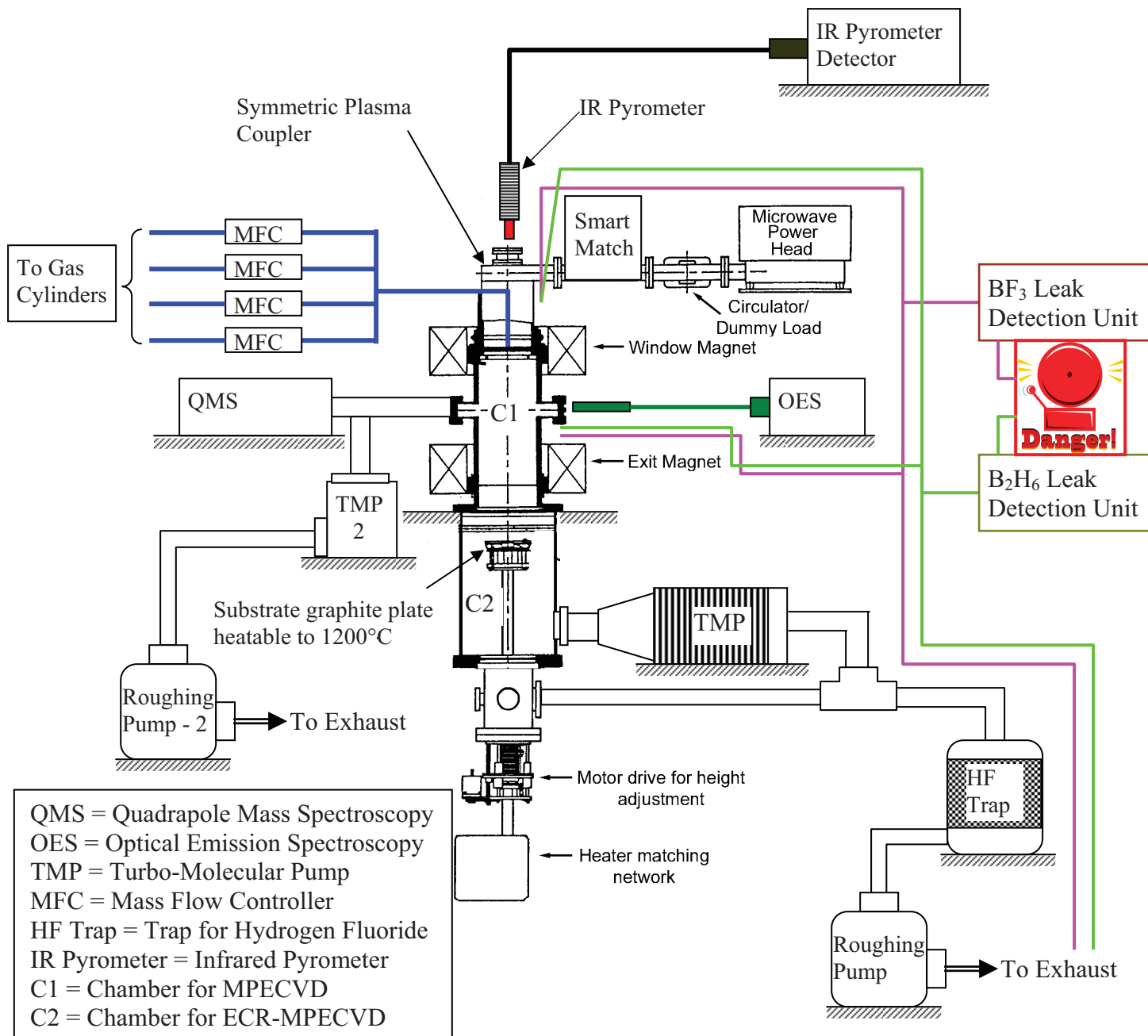


Figure 2.1: Schematic of electron cyclotron resonance microwave plasma enhanced chemical vapor deposition (ECR-MPECVD) system used in this study.

The reactor is evacuated using a combination of roughing pump and turbomolecular pump connected to the bottom chamber. The roughing pump is a D65BCS Leybold rotary pump which provides the low vacuum of around 10^{-3} Torr required as the startup pressure for the turbomolecular pump. The turbomolecular pump is a Turbovac Leybold Turbotronic NT 20 with 1100L/sec pumping capacity. The two pumps together can achieve a base pressure of 10^{-8} Torr.

The system has 4 pressure gauges. Two Baratrons (1000-1Torr and 1- 10^{-3} Torr) and a cold cathode ($10^{-3} - 10^{-10}$ Torr) vacuum gauge connected to the reactor chamber. A Pirani gauge (0.5 to 10^{-4} Torr) connected to the turbomolecular pump measures pressure inside the pump.

The substrate stage is equipped with an induction heating unit capable of reaching temperatures up to 1200°C . A feedback thermocouple that extends into a hole at the bottom of the graphite susceptor, used for induction heating of the stage, is used to maintain and measure the substrate temperature. To obtain substrate surface temperature information an IR pyrometer is focused on the substrate from a viewing window on the top of the symmetric plasma coupler. The stage height can be adjusted in both the chambers of the reactor for up to 4 inches employing a gear drive motor.

Precursor and plasma gases are introduced in the reaction chamber via a circular stainless steel ring surrounding the microwave transparent quartz window at top of the reactor. The flow of the gases is controlled using mass flow controllers (MFCs) along with ON/OFF shut off valves. VCR[®] and Swagelock[®] fittings are used for leak proof and easy maintenance. Different gases connected to the MPECVD system are semiconductor grade Argon (99.9%), Hydrogen (99.999%), Nitrogen (99.999%), Methane (99.9%), Nitrogen (99.7% used only for purging),

Oxygen (99.99%), Diborane (B_2H_6) (5% in H_2), Boron Trifluoride (BF_3) (10% in Ar), and Ammonia (99.8%).

ECR of the plasma is achieved by the two water cooled electromagnets attached to the top chamber of the CVD system. Each magnet has a capacity of 5KW, but the top one called the window magnet is connected to a 5KW power source while the bottom one, called exit magnet, is connected to a 2.5KW power source. The magnets are used for ECR, downstream plasma effect, mirror effect or for magnetic confinement of the plasma. The window and exit magnets are typically operated at 180A and 120A of current respectively, at maximum voltage, to obtain standard electron cyclotron resonance plasma.

The chamber walls and supporting plates are made of non-magnetic stainless steel (SS). The ID of the chamber walls is electro polished for easy cleaning and maintenance. The gas line and exhaust lines, from the pumps to exhaust, are also made of SS. The by product gases generated in the plasma, especially HF – produced during boron nitride experiments with boron trifluoride gas, are trapped using an Activated Charcoal[®] trap before exiting through the rotary pump into the exhaust.

Quadrupole Mass Spectroscopy (QMS) and Optical Emission Spectroscopy (OES) are attached to the CVD system to monitor and control the active species within the plasma. OES is mounted outside the CVD reactor and uses optical lens to capture emissions from the plasma, through a viewing window. The QMS works under high vacuum conditions and uses ionized gas from the plasma as source for analysis. It is therefore connected to the upper reaction chamber of the CVD system via a shut off valve and a needle valve. The shut off valve is used to separate the high vacuum QMS area from the higher pressure plasma side. The needle valve is used to allow a small amount of ionized gas to by-pass the shut off valve and

reach the QMS system. The high vacuum for the QMS is provided by a separate pair of rotary roughing pump and turomolecular pump.

Some of the important advantages and unique features of the system include[1, 2]:

- Can process advanced, non-equilibrium materials like diamond.
- Can deposit a variety of materials like SiN, SiO₂, Si, W, Mo, Ta, Ti, Al, TiN, TiO₂, WC and other ceramics or metals with a few modifications to the system.
- Can control properties of the film by controlling process parameters like temperature, pressure, precursor composition, flow rate, dopants, microwave power, etc.
- Can obtain a base pressure of 10⁻⁸ Torrs and is hence a very clean system.
- Very versatile and flexible and can be easily modified to suit new requirements.
- Can run process between room temperature and 1200°C.
- Magnetic fields can be used to generate ECR, Downstream plasma condition, Mirror effect or simple magnetic confinement.
- Up-to 1500W microwave power may be used to generate the plasma.

2.2 Optical Emission Spectroscopy [8-10]:

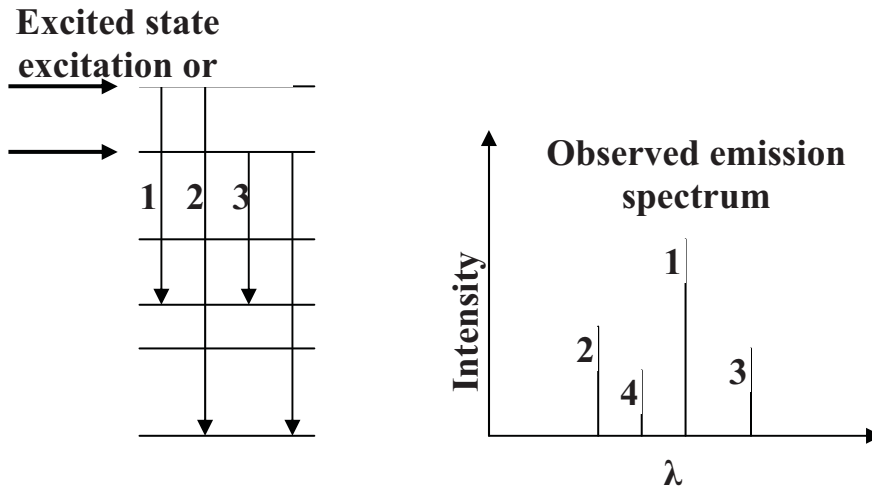


Figure 2.2 Energy levels involved in typical OES experiments

The analysis of light that is emitted from a medium in the absence of external optical excitation is called optical emission spectroscopy (OES). Optical emission generally occurs when electrons or gas-phase species relax from an excited electronic state to a lower state, which may be a ground electronic state, by spontaneous emission, Figure 2.2. The emitted radiation, with wavelength characteristic of the source species/material, is then spectrally dispersed and detected. In plasma assisted processes, such as plasma-assisted etching and deposition, and sputtering deposition, OES is often used to study the different gas-phase species that get generated in the plasma. The optical emission from the plasma is also called plasma-induced emission (PIE).

Optical emission (OE) between vibrational levels in the same electronic state also occur, but are much weaker and of less interest. Materials in thermal equilibrium at a given temperature T also emit light that is called thermal radiation or black body. The spectral

distribution of this OE and its intensity gives valuable information of the temperature of the surface of the material and is known as infrared/optical pyrometry.

In OES since only the excited species in plasma are detected, the observed spectrum gives information only about the excited-state density and does not directly reflect the profile of the ground-state population. These excited-state species generally have densities $<10^{-4}$ of the ground-state density. The other draw-back of OES is that even though emission from specific intermediates and products may dominate OE, emission from the chemically dominant species and important highly reactive species may not be detectable at all. However, when emission is present, OES is a simple and powerful diagnostic tool for practical real time monitoring. The lack of an external excitation source makes OES a robust and an inexpensive instrument for real-time control.

During plasma processing optical emission comes from neutral or ionized atoms, radicals, or molecules that have been electronically excited. Emission from atoms results in sharp lines, while that from molecules is broader and sometimes structured.

The spectrum observed from an OE can be quantitatively analyzed and depends on the density of species, the efficiency of excitation, and the rate of spontaneous emission. The advantage of OES is in its use as a monitor of relative, not absolute, conditions for process monitoring, without an external optical source, for e.g., endpoint detection depends on changes in emission intensities with time. In a steady-state process, the most reliable correlations with process parameters come by rationing the emission intensities of different spectral features.

In plasma the gas-phase species can be excited to the excited state by a number of ways:

1. Electron impact excitation: $A + e^- \rightarrow A^* + e^-$

2. Electron impact dissociation: $AB + e^- \rightarrow A^* + B + e^-$
3. Ion impact: $A^+ + e^- (+M) \rightarrow A^* (+M)$
4. Chemiluminescent recombination: $A + BC \rightarrow AB^* + C$

Where A, B and C represent atoms, radicals, and molecules, AB and BC are molecules and radicals, excited species that emit light are represented by asterisk (*), $e^- (+M)$ is either a neutral species, a negative ion, an electron plus a third body (M), or a surface.

The OE from the plasma is collected by a set of lenses and optical fiber and is focused onto the entrance slit of a spectrometer (Figure 2.3). The light is then dispersed by the monochromator and detected by a photomultiplier. Normally optical emission is collected for 200-900nm range and GaAs and S-20 photomultiplier type detectors show good quantum efficiency in the range. For detecting wavelengths shorter than 190nm, removal of oxygen throughout the collection path and inside the spectrometer is required to avoid absorption by O_2 , and is therefore rarely done. Transitions of wavelengths larger than 900nm from electronic transitions are relatively weak and rare, while those from vibrational transitions are insubstantial in comparison to those from electronic transitions. Such IR emissions compete with the back-ground from blackbody radiation and require noisier detectors.

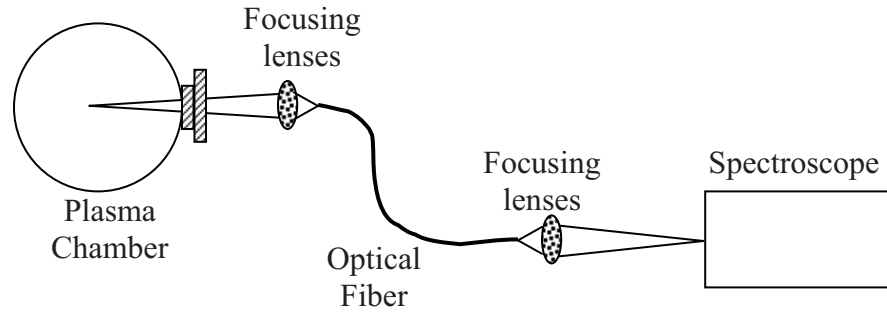


Figure 2.3 Schematic of OES setup used as a plasma diagnostic tool in MPECVD.

1.5 Quadrupole Mass Spectroscopy [11]:

The mass spectroscopy is used to analyze the plasma for its composition. It identifies the constituents of the plasma and measures their absolute partial pressure within the plasma chamber. The constituents of the plasma/sample gas being analyzed are identified by their mass/charge ratio and their partial pressure within the plasma is calculated from the quantity of particles/ions of the particular mass/charge ratio detected by the detector.

A Quadrupole mass spectroscopy (QMS) uses a quadrupole mass analyzer that separates different ions/species by their mass/charge ratio.

A typical QMS consist of the following important parts:

1. An ionizing source
2. Electronic lenses to focus and accelerate the ions towards the detector
3. Analyzer to separate the product ions/species.
4. Detector to count the ions
5. Data processing system to produce mass spectrum.

A mass spectrometer analyzes ions in the following steps

1. Produces ions form the sample to be analyzed (source)

2. Using an analyzer to separate the ions according to their mass/charge ratio.
3. The individual ions are then detected for their mass/charge ratio and abundance and a spectra of the mass/charge ratio and abundance is generated.

In its static mode QMS identifies and quantifies the plasma species and gives the output as a plot between partial pressure of the species and the type of species identified by their mass/charge (m/z) ratio. The QMS can also be used for continuous monitoring of the plasma species in which the variation in partial pressure of the selected plasma species/radicals is monitored with time. The understanding of the type of plasma species generated, their partial pressures, and variation in partial pressure of the plasma species with respect to time and changes in the process parameters provides an understanding of the deposition process. Typical plot of static and dynamic mode of the QMS spectra are given in Figure 2.4.

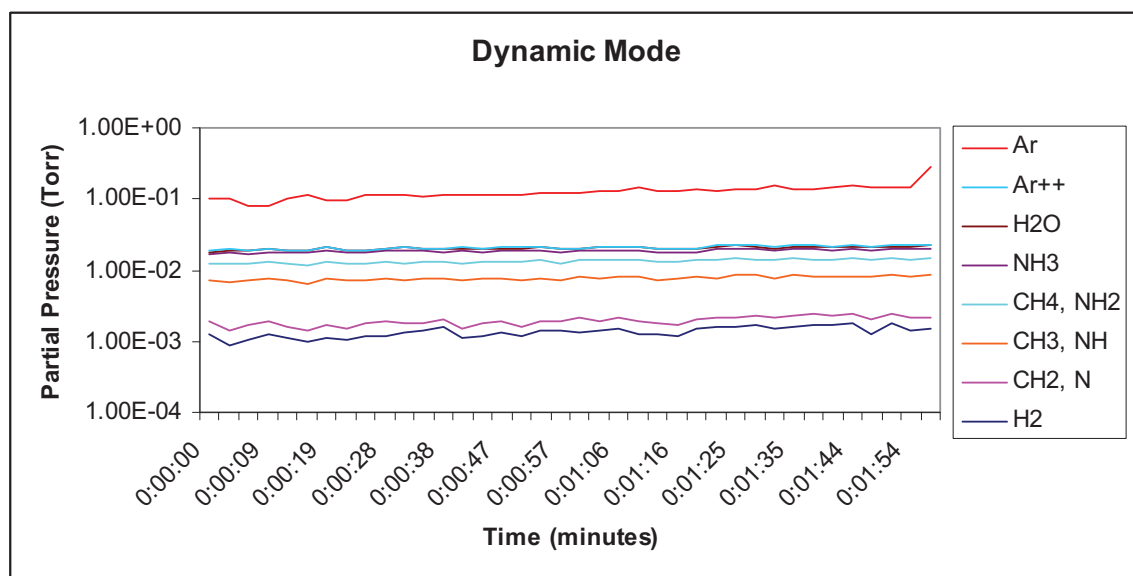
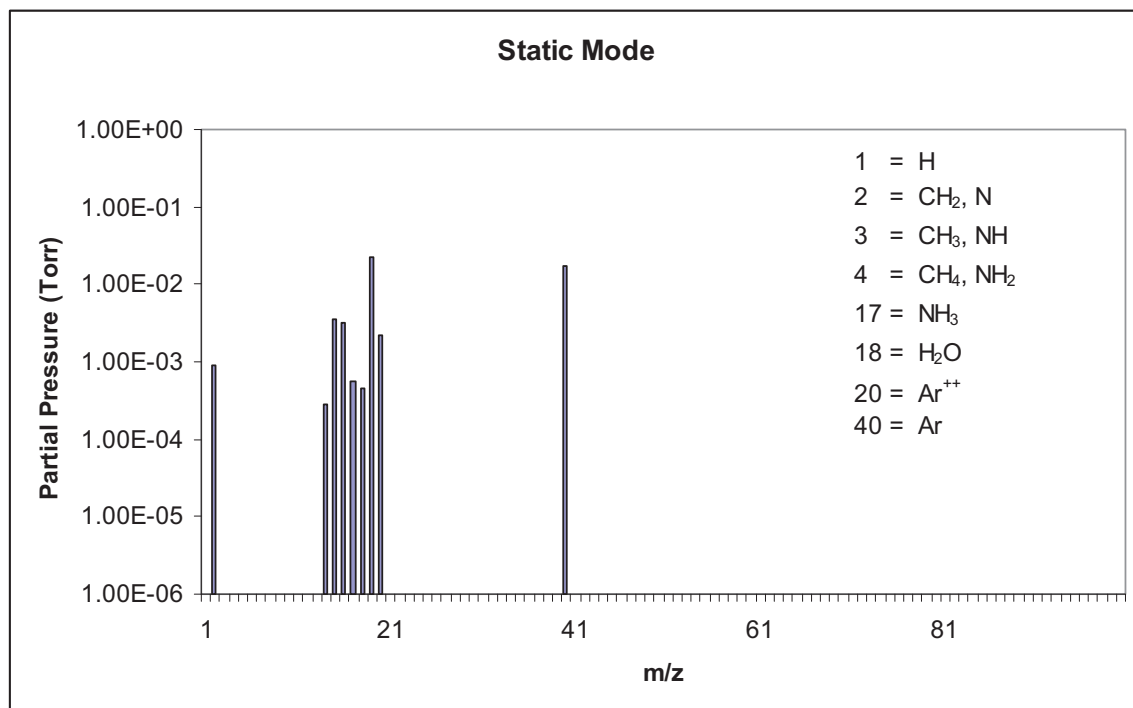


Figure 2.4 (a) Static mode spectra of QMS showing partial pressures of various ions/radicals identified by their mass/charge ratio for Ar+H₂+CH₄+NH₄ plasma. (b) Dynamic mode of QMS showing variation of partial pressure of the plasma species identified in the static mode with time.

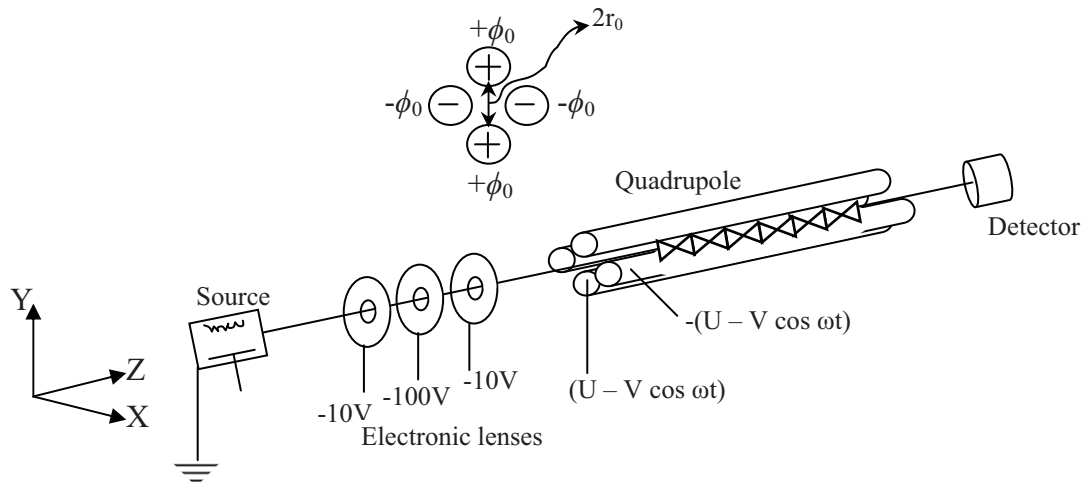


Figure 2.5 Schematic of quadrupole mass spectrometer.

Figure 2.5 Shows the schematic of the Quadrupole mass spectrometer employed for analyzing the plasma. The spectrometer consists of a source, focusing lenses, quadrupole analyzer and detector. It uses plasma from the plasma chamber as the source of ions. The ions are then accelerated and focused along the central axis of the quadrupole towards the detector, using electronic lenses. Once in the quadrupole, ions are stabilized and filtered according to their mass/charge ratio by controlling the stability of the ions along the length of the quadrupole analyzer. Once at the detector the quantity of the ions reaching the detector is measured using Electron Multiplier, Array Detectors, or Photo Multipliers. The quantity of the specific species detected is then converted into the partial pressure of the species within the chamber.

In quadrupole analyzer positive ions entering the space between the rods is drawn towards the negative rod, while the negative ions are drawn towards the positive rod. The ions are prevented from discharging on the rods by altering the potential on the rods, causing the

ions to follow the central axis of the quadrupole to the detector. Selectivity of the ions is achieved by controlling the potential on the rods such that ions with selected mass/charge ratio are deflected back to the central axis while the others reach the rods, get discharged and therefore are not detected by the detector.

The ions travelling along the central axis are subjected to a total electric field made up of a constant DC electric field superimposed with radio-frequency alternating field. The potential applied to the rods is given by:

$$\phi_0 = +(U - V \cos \omega t) \quad \text{and} \quad -\phi_0 = -(U - V \cos \omega t)$$

Where ϕ_0 represents the potential applied to the rods, ω is the angular frequency in rad/s ($\omega = 2\pi f$, where f is the frequency of the RF field), V is the ‘zero to peak’ amplitude of the RF voltage and U is the direct potential.

Ions entering the quadrupole analyzer along the central z-axis are accelerated towards the detector by the electrical lenses. The ions however, are also accelerated in the x and y directions as a result of the induced electric field given by:

$$F_x = ma = m \frac{d^2x}{dt^2} = -ze \frac{\delta\phi}{\delta x}$$

$$F_y = ma = m \frac{d^2y}{dt^2} = -ze \frac{\delta\phi}{\delta y}$$

Where a is the acceleration, m the ion mass and $ze = q$ is its charge. Both x and y determine the position of the ion from the center of the rods. As long as both x and y remain less than r_0 , the distance between two opposite poles of the quadrupole, the ions will be able to pass the quadrupole without touching the rods.

For a quadrupole r_0 is constant, ω is maintained constant, while U and V are variables. The positions x and y for an ion of mass m can be determined during a time span as a function of U and V . Changing U and V helps in selectively stabilize ions with specific mass that can then be detected for their quantity at the detector. The diagram below, Figure 2.6, shows that by scanning along a line maintaining the U/V ratio constant allows the successive detection of ions with different masses.

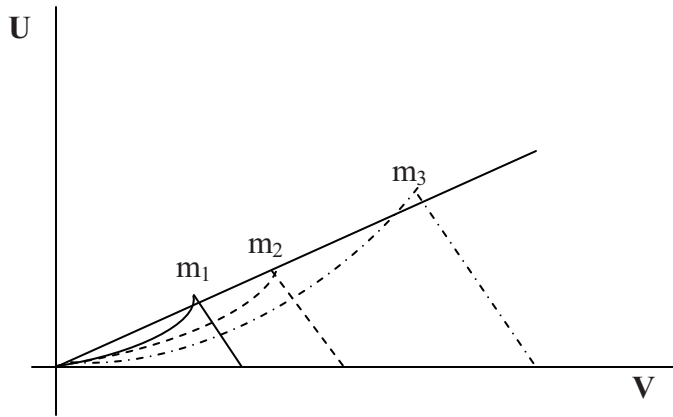


Figure 2.6 Stability areas of ions with different masses as a function of U and V .

PART II

MPECVD For Synthesis of Beta-Carbon Nitride

Chapter 1

Introduction

Hardness is a complex property related to the extent to which solids resist both elastic and plastic deformation. For materials with defects, hardness can be limited by many factors including point defects, dislocations, and macroscopic defects. On the microscopic level, for ideal systems, hardness is determined by the bulk modulus, which in turn depends on the nature of its chemical bonding. It is the strength and compressibility of the bond that plays the primary role in a solid's ability to resist deformation. The property bulk modulus, which defines the strength of a material, is the highest for covalently bonded materials. Diamond, a covalently bonded material, has the largest bulk modulus of 443 GPa, and is also the hardest known solid with a hardness of 100 GPa. *c*-BN, the next hardest material has bulk modulus of 369 GPa [12] corresponding to hardness of 21.9 GPa.

Using an empirical model for the bulk moduli of covalent solids with scaling arguments based on the Philips-Van Vechten scheme for characterizing covalent and ionic nature of tetrahedral solids by means of their spectral properties Liu and Cohen in 1989, demonstrated that a covalent solid formed between C and N isomorphous to Beta Silicon Nitride (β -Si₃N₄), could have a larger bulk modulus than diamond, and thus would be harder than diamond. With a bond length calculated as 1.4Å and lattice constants of $a = 6.4017\text{\AA}$ and $c = 2.4041\text{\AA}$, the bulk modulus of β -C₃N₄ was estimated to be 427 GPa [10-12]. The predication of such a high

modulus material with associated industrial applications inspired scientists around the world to extensively study the synthesis of hypothetical β - C_3N_4 .

While attempting synthesis of hypothetical β - C_3N_4 , various different forms of carbon nitrides were discovered including amorphous carbon nitride (a - C_3N_4) face centered cubic and pseudocubic Carbon Nitride, alpha carbon nitride and graphitic carbon nitride [13-15]. These different forms of Carbon nitrides were shown to possess interesting properties related to electronic, electrical and mechanical applications that make the whole genre of Carbon Nitride materials even more fascinating and intriguing. Some of the other interesting properties (other than high hardness) of the carbon nitride (CN_x) materials include wide band gap (3.2 eV indirect and 4.0 eV for direct measurements) [13], high thermal conductivity, high strength, excellent resistance to corrosion and wear, and smooth surface [14, 15].

Based on the above properties some of the predicted applications of CN_x materials are fabrication of high-hardness, high temperature, high-power and high-frequency devices used in microelectronic, and space flights, over-coating films on magnetic recording disks to protect computer disk drives, luminescence semiconductors [16], field emission materials [17], cutting tools and wear resistance and corrosion resistant coatings. Semiconductors with variable band gaps may also be obtained by controlling the nitrogen concentration in the films [14, 15].

Although amorphous and graphitic carbon nitride thin films and their bulk materials have been successfully synthesized, phase pure alpha or Beta carbon nitride thin films and their bulk materials are till date hypothetical materials. The short C-N bond length in the β - C_3N_4 structure resulting in extremely small N lone pair-N lone pair distance of 2.46Å, which cause great repulsion between the lone pairs was found to be the main reason for the instability of β - C_3N_4 [18]. Another hurdle in the synthesis of C_3N_4 was the difficulty observed in getting a

stoichiometric ratio of C and N in the CN_x thin films. The N/C ration was mostly observed to be below the required value of 57% [19].

Over the years some success has been reported in the synthesis of crystalline carbon nitride (CN_x) thin films using low pressure techniques [16, 17, 22-35]. These thin films were stabilized mostly by Si and showed characteristic peaks of both $\beta-C_3N_4$ and $\alpha-C_3N_4$ along side peaks of Si_3N_4 in XRD and Raman spectra of the deposited thin films. High pressure synthesis of carbon nitride resulted in mostly amorphous powder [20]. Some of the low pressure techniques that showed good results of crystalline Si-stabilized carbon nitride thin films include Pulsed Laser Deposition, Ion Implantation, Vacuum Cathode Arc Method, RF Reactive Magnetron Sputtering and MPECVD. However till date phase pure $\beta-C_3N_4$ remains a hypothetical material.

In this study, synthesis of $\beta-C_3N_4$ is attempted using Microwave Plasma Enhanced Chemical Vapor Deposition (MPECVD) system equipped with in-situ plasma analysis techniques such as Quadrupole Mass Spectroscopy and Optical Emission Spectroscopy. Chemical vapor deposition techniques itself is a very versatile technique with applications in thin film deposition of ceramics, metals and polymers for semiconductor and packaging industry. Addition of plasma improves the capabilities of a CVD system to the extent that meta-stable materials such as diamond can be easily synthesized. Using microwaves as a plasma source adds to the advantages of a plasma CVD system. Microwaves not only increase the density of the plasma but also make it possible to deposition thin films at lower deposition temperatures. In addition to Microwave plasma the QMS and OES units installed on our MPECVD system, that provide instant chemical analysis of the plasma, makes our CVD

system well tooled for research and development work on difficult-to-synthesize materials such as β - C_3N_4 .

The inspiration behind attempting the synthesis of hypothetical β - C_3N_4 thin films comes from the deposition of diamond thin films. In the synthesis of diamond thin films once the nucleation layer of diamond is formed, i.e. once the diamond structure is established, further growth of diamond thin films becomes very easy. Similarly it was thought that once a β - C_3N_4 structure is established, with the help of Si from the substrate, growth of the Si incorporated thin films over time could potentially result in phase pure β - C_3N_4 on the top surface of the thin films.

In this study Si incorporated CN_x thin films were successfully deposited on Si substrates using $CH_4+NH_3+H_2$ plasma. Although phase pure β - C_3N_4 was not produced in long term growth experiments it was discovered that the morphology and type of CN_x thin film deposited by MPECVD can be controlled by controlling the sequence of introduction of the precursor gases in the plasma chamber. It was found that if after stabilizing the initial H_2 plasma, N_2 is introduced first, well crystallized hexagonal Si-incorporated CN_x particles are deposited. These particles exhibit characteristic peaks of β - C_3N_4 , α - C_3N_4 and β - Si_3N_4 in their Raman Spectra. On the other hand if after stabilizing H_2 plasma CH_4 is introduced first, graphitic CN_x is formed with some Si incorporated in it. The graphitic CN_x particles show characteristic peaks of graphite in their Raman spectra. The observations were confirmed by repetitive experiments. Effect of other deposition parameters including deposition pressure, microwave power and precursor gas ratios were also investigated.

Chapter 2

Literature Review

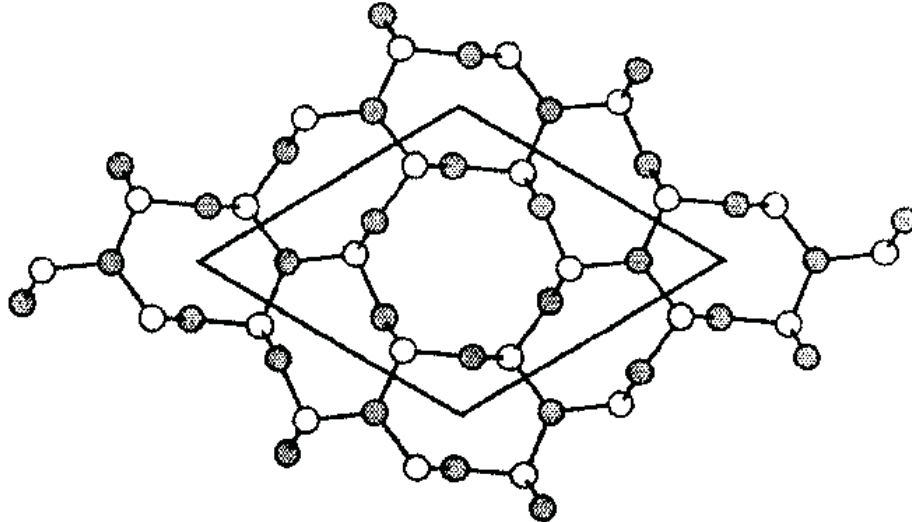


Figure 2.1: Crystal structure of β - C_3N_4 with C and N atoms as white and grey respectively [10, 37, 38]

2.1 Structure of Carbon Nitride

Liu and Cohen chose β - Si_3N_4 structure with C substituting for Si as a prototype for a covalent C-N solid. The octet rule for covalent bonding is satisfied in this structure, and no anti-bonding states are occupied [12].

In Figure 2.1, the structure is shown to consist of bulked layers stacked in AAA... sequence. The unit cell is hexagonal and contains two formula units (14 atoms) with local order such that C atoms occupy slightly distorted tetrahedral sites while N atoms sit in nearly planar triply coordinated sites. This structure can be thought of as a complex network of CN_4 tetrahedra that are linked at the corners. The atomic coordination suggests sp^3 hybrids on the C

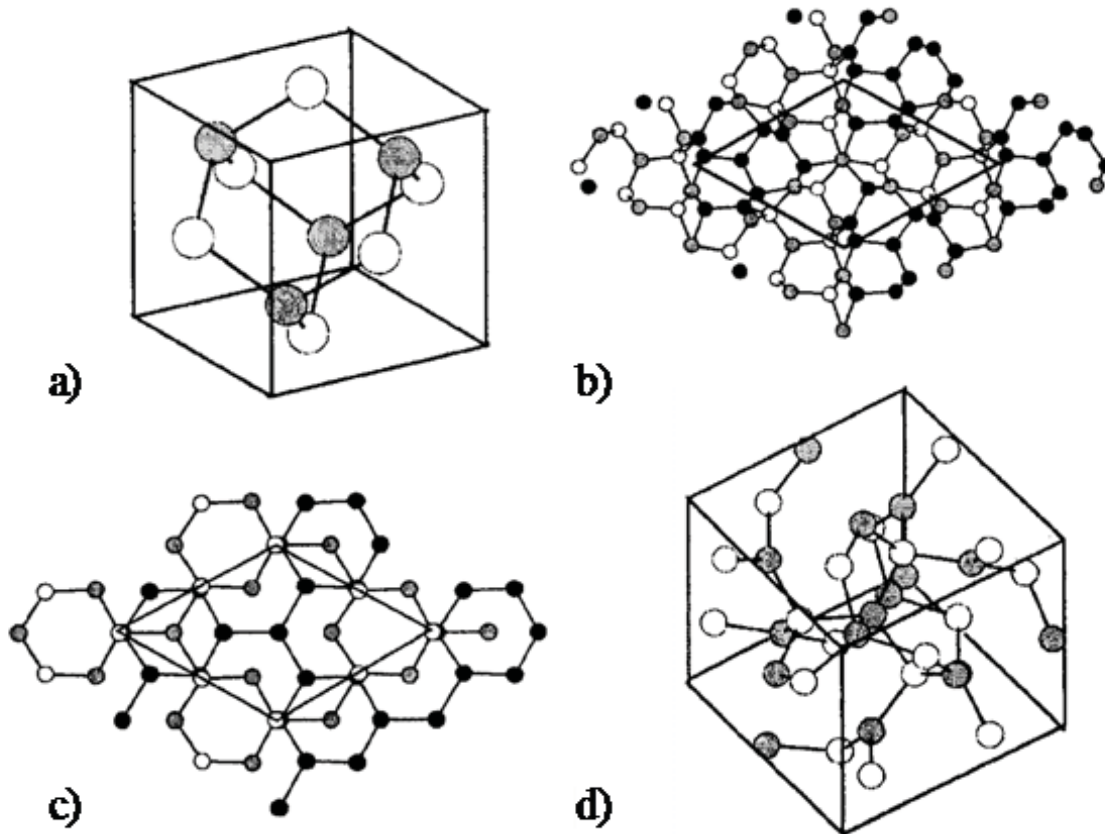


Figure 2.2: Ball and stick models of C_3N_4 phases. For the defect zinc-blende (a) and cubic (d) the carbon and nitrogen atoms are white and grey respectively. The α structure (b) and the graphite phase (c) both consist of two layers. The upper layer shows the C atoms in white and the N atoms in light grey. In the lower layer, the C and N atoms are dark grey and black respectively.

atoms and sp^2 hybrids on the N atoms with lattice constants calculated to be $a = 6.4017\text{\AA}$ and $c = 2.4041\text{\AA}$. The short bond length between C-N of approximately 1.4\AA in the β - C_3N_4 structure however results in extremely short non-bonded N-N distance (2.46 and 2.69\AA) that makes the β - C_3N_4 structure metastable.

Other forms of carbon nitride (CN_x) discovered include α - C_3N_4 , analogue to α - Si_3N_4 , face centered (FCC) cubic and pseudocubic (Zinc-blende) C_3N_4 , and graphitic carbon nitride (g - C_3N_4). In α - C_3N_4 , similar to α - Si_3N_4 , all N sites are sp^3 hybridized because the C-N rings of α - C_3N_4 are 6-membered, and all the N sites are attached only to them [1-3]. Also since all the

N sites are attached to C-N rings α -C₃N₄ are less bulky than α -Si₃N₄. This structure of α -C₃N₄ is the reason for its negative Poisson's ratio in all dimensions i.e. to say that the C-N-C bonds of α -C₃N₄ will become more planer under tension [1-3]. Other predicted C₃N₄ structures include face centered (FCC) cubic and pseudocubic (Zinc-blende) C₃N₄ [21]. Both of these structures are predicted to consist of sp³ hybridized nitrogen. Like graphite and diamond are the allotropes of carbon, another structure of C₃N₄ is graphitic-C₃N₄. It is proposed that graphitic-C₃N₄ is more stable than β -C₃N₄ [21]. For graphitic-C₃N₄ sp² hybridized N in C₃N₄ is assumed with planer or non-planer geometry [21]. Figure 2.2 shows the four predicted structures (other than β -C₃N₄) of crystalline C₃N₄ [1-3].

2.2 PROPERTIES OF CARBON NITRIDE:

Following are some of the exciting properties of CN_x films [7-9, 25, 27-40, 43]:

1. High bulk modulus (427 GPa) ,
2. Wide band gap ; 3.2 eV indirect and 4.0 eV direct,
3. High thermal conductivity,
4. high strength, Excellent resistance to corrosion and wear. CN_x films with x on the order of 0.4 have better wear resistance than the usual hard carbon films used as protective overcoats,
5. Semiconductors with variable band gaps may be obtained by controlling the nitrogen concentration in the films.
6. Smooth surface,
7. Negative Poisson's ratio,
8. Transparent , and

9. Calculated optical band gap of -6eV and observed value of -2.8eV .

2.3 APPLICATIONS OF CARBON NITRIDE THIN FILMS

Based on the above properties some of the predicted applications of CN_x materials are [7-9, 31, 33-46, 49]:

1. Fabrication of high-hardness, high temperature, high-power or high-frequency devices for microelectronic, and space flight applications.
2. Over-coating films on magnetic recording disks to protect computer disk drives,
3. luminescence semiconductor ,
4. field emission ,
5. wear and corrosion resistant coatings for cutting tool, and
6. Semiconductors with variable band gaps.

2.4 SYNTHESIS

Almost all the possible techniques, from cryogenic [17] to high pressure high temperature technique [17, 20] have been explored for the synthesis of hypothetical $\beta\text{-C}_3\text{N}_4$. The most commonly used low pressure techniques are Microwave Plasma Chemical Vapor Deposition (MPCVD) [7, 9, 33, 36-42], Pulsed Laser Deposition (PLD) assisted with various plasma processes [8, 28, 31, 42, 44], Plasma Ion Plating [1, 22], Vacuum Cathode Arc Method [23], and Radio Frequency Reactive Magnetron Sputtering (RF-MS) [13], to name a few. However, so far no film with 100% crystalline $\beta\text{-C}_3\text{N}_4$ has been deposited, although RF-MS, MPCVD, and PLD techniques have shown some promising results. High pressure high temperatures technique was also explored with minimum success [20]. The technique is

explained further in the section below. MPCVD, PLD and Ion Implantation techniques that showed some promising results are also discussed in more detail in the following section. Different substrates and precursors explored are summarized separately.

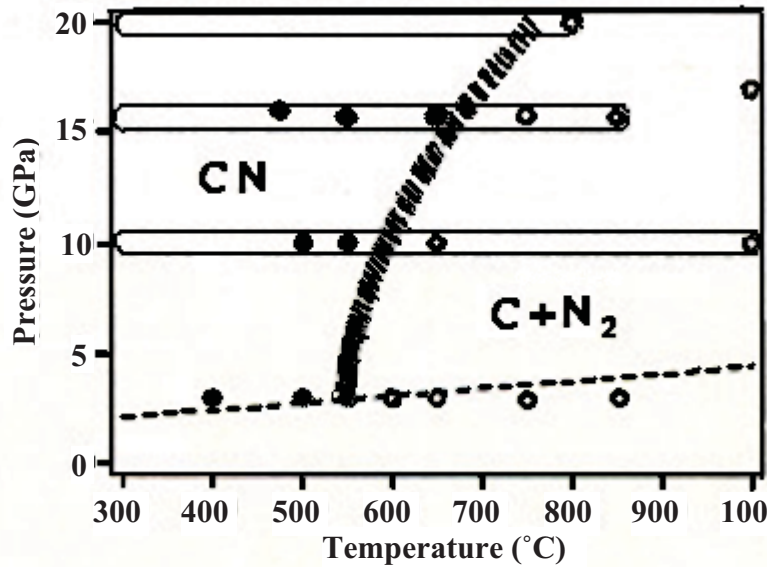


Figure 2.3 Stability phase diagram of pCN [24]

2.4.1 HIGH PRESSURE SYNTHESIS:

It has been proven that in a C-N-H atmosphere, under high pressure, N does not stay on diamond surface, but escapes as HCN and no C-N compound can be formed. Thus exclusion of H from the precursor material for the synthesis of CN_x materials under HPHT conditions was proposed. Studies [25, 26] have established that CN_x materials go through a permanent decomposition into molecular N and C at a definite temperature that increases with increasing pressure. It has also been suggested theoretically that carbon nitride species with sp^3 bonding should have greater stability at higher temperature [18]. However, it is unknown if the kinetic energy barrier for the formation of $\beta-C_3N_4$ can be overcome at temperatures below the decomposition temperature of sp^2 -bonded CN_x material into C and N_2 [24]. Using

paracyanogen (pCN) precursor, and Boyd and England type piston cylinder apparatus and a Walker type multianvil press, it was demonstrated [24] that upper stability point of precursor paracyanogen (pCN) at 3GPa is 550°C and increases to approximately 750°C at 20 GPa as shown in Figure 2.3. It was shown that within the data range of pressure and temperature where pCN was stable, density of the formed CN_x increased close to that of graphite indicating that pCN retains sp^2 hybridization in the CN_x film. Thus, it was concluded that simply going to HTHP conditions with precursors that retain their sp^2 hybridization is not the best approach for the synthesis of sp^3 CN_x . Precursors that help overcome the barrier for sp^3 hybridization are needed.

2.4.2 LOW PRESSURE SYNTHESIS:

Other than the instability of β - C_3N_4 low pressure techniques investigated for the synthesis of CN_x thin films have a generic problem; achieving the required percentage (57%) of atomic nitrogen in the thin films. Using plasma diagnostic measurements it was shown that for any low pressure technique employed for synthesis of crystalline carbon nitride, high concentration of active radical species (e.g. CN^\cdot and N^\cdot) are necessary to obtain high nitrogen concentrations [19]. To produce high concentration of active radical species higher energies are required. Energy of the radicals produced in a plasma or a CVD system depend on pressure, power or plasma source and temperature of the substrate. Under low pressure conditions too high temperature often results in re-evaporation/desorption of the depositing species; etching of the substrate or formation of substrate-vapor gas compound. Temperature of the substrate should therefore be high enough to support deposition of the thin film on the substrate, and low enough to prevent desorption of the depositing radicals. High substrate

temperature also catalyzes the decrease in the N/C ratio [19]. It has been observed that the N/C ratio (i.e. N composition in the films) increases as the substrate temperature increases up-to 850°C and it decreases with a little rise above 850°C [27]. Temperature also decides what compound would form during the deposition. Shi et. al. [28] showed that β -Si₃N₄ grows very rapidly as the substrate temperature increases, while on the other hand if the substrate temperature is too low carbon phase appears on the films.

Decreasing pressure in the MPECVD system helps in increasing the energy of the depositing radicals and increases their density in the plasma. It also increases the energy of bombardment of the ions/radicals. The disadvantage observed in the synthesis of hypothetical β -C₃N₄ thin films under low pressure conditions is that physical impact, e.g. in the form of ion bombardment, leads to a strong reduction of the nitrogen content by chemically enhanced preferential sputtering of nitrogen atoms and preferential desorption of volatile N containing species [19]. As a consequence, physical impact and/or high temperatures have to be avoided in order to achieve high nitrogen concentrations (e.g. 57% as required for β -C₃N₄). This, in turn, means that a high degree of ‘chemical’ impact (activation) is required if carbon nitride films with high N/C ratios are to be deposited [19]. Chemical activity/reactivity of the depositing radicals can be increased by controlling pressure or by increasing the density of the radicals in the plasma by increasing energy of the plasma source (microwave power in case of MPECVD system).

Increasing energy of the plasma source/ion gun/laser up-to a certain level helps in increasing the density of the plasma/active radicals. Above the critical energy increasing energy of the plasma source/ion gun/laser can cause deposition of un-wanted material, etching of the substrate or re-evaporation of the depositing species. Other key factors in the synthesis

of C_3N_4 material, under low pressure conditions, is purity of carbon and nitrogen precursors (to avoid the formation of unwanted compounds like C-H-N polymers) and control of energies of active radical species of C and N (to trap metastable phase kinetically) [29].

Techniques with some success in the synthesis of CN_x thin films under low pressure conditions are listed in Table 2.1.

Table 2.1: Comparison of some of the techniques used for the synthesis of CN_x films.

No.	Method	Sub.	Precursors	Films formed	Ref.
1.	MPCVD	Si, Mo, Ta, Pt, Ni	CH_4 , N_2 , Ar & H_2	Interlayer of SiC, Si_3N_4 , and crystals of Si-C-N, and α - and β - C_3N_4	[19, 23-31, 44]
2.	Pulsed LASER deposition	SiO_2 , Si	N_2 -Plasma/ Ion beam and LASER ablated C/graphite	Interlayer of SiC, Si-C-N, C=N, $C\equiv N$, hexagonal crystals α - and β - C_3N_4	[17, 25, 28-31]
3.	Ion Implantation	SiO_2 , Si and a-C	N-Ion beam and Graphite / Diamond target	SiC, a- CN_x	[22]
4.	Vacuum Cathode Arc method	Si	N_2 , Ar gas and Graphite target	SiC, Si-C-N, C=N, $C\equiv N$,	[23]
5.	RF Reactive Magnetron Sputtering	Plastic (CR-390)	N_2 -Plasma and Graphite target	C=N, $C\equiv N$, and some C – N	[21, 49]

From the table above it can be seen that MPCVD, PLD and Ion implantation techniques show promising results. These techniques are therefore discussed briefly in the following subsections.

2.4.2.1 MICROWAVE PLASMA CHEMICAL VAPOR DEPOSITION (MPCVD)

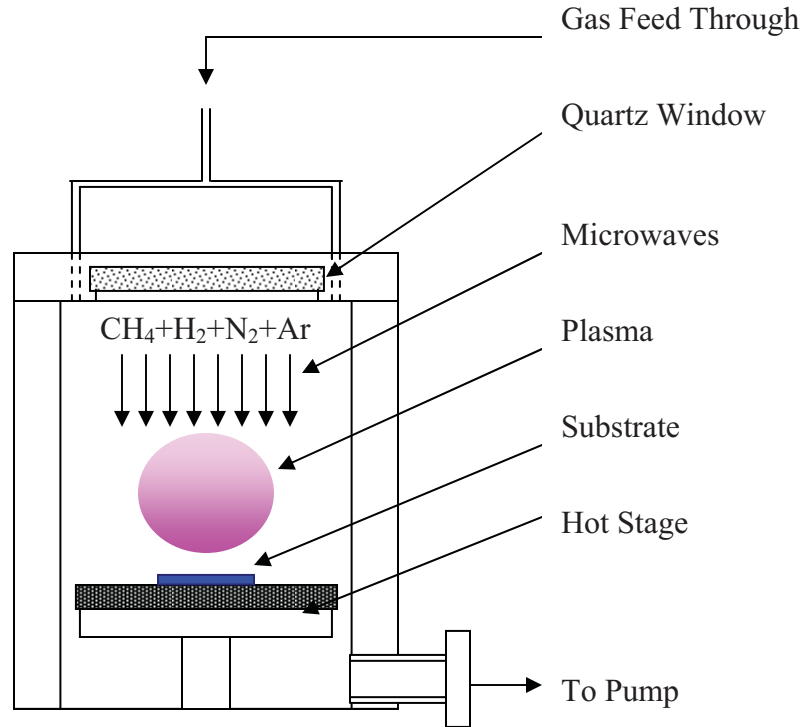


Fig. 2.4: Schematic of typical MPCVD setup for synthesis of CN_x films

MPCVD is a widely used technique for the synthesis of CN_x films on Si substrates [3, 5, 24, 27-33]. Figure 2.4 shows a typical setup of MPCVD used for the deposition of CN_x films. The experimental parameters that have given the most promising results for this process are: flow rates of Nitrogen as 100 sccm, CH₄ as 0.5-1.0 sccm, pressure of 18.75 – 22.5 Torr, microwave power of 500-700W, deposition time of 1.5 hrs. and deposition temperatures of 700-900°C. These deposition parameters produced hexagonal α - and β -C₃N₄ with N/C ratios from 0.8 – 2.0 [3, 27, 29]. But the films were not composed of only α - and β -C₃N₄ phases, phases such as α - and β -Si₃N₄, SiC, Si-C-N, etc., are also seen [7, 36, 39]. β -Si₃N₄ grows more easily near the substrate surface. N and Si with electronegativities of 3.0 and 2.0, respectively,

results in the easier formation of covalent bond of Si-N than C-N covalent bonds (C has electronegativity of 2.5). The average growth rate ratio between Si-N and Si-C-N was found to be 21/1 [30]. At higher temperatures growth rate of β -Si₃N₄ increases [31]. Since Si stabilizes the crystalline structure of carbon nitride and also increases nitrogen concentration in the films, its diffusion into the film, which is achieved at higher temperatures, in a limited amount is essential for successful synthesis of CN_x films [28, 30]. Cross-section of films prepared with 10% H₂ in N₂ + CH₄ plasma, revealed three layers, Si-O, Si-C-N and Si-N, which was confirmed by selected area EDS analysis. Another systematic study of nitrogen incorporation (0 – 100%) in H₂ plasma showed that diamond is formed at very low concentrations of nitrogen (0-3%), however Si-C-N was formed with higher nitrogen concentrations [30] in a MPCVD environment. The above observations prove that the concept of electronegativity is followed, Si diffusion in the growing film is important for stability of the crystalline CN_x thin films, and that H₂ should be avoided in the precursor gas to promote formation of pure CN_x thin films using MPECVD.

2.4.2.2 Pulse Laser Deposition (PLD)

Figure 2.5 shows setup for Radio Frequency (RF) Pulsed modulation assisted Pulsed Laser Deposition of CN_x films. In PLD, a laser (e.g. ND:YAG [29, 32], KrF [8, 46, 47], XeCl [33] or ArF [33]) is used to ablate high purity graphite target in the presence of a nitrogen plasma. The atomic/ionic nitrogen from the plasma reacts with carbon from the fluence, obtained by laser ablation of graphite target, to form CN radicals that deposit on the Si (100) substrate. Most of the films obtained by PLD process are sp² bonded carbon nitride with some C–N (sp³) and C≡N (sp¹) bonded phases, with [N] content ranging from 35 – 53% [32]. It was

also observed that the $C\equiv N$ triple bond in the films increased with increasing $[N]$ in the films [15, 32]. A correlation between the nitrogen composition and the film growth rate [32] suggested that a key step in the carbon nitride growth mechanism by PLD involves a reaction between carbon and nitrogen at the growth surface and not in the gas phase.

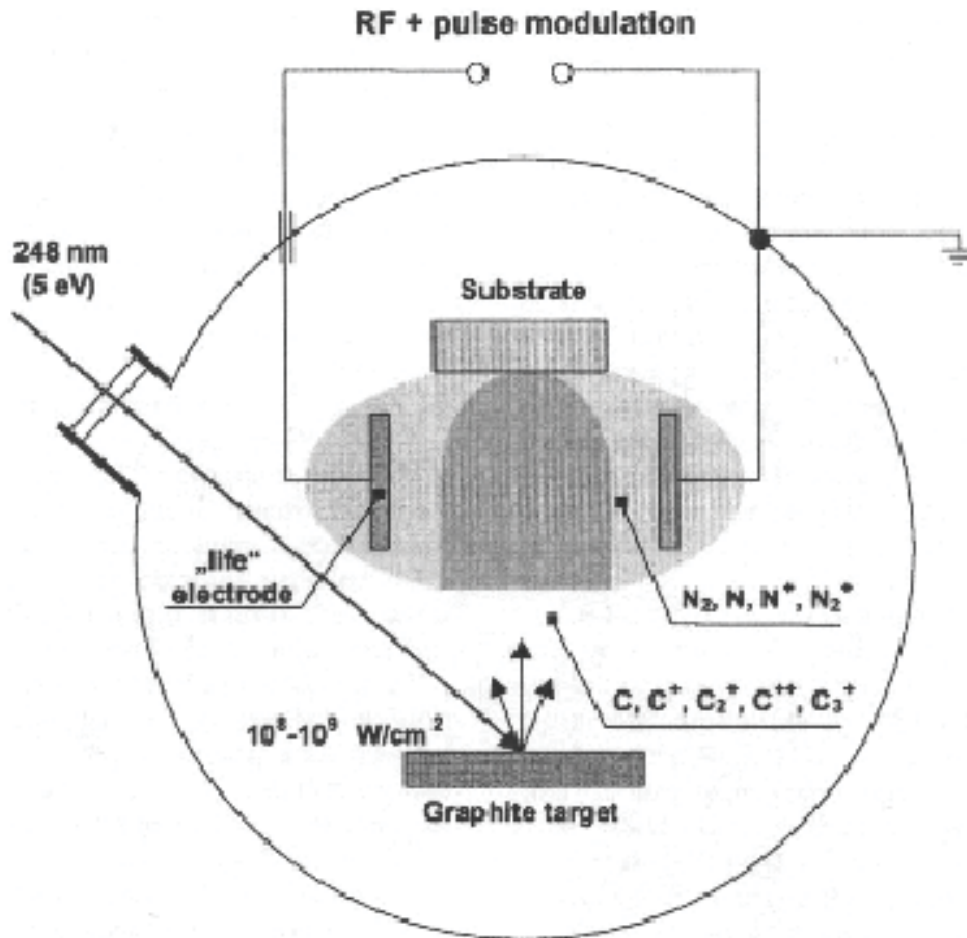


Figure 2.5: Setup for RF pulsed modulation assisted Pulsed Laser Deposition of CN_x film [19].

PLD technique for CN_x films are always combined with different techniques of nitrogen supply some of them are given in Table 2.2 below:

Table 2.2: Comparison of different techniques of Nitrogen addition in PLD of CN_x films.

No.	Technique	Sub.	N ₂ source	C source	Laser	Pressure	Film deposited	Ref.
1	ECR MWP*	Si (100)	N ₂ Plasma	Graphite target	ND:YAG	0.22 mT	mostly sp ² with some sp ³ bonds	[15]
2	ICP-CTR**	Si (100)	N ₂ Plasma	Graphite target	KrF	0.25-2.25 T	mostly sp ² with some sp ³ bonds	[19]
	PLD-RFP***	Si (100)	N ₂ Plasma	Graphite target	KrF	0.15T	mostly sp ² with some sp ³ bonds	
3	Ion Assisted	Si (100)	N ₂ ion gun	Graphite target	ArF & XeCl		mostly sp ² with some sp ³ bonds	[33]
4	Atomic nitrogen beam	Si (100)	atomic N beam	Graphite target	ND:YAG & KrF		mostly sp ² with some sp ³ bonds	[32]
5	ECR MWP	Si (100)	N ₂ Plasma	Graphite target	G target by PLB	0.22 mT	mostly sp ² with some sp ³ bonds	[14]
6	RF discharge	Si (100) and SiO ₂	N ₂ Plasma	Graphite target	ND:YAG & KrF	10e-5 to 10e-4 T	mostly sp ² with some sp ³ bonds	[34]

* ECR MWP = Electron Cyclotron Resonance Microwave plasma

** ICP-CTR = Inductively coupled plasma CVD utilizing chemical transport reactions

*** PLD-RFP = Pulsed laser deposition with additional R.F. plasma discharge.

From the table above it is seen that irrespective of the techniques used for addition of nitrogen into the system the films formed by PLD process were mostly sp² bonded CN_x films with some sp³ bonded phases embedded in them. The reason for the low sp³ and higher sp² phases in the film can be cited as the high impingement energies of the radicals, growth rate dependence of the composition of the film [29], and incomplete reaction between the ablated carbon and ionic/atomic nitrogen.

2.4.2.3 ION IMPLANTATION

[N]/[C] ratio ranging from 0.7-3.5, can be achieved by selecting appropriate energies and doses of N and C atoms in ion implantation [35]. The films obtained on Si substrate were

of pure carbon and nitrogen, with segregation of C and N ions near SiO₂/Si interface. The C and N atoms implanted in the samples showed no bonding between them. However after annealing at 1000°C for 3 hrs., some C≡N triple bonding was observed in the FTIR spectrum at ~2250cm⁻¹. XPS analysis of the film showed that a majority of the nitrogen was not bonded to Si or O, suggesting that the formation of C-N bonds was energetically more favorable [35] under the deposition conditions used. In implantation of nitrogen in diamond [22] with lower energies on Diamond thin films, the nitrogen ions did not have enough energy to damage the diamond film and were bonded to either sp² hybridized or sp³ hybridized carbon. With higher implantation energies, diamond got graphitized and most of the nitrogen ions bonded with sp² hybridized carbon [22]. The films deposited were therefore mostly sp² bonded, although with good amounts of N concentration in them.

2.4.3 SUBSTRATES

Some of the substrate materials studied for the synthesis of hypothetical β-C₃N₄ are listed in Table 2.3. While those that are more promising, like Si, Pt and α-Si₃N₄ are discussed in detail in the subsections that follow.

Table 2.3: Different substrates investigated for deposition of Carbon Nitride thin films.

No.	Substrate	Films Obtained	References
1.	Si (100)	Si, SiC, Si ₃ N ₄ , Si-C-N, a-CN _x , C=N, C≡N, α- and β-C ₃ N ₄	[17-19, 22, 26-32, 45, 48]
2.	Pt	Pt, C=N, C≡N, α- and β-C ₃ N ₄	[35, 37]
3.	α-Si ₃ N ₄	α-Si ₃ N ₄ , C=N, C≡N, α- and β-C ₃ N ₄	[36]
4.	Mo	Mo, Mo ₂ N, MoN, MoC _x , C=N, C≡N, α- and β-C ₃ N ₄	[37]
5.	Ta	Ta, TaC, C=N, C≡N, α- and β-C ₃ N ₄	[37]
6.	Ni	Ni, C=N, C≡N, α- and β-C ₃ N ₄	[33]
7.	SiO ₂	a-CN _x , C=N, C≡N, α- and β-C ₃ N ₄	[22, 34]

2.4.3.1 SILICON (Si)

Silicon (100) is by far the most commonly used substrate for the synthesis of CN_x films, because of its useful semi-conducting properties. Also, silicon is believed to catalyze the

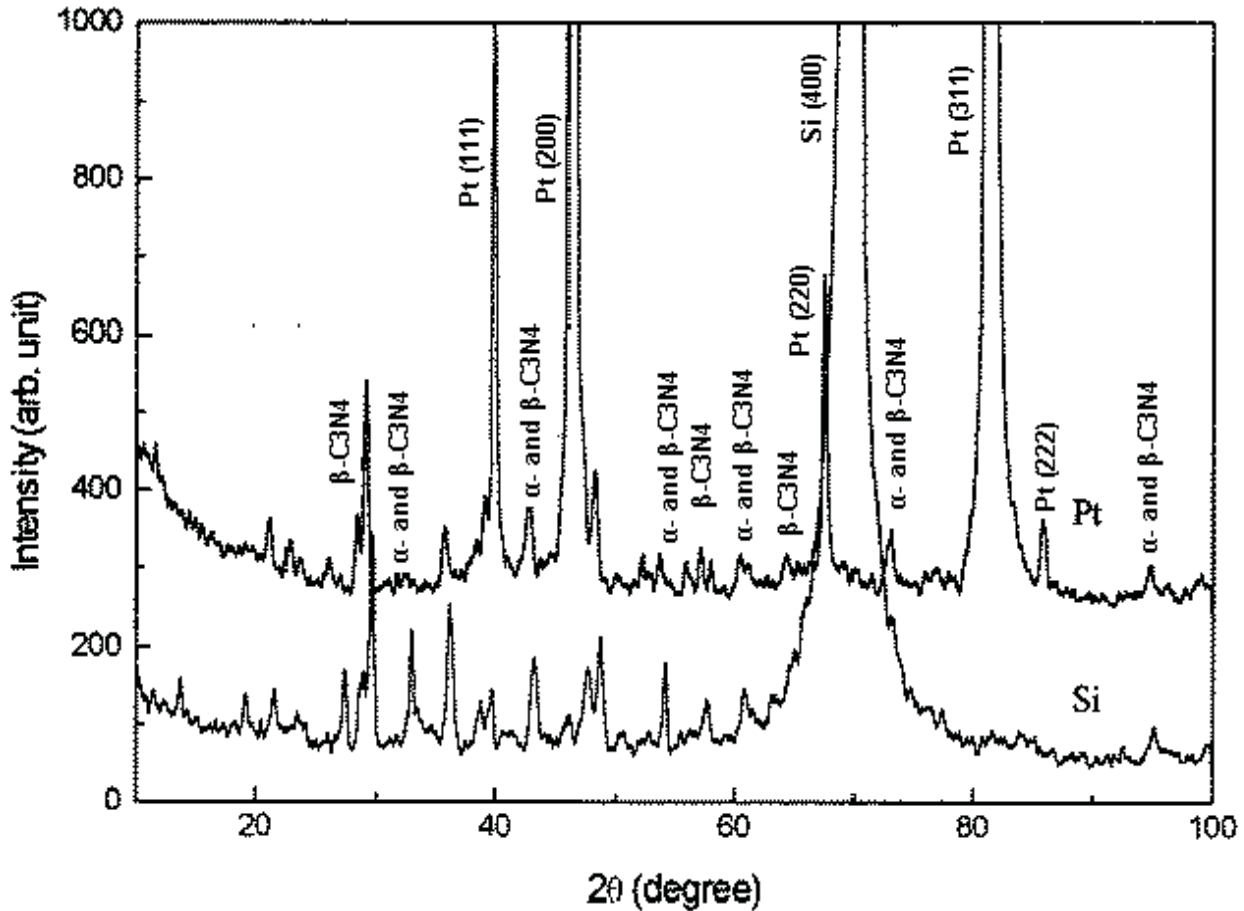


Figure 2.6: Comparison of X-ray diffraction peaks of CN_x films deposited on Pt and Si substrate [37].

chemical reactions in the plasma during the deposition of CN_x films that eventually leads to the formation of crystalline and stable C-N network [38]. An intermixing zone is formed during deposition on Si substrate consisting of substrate Si atoms and incident N and C atoms that play a role in reducing lattice mismatch and relaxing intrinsic stresses. However, the associated disadvantages of using Si as substrate for the synthesis of CN_x materials is the diffusion of Si

into the film, forming compounds, such as Si-N, Si-C, and Si-C-N. These compounds form more easily than CN_x because of the electronegativities of Si, N and C (Si = 2, N=3, C=2.5). The characterization of CN_x thin film deposited on Si substrate becomes difficult because of the overlapping of the CN_x characteristic peaks with the characteristic peaks of Si based Si-C-N compounds.

2.4.3.2 PLATINUM

Since Platinum does not have any simple compound with C and N, it was used as a substrate for deposition of CN_x films. However, the films on Pt substrate were amorphous. With the addition of a small amount of Si impurity, increase in the $[N]/([C] + [Si])$ atomic ratio and crystallization of carbon nitride films was observed. The $[N]/([C] + [Si])$ atomic ratio of carbon nitride films containing 5.53% Si can reach 1.35 (with small crystallites of α - and β - C_3N_4), close to the stoichiometric value of 1.33 of hypothetical C_3N_4 [37]. EDX showed that N/C atomic ratio in the films was close to 4/3 [31]. A comparison of X-ray diffraction peaks of CN_x thin films on Pt and Si substrate shows that except for the strong peaks of the substrate and β - Si_3N_4 , all the low index, high intensity peaks of β - C_3N_4 were almost the same, Figure 2.6. Suggesting that Platinum is as good as a substrate for CN thin films as is Silicon.

2.4.3.3 AMORPHOUS SILICON NITRIDE (α - SiN_x)

The use of α - SiN_x substrate was tried with a direct dual ion beam deposition technique for the synthesis of CN_x thin films [36]. Since the activation energy barrier of C-N bond is higher than that of Si-C bond, Si-C bond is more likely to form than the C-N bond when depositing on Si substrate. The Si-N double bond in α - SiN_x is more difficult to break than Si-Si

double bond in Si substrate. Because of these facts C-N bonds form directly on the α -SiN_x substrate without formation of any intermediate layer [36] or without much diffusion of Si in the growing thin film. The result of XPS and the Raman analyses of the films deposited on α -SiN_x substrate show that the sp³/sp² and the I_D/I_G ratios are relatively higher than those of the films on Si substrate [36]. These results suggest that α -SiN_x is a promising substrate for the synthesis of CN_x.

From the discussions made above it can be concluded that Si, Pt and α -SiN_x are promising candidates for substrate material for the deposition of hypothetical β -C₃N₄. Platinum however is every expensive and therefore is not explored extensively as a substrate material for CN thin films. In this study Si substrates were used because of their ability to stabilize the C-N structure.

2.4.4 PRECURSORS

In most CVD processes using Microwave Plasma, synthesis of carbon nitride is brought about by the use of N₂ and CH₄ precursor gases [7, 9, 33, 36-43]. In some cases H₂ [7, 33, 34], SiH₂ [38], and Ar [39] were also added. Most MPECVD processes using 100 sccm of N₂ and 1 sccm CH₄ produced hexagonal crystalline rods of Si-C-N, as shown in Figure 2.7 [9, 33, 36, 37, 39, 42, 43]. It was also observed that with increase in CH₄ content the Nitrogen in the film decreased [40]. Increasing nitrogen content in H₂ + CH₄ plasma showed that with the addition of minute amount of nitrogen (tens of ppm), it is possible to grow (100)-textured films of diamond on Si. With increase in N to 1% the grain size of diamond film decreased significantly. Up-to 3% N, diamond films of cauliflower morphology with rough surface were formed [40]. Also, the growth rate of diamond thin films decreased with increasing N

concentration. At 6% nitrogen small ball-like separated particles were observed. The same affect is observed for 22%N₂. Above 72%N, crystals with a type of hexagonal facets started appearing. At 92% N diamond crystals disappeared. At 98% N₂ uniform coatings of hexagonal crystals of C-Si-N (with high nucleation rate) were observed [41].

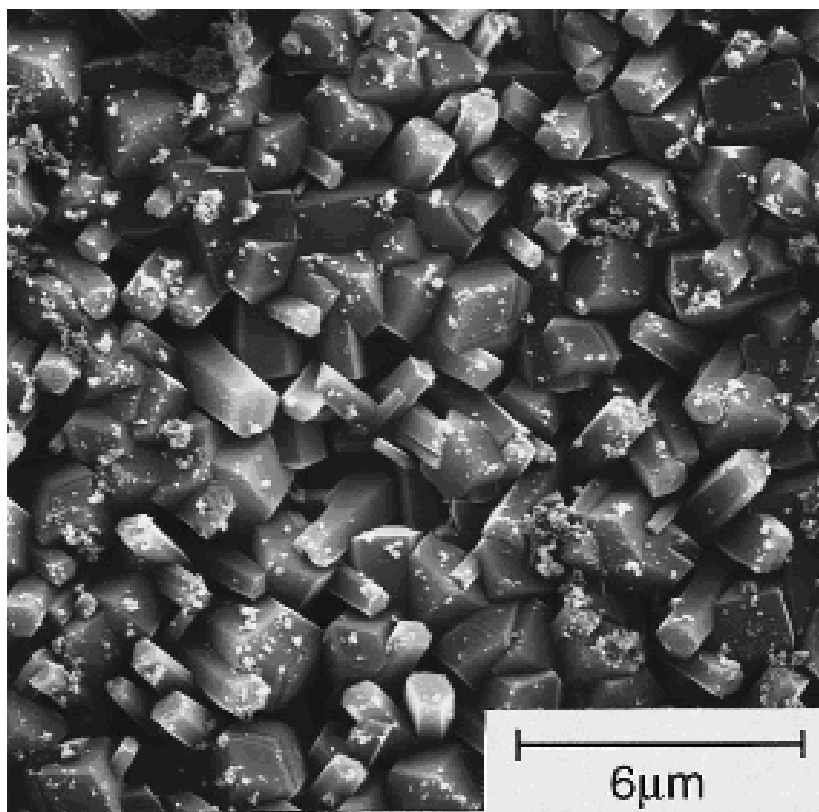


Figure 2.7: Typical SEM image of Hexagonal crystalline Si-C-N film [38]

The addition of H₂ (10sccm) in a N₂ and CH₄ system resulted in a polycrystalline Si-C-N film when deposited for short period (20minutes), and hexagonal crystals of Si₃N₄ were obtained with 6hrs deposition time, indicating that under those conditions Si₃N₄ is more favorably formed. Incorporation of small amounts of N in Ar + CH₄ plasma gave

ultrananocrystalline diamond [39]. Addition of SiH₂ into N₂, H₂ and CH₄ system helped reduce the temperature of deposition of Si-C-N thin films [38].

In the CN_x films obtained by Ion Implantation using C ions with 80 KeV energy and N ions with 90keV energy, it was observed that no C-N bonds were present in the as deposited films. However, annealing of the films at 1000°C for 3 hours in N₂ atmosphere, produced C-N (sp³) bonds in the film [35].

In Pulsed Laser Deposition of CN_x films, carbon is provided by laser ablation of graphite/a-C target [14, 15, 19, 32-34], while N was incorporated by numerous methods such as electron cyclotron resonance microwave plasma (ECR MWP), inductively coupled plasma (ICP), RF plasma, N₂ ion gun etc. (Table 2.2) [17, 18, 32, 33, 45]. Most of the processes mentioned above gave amorphous films with some crystallites embedded in the amorphous matrix.

As seen from the above, precursor gases for CN_x films are supplied separately irrespective of the technique used. It is also observed that carbon sources such as graphite powder, graphite target, amorphous carbon films and CH₄, and Nitrogen sources such as ICP plasma of N₂, ECR MWP of N₂, and N₂ gas can produce films with composition and bonding close to that expected for β-C₃N₄.

2.5 CHARACTERIZATION

Several techniques have been used to characterize CN_x films. The four most important methods, x-ray photoelectron spectroscopy (XPS), X-rays diffraction (XRD), Raman spectroscopy and FTIR spectroscopy are described below.

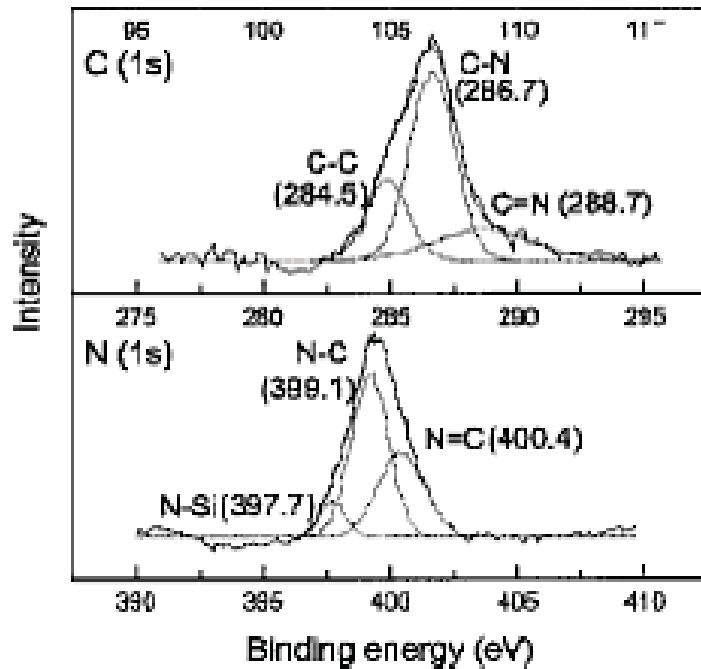


Figure 2.8: XPS spectrum of Si-C-N crystal showing C (1s) and N (1s) core level spectra [37]

2.5.1 X-RAY PHOTOELECTRON SPECTROSCOPY (XPS)

XPS can give accurate estimates of light elements in the surface layer and information on the chemical environment around C and N can be obtained. With XPS we can delineate small binding energy differences occurring in various bonding states between C and N [27]. The spectra of C-1s and N-1s are broad and asymmetric indicative of several overlapping peaks. After deconvolution of C-1s and N-1s spectra into their components, the three bonding states between C and N (C-N, C=N, and C≡N triple bond) can be revealed as shown in Figure

2.8. The N/C ratio in each phase can be calculated from the areas under the fitted Gaussian distributions of XPS peaks divided by their sensitivity factors. Thus, XPS is an important technique to characterize carbon nitride films for their N/C ratio and the bonding states between C and N. Table 2.5 gives some discrepancies observed in the assignment of C-1s and N-1s core level spectra by different authors.

Table 2.5: XPS peaks of different carbon nitride and silicon phases

No.	Spectra	Binding energy Peaks (eV)	Components	References
1.	C-1s	286.1 – 286.9	Sp ³ C-N	[11, 13, 25, 26, 33]
		287.1 – 287.8		[25, 39, 40]
		285.7 – 286.2	Sp ² C-N	[16, 17, 20, 34, 35]
		288.0 – 288.9		[13, 25, 26, 33]
		287.6 – 287.8	Sp C-N	[13, 17]
		289.4 – 288.9	C-O	[34]
		285.3 – 287.7	C-Si	[38]
		284.5	SiCN	[38]
		284.2 – 284.5	Sp ³ C-C	[7, 25, 26, 39, 40]
		284.6	Sp ² C-C	[14, 17]
2.	N-1s	398.1 – 399.08	Sp ³ C-N	[16-18, 20, 23, 24, 34, 35, 48]
		399.8 – 400.82	Sp ² C-N	[30-32, 34, 42, 45, 46, 58]
		397.7 – 397.72	Sp C-N	[17, 36]
		401.5 – 402.3	N-O	[25, 26, 30, 31, 39, 40, 49]
		403.65	N-N	[36]
		395.01	Atomic N	[13]

2.5.2 X-RAY DIFFRACTION (XRD)

Almost all CN films reported in published papers are composed of multiple phases, especially those deposited on substrates that form direct compounds with the precursors, such as Si, Mo, Ta, Ni, SiO₂ and α -SiN_x. Some disagreement in the calculated and experimental data for X-ray of CN_x films are observed. Three major reasons were proposed for this inconsistency [37]: First, there are no standard samples for hypothetical β -C₃N₄, so the calculated spectrum are based on theoretically predicted crystal structures. Secondly X-ray diffraction experiments

were done on thin films rather than on powder in standard diffraction set up. Constraints from thin films, such as texture and preferred orientation, strains, substrate effect, can also contribute to the discrepancies. Third, defects, such as impurity and dislocations, can also contribute to this disagreement by distorting the shape of the lattices. Other than that it is also observed that the diffraction peaks of different phases overlap (for example α - and β - C_3N_4 have almost the same structure and properties and most of the X-ray peaks of α - C_3N_4 overlap with those of β - C_3N_4 as can be seen in Table 2.5) [28]. Also, due to the low mass number of C and N, the intensity of observed XRD spectra from CN_x films is generally very weak owing to the low scattering efficiency of both C and N. Peaks from substrate material for thinner films become dominating in the XRD spectra because of the greater penetration depth of the X-rays in the low scattering material thin CN_x films.

Table 2.5: Some of the overlapping peaks (calculated) of α - and β - C_3N_4 [27, 28].

No.	α - C_3N_4		β - C_3N_4	
	hkl	$d(\text{\AA})$	hkl	$d(\text{\AA})$
1	(100)	0.560	(100)	0.554
2	(110)	3.233	(110)	3.201
3	(200)	2.800	(200)	2.772
4	(102)	2.171	(101)	2.206
5	(210)	2.117	(201)	2.095
6	(211)	1.931	(111)	1.922

It is observed that β - Si_3N_4 dominates near the interface between the film and the substrate in films deposited on Si [28]. As the film gets thicker the area near the surface gets richer in C_3N_4 , however the effect of the substrate and the interlayer is still present if the penetration depth of the X-rays is greater than the thickness of the C_3N_4 films [9, 31]. XRD spectrum were also used to calculate the lattice parameters. Lattice parameters calculated [33] from one such

XRD spectrum are, $a = 6.38\text{\AA}$ and $c = 4.648\text{\AA}$ for $\alpha\text{-C}_3\text{N}_4$ and $a = 6.24\text{\AA}$ and $c = 2.36\text{\AA}$ for $\beta\text{-C}_3\text{N}_4$.

2.5.3 FURRIER TRANSFORM INFRARED SPECTROSCOPY (FTIR)

FTIR is used to study the vibration modes of carbon nitride films. The vibrations of D and G bands of carbon network are generally not observed in infrared spectrum. However, addition of nitrogen in the carbon network breaks the carbon symmetry making the carbon-nitrogen structure IR-active [15]. The common IR peaks observed for films prepared by MPECVD are given in Table 2.6.

Table 2.6: FTIR peaks assigned to various phases of carbon nitride and silicon nitride.

No.	Phase	FTIR peaks	References
1.	$\beta\text{-C}_3\text{N}_4$	573 – 888 cm^{-1}	[19, 23]
		1000 – 1400 cm^{-1}	[15, 17, 26, 34]
2.	$\alpha\text{-C}_3\text{N}_4$	449 – 1464 cm^{-1}	[16]
3.	Si_3N_4	850 – 1200 cm^{-1}	[31]
4.	C=N	1500 – 1700 cm^{-1}	[23, 25, 35, 47]
5.	C≡N	2100 – 2200 cm^{-1}	[23, 25, 35]

2.5.4 Raman Spectroscopy

Table 2.7 below lists the calculated Raman shift peaks for beta carbon nitride and the observed peaks for beta silicon nitride. As can be seen from the table the peaks for the two compounds are very close to each other. Since Si helps in stabilizing the crystalline CN_x phase, formation of some silicon nitride or silicon carbide is unavoidable. The presence of the two types of nitride with similar crystal structure causes overlapping of the peaks in a Raman spectra making it difficult to quantify the % CN in the thin films. Table 2.7 shows the characteristic Raman peaks for $\beta\text{-C}_3\text{N}_4$ and $\beta\text{-Si}_3\text{N}_4$ for comparison.

Table 2.7: characteristic Raman peaks for β -C₃N₄ and β -Si₃N₄ [16, 27].

β -C ₃ N ₄ ^{19,30} (cm ⁻¹)	β -Si ₃ N ₄ (cm ⁻¹)
206	210
266	229
300	--
327	451
645	619
672	732
885	865
1048	939
1237	1047
1327	--
1343	--
1497	--

2.6 SUMMARY OF LITERATURE REVIEW ON CARBON NITRIDE

Synthesis of C₃N₄ phase with nitrogen content of 57% and in bulk amount remains unsubstantiated for demonstrating its unique properties. Although MPCVD and PLD techniques have shown promising results, with nitrogen content up-to 53%, synthesis of β -C₃N₄ films with nitrogen content of 57% is still a challenge. From the discussion above the following can be concluded for research in deposition of crystalline thin films of carbon and nitrogen:

- 1.6.1. Hydrogen should be avoided in order to prevent the escape of N as HCN.
- 1.6.2. Si helps in stabilizing the CN_x structure, and therefore some Si incorporation in the CN_x thin films is essential.

- 1.6.3. Deposition temperature should be controlled such that Si diffusion (from Si substrate) in the growing film is limited to such levels that help stabilize the CN_x structure and not result in deposition of Silicon Nitride thin film.
- 1.6.4. Carbon and Nitrogen precursor flow rates don't follow the stoichiometric ratio. Nitrogen precursor in much higher volume than carbon precursor is needed for appreciable incorporation of N in the CN_x thin films.
- 1.6.5. XPS, XRD, Raman and FTIR have been most successfully employed for the characterization of CN_x films.

2.7 SUGGESTIONS FOR FUTURE RESEARCH:

- 2.7.1** Experiments with minimum hydrogen in the precursor gases should be attempted. With reduction in the hydrogen content in the precursor gases the chances of losing nitrogen as HCN species are reduced. Thus more nitrogen is available for deposition of CN_x films.
- 2.7.2** MPECVD experiments using N + CH₄ plasma, run for longer deposition period should be tried with higher power (for high chemical activity), so as to have a thicker film with less amount of silicon in the top layers.
- 2.7.3** Higher temperature (800-1000°C) with higher plasma energies (900-1200W) and addition of elements like Si, B etc., that can help in stabilizing the crystallinity of the CN_x thin film can be explored. Under the conditions of high temperature and power CN radicals important for the deposition of CN_x films, have high mobility and the films formed can be stabilized.

CHAPTER 3

OBJECTIVES AND RESEARCH PLAN

The major objectives of this part of the research include:

1. Using MPCVD technique, study the effect of Nitrogen addition to diamond thin film deposition conditions.
2. Optimize conditions for and, study the effect of, deposition parameters on synthesis of crystalline Si-C-N thin films on Si substrate
3. Explore the influence of deposition time on Si-C-N thin films assuming that with increasing deposition time diffusion of Si in the top layers of the depositing film would decrease resulting in almost phase pure β -C₃N₄ at the surface.

Synthesis of diamond thin films by MPECVD is a well established technique. Since CH₄ is the common precursor for diamond and CN_x thin films, conditions suitable for diamond deposition were used as the starting point for the synthesis of CN_x thin films. Nitrogen was systematically added to the CH₄+H₂ plasma and the films deposited were characterized for carbon nitride.

In the second step, results from nitrogen-addition-to-diamond-deposition-condition experiments were used to establish conditions for further experiments towards synthesis of carbon nitride thin films. Si substrate was used with the knowledge that Si diffusion in the growing CN_x thin film helps in stabilizing the C₃N₄ structure. Since β -C₃N₄ and β -Si₃N₄ have the same crystal structure, the hypothesis is that a base structure of β -Si₃N₄ formed as interfacial layer should facilitate the growth of β -C₃N₄. With increase in film thickness with

increasing deposition time the Si diffusion in the films should decrease and eventually result in almost phase pure β -C₃N₄ as the top layer of the thin film.

CHAPTER 4

EXPERIMENTAL

The ASTEX microwave plasma enhanced chemical vapor deposition system described in Part I was used for the synthesis of carbon nitride thin films. Semiconductor grade CH₄ (99.9%), N₂ (99.999%), H₂ (99.999%) and Ar (99.9%) were used as precursor gases. Si (100) wafers of 0.5mm thickness were used as substrates.

4.1 Substrate Preparation

Si (100) wafers were cut into 10mm x 10mm squares pieces so that 4 such pieces could be placed below the plasma. The plasma ball varies in size from 1 inch to 2 inches depending on the deposition conditions being used. Using 10 x 10mm square pieces establishes uniform coverage of the substrates by the plasma and helps in deposition of thin films on substrates with different pre-treatments.

Si (100) substrates were first cleaned with Acetone to remove oil and other carbohydrates if present on the surface. The substrates were then cleaned with Ethyl alcohol and di-ionized water to remove any acetone remains from the surface. After cleaning with DI water the substrates were immersed in 2% HF solution for 5 minutes to etch native oxygen from the surface.

The cleaned and HF treated Si substrates were immediately transferred to an ultrasonic bath containing 20-40 μ m diamond slurry for Nitrogen-addition-to-diamond-deposition-conditions experiments. Ultrasonic activation in diamond slurry was performed for 2 hours to

activate the Si substrate surface for diamond nucleation. For all other experiments no additional treatment was given to the Si substrates before placing them in the plasma chamber.

The substrates after pre-treatment with just 2%HF or ultrasonic activation, were cleaned with ethyl alcohol and DI water, and dried with dry Nitrogen. The substrates were then immediately transferred to the plasma chamber where they were placed on a 1 mm thick Molybdenum disc that seated directly on the inductively heated hot stage. Before starting each experiment the substrates were given H₂ plasma treatment for 10 minutes to remove any native oxide layer that might have been formed between the time the substrate was cleaned and the plasma started.

4.2 Deposition conditions

After loading the samples, the plasma chamber is pre-evacuated to 10⁻⁶ Torr at 350°C. Hydrogen is then introduced in the chamber and a pressure of around 10 Torr stabilized using throttle valve. Microwave power of around 350W is then employed to start the plasma. Once stable plasma is established precursor gases and other parameters are set as per the deposition conditions.

Synthesis of diamond thin films by MPECVD is a well established technique, and therefore effect of nitrogen addition to the 1% CH₄ + H₂ plasma, for diamond deposition, was used as the first step towards synthesis of β-C₃N₄ thin films. Nitrogen flow rates of 0.6, 1.0, 1.5, 2.0, 5.0 and 10.0 sccm were used. Effect of systematic increase in N₂ gas to the CH₄ + H₂ plasma was studied with respect to carbon nitride thin films in this part of the study. Table 4.1 gives the experimental conditions used:

Table 4.1: Process parameters for N₂ addition in 1%CH₄ + H₂ plasma used for diamond deposition by MPECVD

Substrate	Si (100)
Gas Flow Rate	Net 100 sccm
CH ₄	1 sccm
N ₂	0.6 – 10 sccm
H ₂	Remainder
Pressure	30 Torr
Power	900W
Substrate Temperature	750°C
Growth Time	8 Hrs

In the second step towards synthesis of β -C₃N₄, thin films results from the first step were used to decide deposition conditions for further experiments. A large variation of precursor gas flow rates, deposition pressure, microwave power and substrate temperature were studied. Table 4.2 gives a global view of the conditions used.

Table 4.2: Process parameters for the synthesis of CN_x thin films by MPECVD

Substrate	Si (100)
N ₂	10 – 50 sccm
CH ₄	1 – 10 sccm
H ₂	90 – 40 sccm
Pr	12 – 95 Torr
W	750 – 1200 Watts
Sub. Temp.	750 – 900°C

4.3 Characterization Techniques

The thin films were characterized using optical microscope, scanning electron microscope (SEM), energy dispersive spectroscopy (EDS), X-ray diffraction (XRD) and,

Raman spectroscopy. The results obtained were correlated with the deposition conditions and an understanding of the growth mechanism was established.

CHAPTER 5

RESULTS AND DISCUSSION OF CARBON NITRIDE THIN FILMS

DEPOSITED BY MPECVD

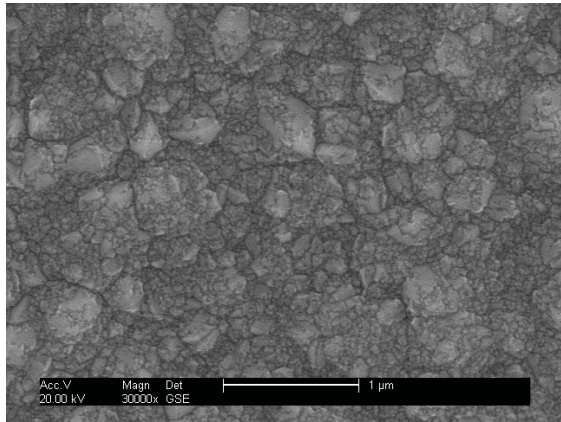
Thin films deposited in the first set of experiments involving systematic increase in Nitrogen percentage to the Methane plus Hydrogen plasma conditions suitable for diamond deposition were characterized using SEM and XRD.

5.1 Effect of Nitrogen Addition to Diamond Thin Film Deposition Conditions

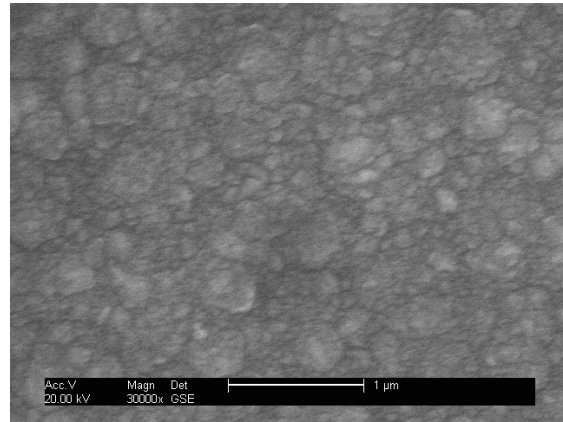
The aim of this part of the research was to exploit the well established knowledge of deposition of diamond thin films as the starting point for the synthesis of CN_x thin films. The hypothesis is that with gradual increase in Nitrogen gas to the diamond deposition conditions the diamond in the thin films will decrease and would get replaced by CN_x thin films.

Experiments in this part of the research were performed using conditions given in Table 4.1 of Part I of this thesis. Thin films deposited with increasing Nitrogen addition to diamond deposition conditions were characterized using SEM and XRD for morphology and phase analysis.

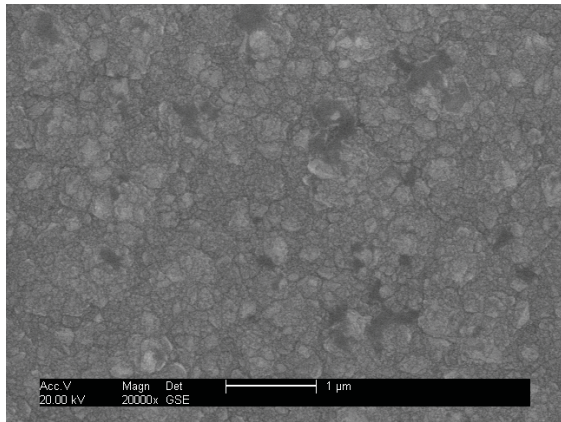
5.1.1 Morphology Analysis Scanning Electron Microscopy



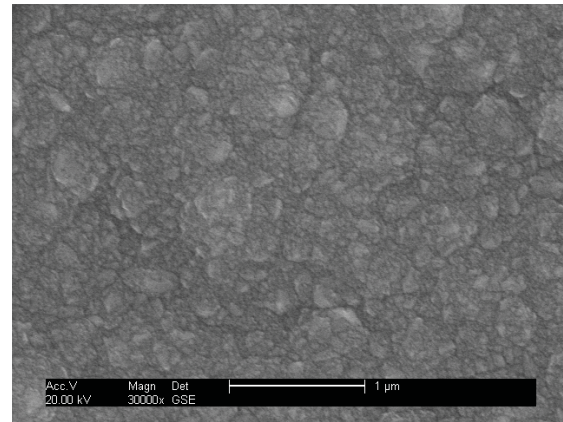
0.6%N₂ 1.0% CH₄ 98.4% H₂



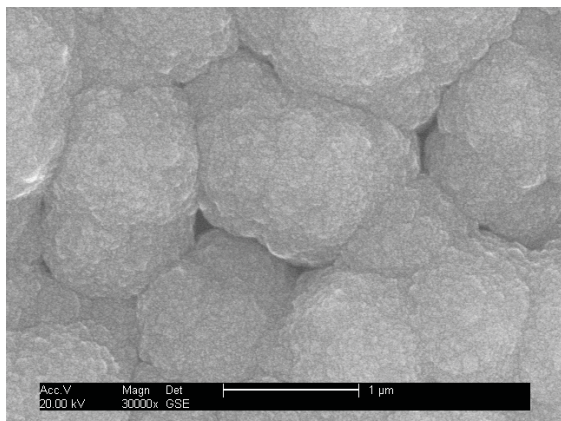
1.0%N₂ 1.0% CH₄ 98.0% H₂



1.5% N₂ 1.0% CH₄ 97.5% H₂



2.0 %N₂ 1.0% CH₄ 97.0% H₂



5.0 % N₂ 1.0% CH₄ 94.0% H₂

Figure 5.1: SEM micrographs showing changes observed in the morphology of diamond thin films with increase in Nitrogen addition to the diamond deposition conditions

From SEM investigation it is observed that even at 0.6% N₂ addition to the precursor gases diamond structure starts getting distorted. Instead of big micron size smooth and well faceted diamond crystals rough grains of much smaller sizes are observed. This is because N in diamond structure breaks the uniformity of the zinc-blend structure preventing the growth of diamond nuclei into a smooth well faceted micron size crystal. Similar degrading effect is observed for film deposited with higher percentages of N up-to 5%. The diamond structure becomes more and more distorted and the nano-sized diamond crystals start to agglomerate to form cauliflower type grains. With further increase in Nitrogen percent (10% and above) non-uniform /no thin films were deposited.

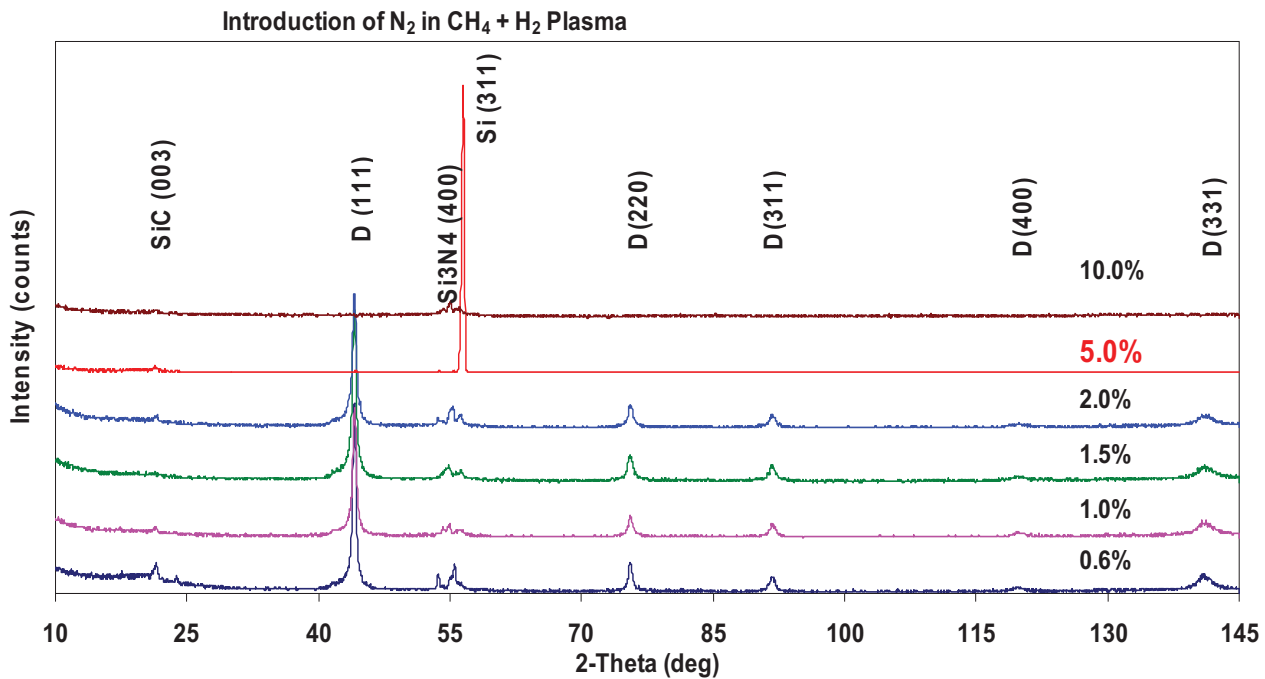


Figure 5.2: XRD data showing effect of increasing N₂ in 1%CH₄+H₂ plasma on quality of diamond thin films.

5.1.2 Phase Identification by X-Ray Diffraction

X-ray diffraction patterns (Figure 5.2) of the deposited films reveal that diamond is formed for nitrogen flow rates below 5%. Which suggests that in the deposition of CN_x thin films to avoid diamond deposition Nitrogen flow rates in excess of 5% should be used. Under conditions of further increase in N addition to 1% $CH_4 + H_2$ plasma non-uniform films were deposited. Which suggested that under the deposition conditions any solid phase that forms during deposition was getting etched away. Since in the employed plasma chemistry carbon is the main element that can deposit as a solid phase it can be construed that higher flow rates of CH_4 are needed to get any deposit under the high nitrogen deposition conditions. Further experiments were therefore performed as per conditions in Table 4.2 with higher N_2 and CH_4 flow rates.

5.2 Synthesis of CN_x Thin Films

In the second set of experiments thin films deposited employing conditions in Table 4.2 of Part II, were characterized using optical microscopy, SEM, EDS, and Raman spectroscopy. As realized from the nitrogen addition experiments to diamond deposition conditions, higher percentages of CH_4 were used for the synthesis of CN_x thin films. The effect of variation in deposition conditions was established to optimize the synthesis process. Optical emission spectroscopy and quadrupole mass spectroscopy were used to study the plasma chemistry.

5.2.1 Surface Morphology Study by Optical Microscopy

Optical microscopic examination (Figure 5.3) of thin films deposited using conditions from Table 4.2 of Part II showed two different morphologies, rod like crystals (RLCs) and spheroids as shown in Figure 5.3(a).

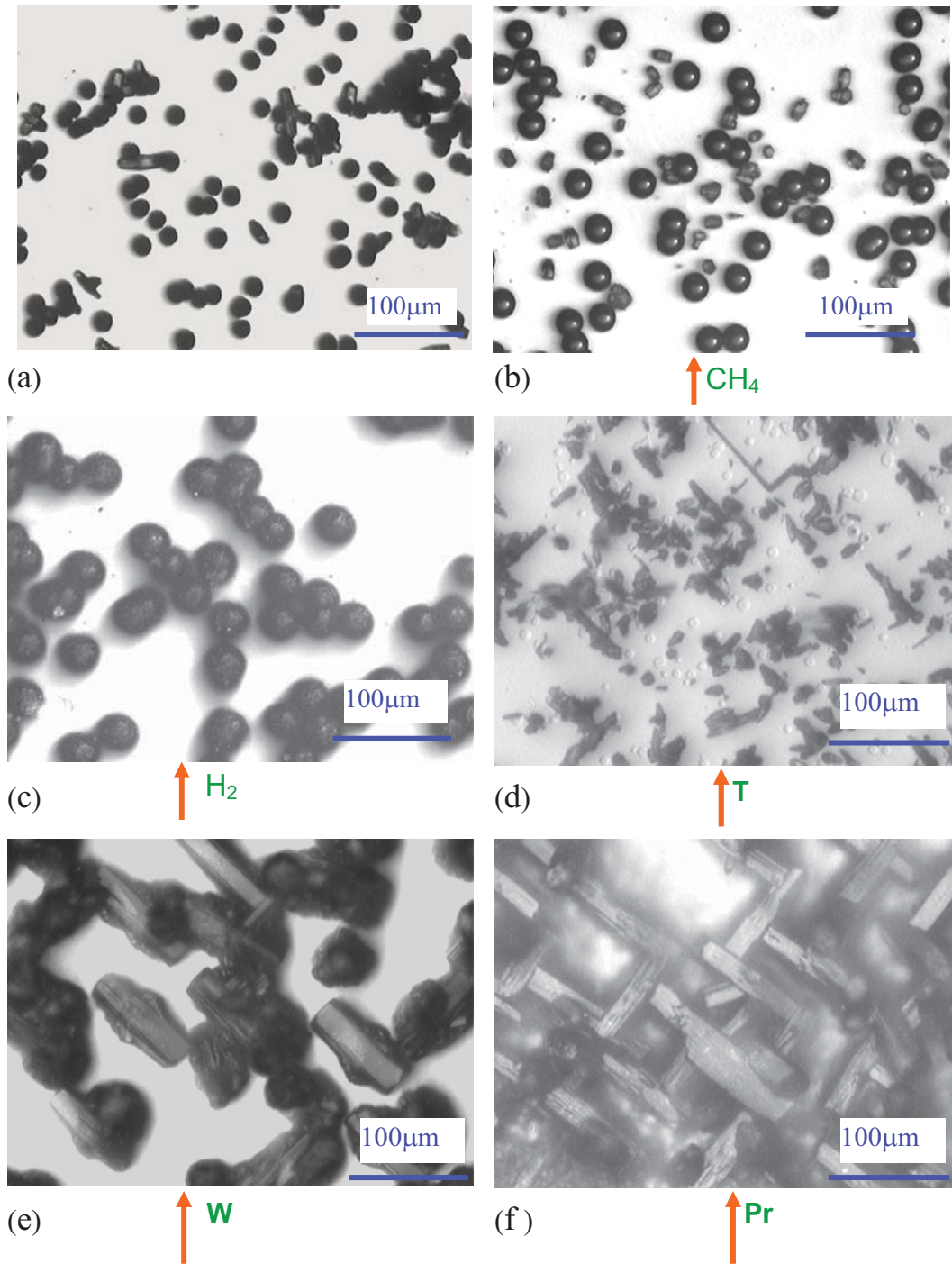


Figure 5.3: Effect of variation of process parameters on the type and morphology of CN_x thin films. (a) The two morphologies observed, (b-f) effect of increasing (b) CH₄, (c) H₂, (d) substrate temperature, (e) microwave power and (f) deposition pressure.

It was observed that increasing methane and hydrogen in the plasma increased the quantity and size of the spheroids, respectively, in the films. Increasing temperature increased the amount of RLCs, increasing pressure and power helped in increasing the size of these RLCs reaching over 100 μ m. Figures 5.3b – f show the effect of increasing CH₄, H₂, temperature, power and pressure, on spheroids and RLCs.

Further control over the morphology of the CN_x films is achieved by controlling the sequence of introduction of the precursor gases. It was realized that after stabilizing all other deposition parameters if CH₄ is introduced first into the deposition chamber the synthesized film is composed mainly of spheroid, and when N₂ is introduced first mostly RLCs get deposited on the Si substrate. In Table 5.1 and Figure 5.4 below it is shown that under low pressure conditions, when N₂ is introduced first RLCs with some spheroids are deposited. When CH₄ is used as the first precursor gas under low pressure condition, mostly spheroids get deposited. With increase in pressure the size and quantity of RLCs increases. Almost no spheroids are observed when N₂ is used as the first precursor gas under higher pressure conditions. For thin films with methane as the first precursor gas under higher pressure conditions the quantity of spheroids increases.

Table 5.1: Effect of first precursor gas and pressure on the morphology of the CN_x thin films deposited.

Exp. No.	Starting gas	Pressure (Torr)	Power (W)	Time (hrs)	Temp (C)	N₂ (sccm)	CH₄ (sccm)
1	N ₂	13	900	8	900	10	8
2	CH ₄	13	900	8	900	10	8
3	N ₂	30	900	8	900	10	8
4	CH ₄	30	900	8	900	10	8

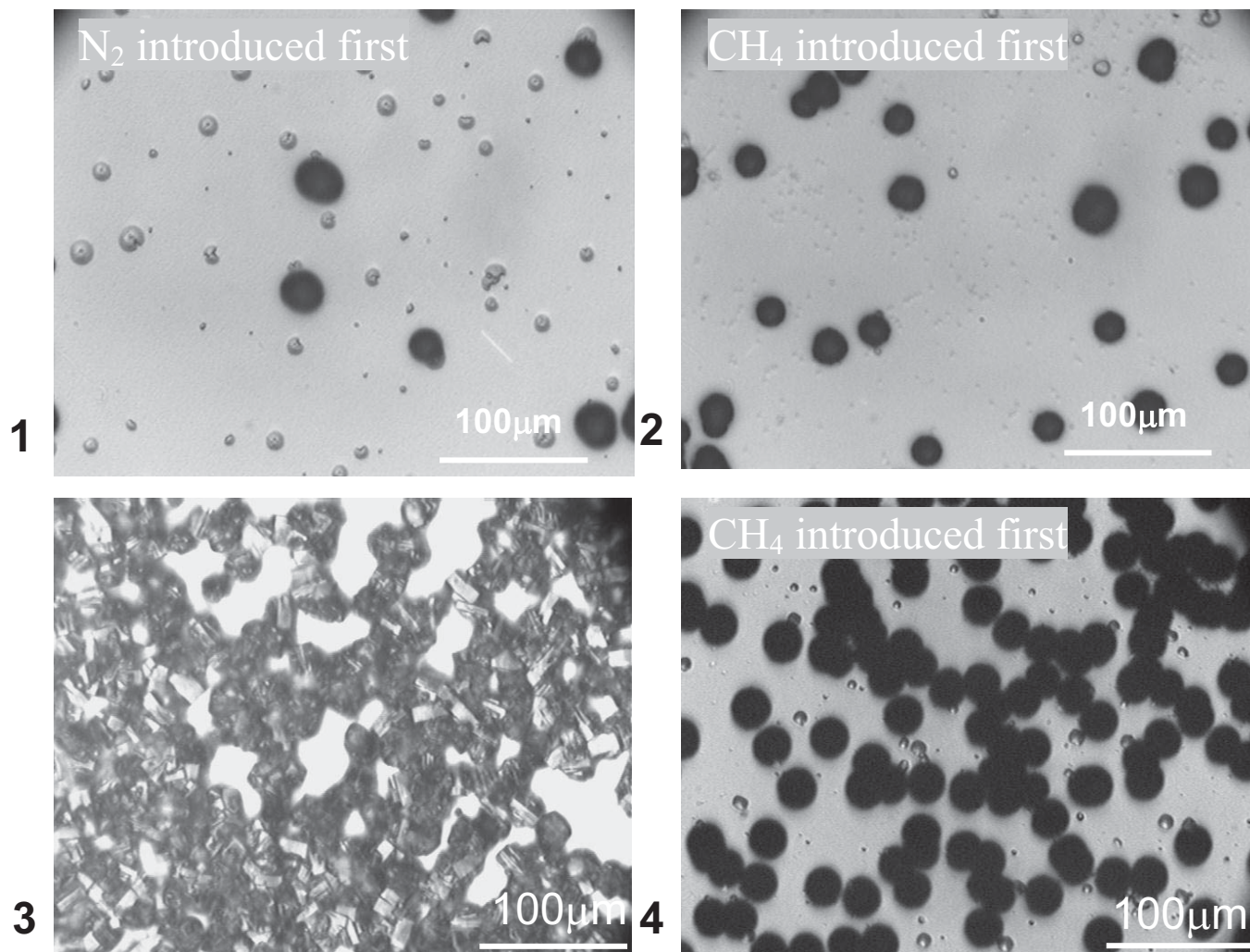


Figure 5.4 Effect of sequence of introduction of precursor gases and deposition pressure on the morphology of the CN_x thin films.

5.2.2 SEM, EDS and Raman spectroscopic Investigation of CN_x Thin Films by MPECVD

SEM and EDS investigation of the films, Figure 5.5 and Table 5.2, respectively, show that the spheroids are agglomerated nano-meter sized needles of C, Si and N, while the RLCs are micro-meter sized well crystallized hexagonal crystals of N, C and Si.

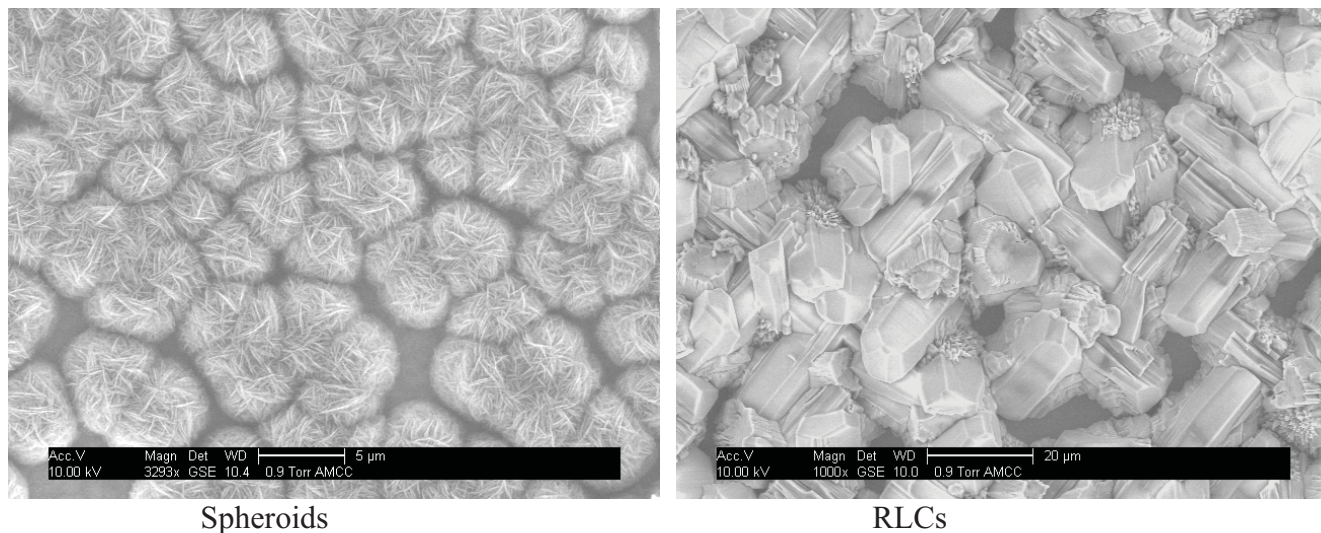


Figure 5.5. SEM micrographs show that the spheroids are agglomerates of nanometer sized needles while the RLCs have a well defined crystalline morphology.

Table 5.2: Quantitative EDS data observed for Spheroids and RLCs.

Elements		Spheroid	RLC
Atomic %	C	92.62	18.2
	N	2.82	73.11
	Si	4.56	8.69
Weight %	C	86.90	14.7
	N	3.08	68.88
	Si	10.01	16.41

Raman spectrum of spheroids, Figure 5.6, shows two peak around 1350cm^{-1} and 1550cm^{-1} representing disordered and ordered vibrational modes of graphite. This confirms that the needles in the spheroids are graphitic with some Si and N incorporated in them, as observed from EDS spectra. Raman spectra of the RLCs show clear peaks around 260cm^{-1} and 880cm^{-1} that match closely to the calculated peaks for $\beta\text{-C}_3\text{N}_4$ and $\alpha\text{-C}_3\text{N}_4$, respectively. Also observed are the Si and $\beta\text{-Si}_3\text{N}_4$ [16, 27] peaks at 520cm^{-1} and 930cm^{-1} , respectively. The presence of $\beta\text{-Si}_3\text{N}_4$ peaks confirms the diffusion of Si and formation of Si_3N_4 in the thin films. According to Gu et al. [37] the diffusion of Si helps in stabilizing the C_3N_4 network.

Raman spectra for N-C-Si crystals (RLCs) and C-Si-N agglomerated needles (spheroids)

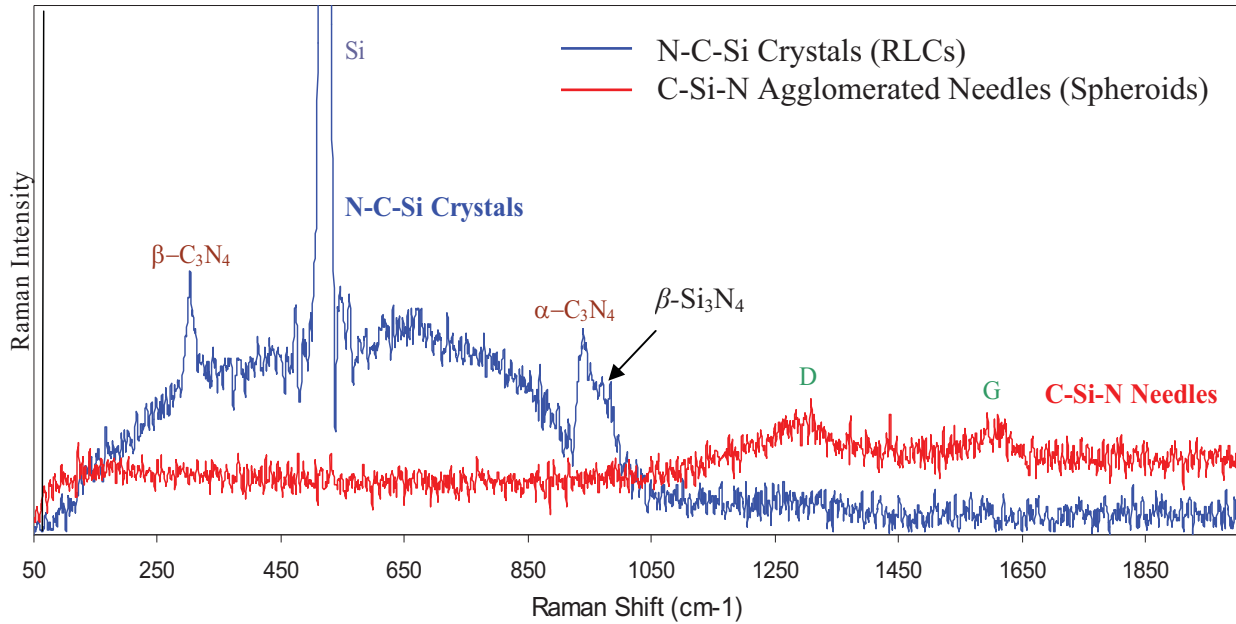


Figure 5.6: Raman spectra for N-C-Si crystals (RLCs) and C-Si-N agglomerated needles (spheroids)

Amorphous CN_x films formed when deposition was done on a pure Pt substrate. However, when Si impurity was added to the Pt substrate, crystalline CN_x could be obtained, emphasizing the role of Si in stabilizing the crystalline structure.

It is proposed that when N_2 is introduced first, under the conditions of high temperature, N with electronegativity of 3 reacts easily with Si, electronegativity of 2, to form covalent Si-N bonds [30]. When CH_4 is introduced to the plasma already containing N_2 , CN^\cdot radicals that get generated in the plasma impinge on Si-N surface instead of Si substrate surface. Carbon, with electronegativity of 2.4, from the CN^\cdot radical bonds with N or Si, while N from CN^\cdot radical bonds with Si, if available, or adjacent C atom to form covalently bonded Si-C-N rod like crystals. According to Wu et al. [30] the growth rate ratio between Si-N and Si-C-N is around 21/1 which explains the high N and Si content in the crystals.

For the experiments with CH₄ as the first precursor gas, as is well known for diamond deposition [42] that SiC layer is formed between Si substrate and diamond thin film when depositing diamond on Si substrates using MPECVD technique. It is also well known that a lot of graphite is deposited along with diamond when the CH₄ percent in the plasma is increased above 2% for diamond deposition. In our experiments when CH₄ is introduced first in the plasma, because of its high percentage, a large amount of graphite gets deposited. Under the deposition conditions used there is not enough H₂ available to etch the graphite that gets deposited. Thus, the formation of Si-C bonds is hindered or limited. When N is introduced in the plasma chamber, CN' radicals that get generated within the plasma impinge on the graphite covered Si surface. C from the CN' radicals combines with graphite to form more graphite, while N from CN' radical either combines with N from the plasma and escapes as N₂, combines with C to form CN_x or combines with diffused Si to form Si-N bond. The low amount of N observed in C-Si-N needles from EDS suggests that most of the N from the depositing CN' radicals re-attaches with other N ions from plasma and escapes as N₂ molecule.

5.2.3 Plasma Analysis by OES and QMS

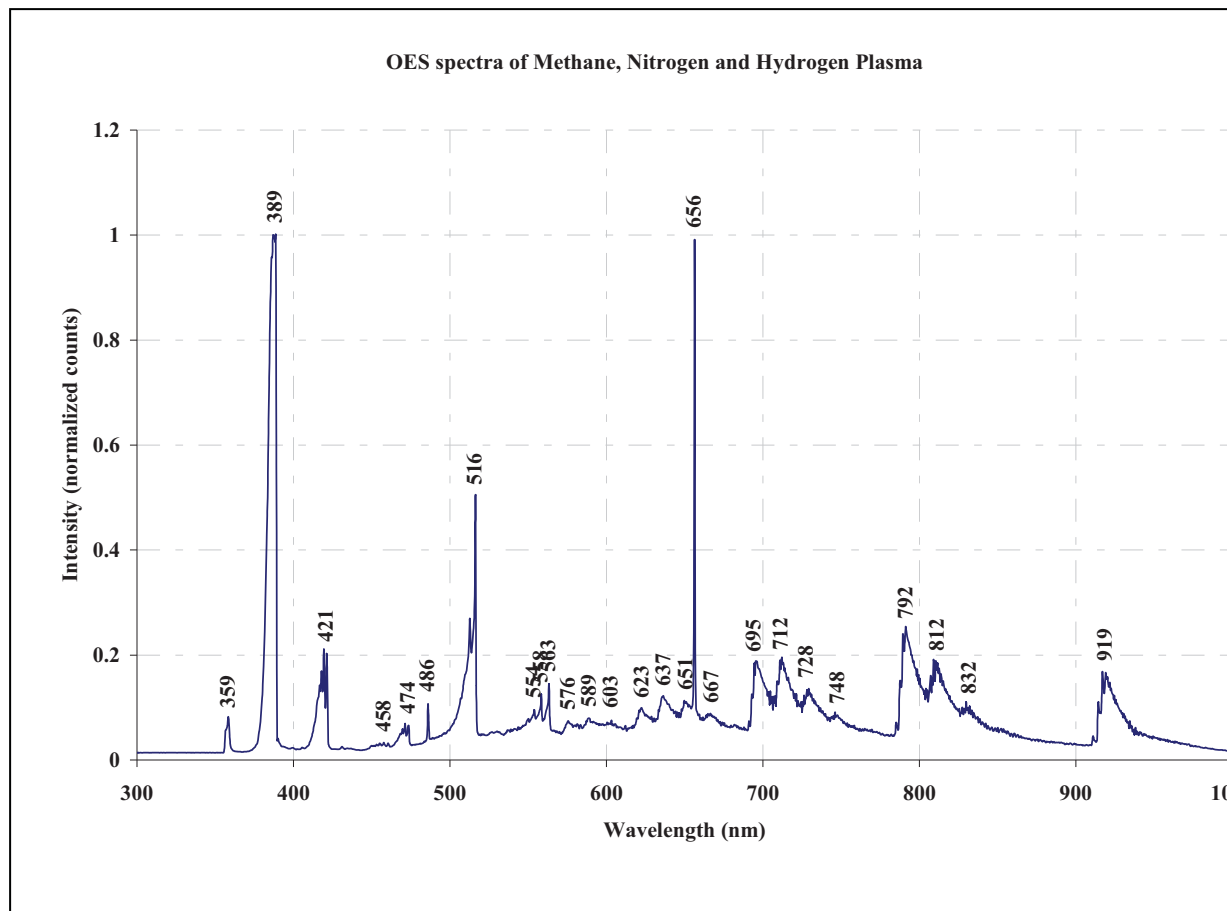


Figure 5.7 OES spectra of methane, hydrogen and nitrogen plasma

OES spectra of the methane, hydrogen and nitrogen plasma is dominated by broad and structured emission peaks of Nitrogen molecules. Emission from CN radicals generated in the plasma and, H atom and H₂ (Fulcher band) are also observed. Figure 5.7 shows typical optical emission spectra observed for plasma containing hydrogen, methane and nitrogen gas. Table 5.7 lists the emission peaks observed at different wavelengths and their corresponding emission sources.

Table 5.3: Observed OES peaks and their excitation source for hydrogen, methane and nitrogen plasma

OES Peaks Wavelength (nm)	Excitation Source
359	CN
389	CN/First negative series N_2^+
421	CN/SiN/ First negative series N_2^+
458	First negative series N_2^+
468	H_2 / First negative series N_2^+
516	First negative series N_2^+
554	First negative series N_2^+
558	First negative series N_2^+
576	N/ H_2 Fulcher band
583	H/Second positive series N_2
589	N/ H_2 Fulcher band
603	H_2 Fulcher band
623	H_2 Fulcher band
637	Second positive series N_2
651	H alpha
667	N
695	CN
712	CN
728	N
748	Second positive series N_2
792	Second positive series N_2
812	Second positive series N_2
832	Second positive series N_2
919	Second positive series N_2

From Table 5.3 it is observed that the methane, nitrogen and hydrogen plasma employed for the synthesis of CN_x thin films contains active CN^{\cdot} radicals that are thought to be the building blocks of CN_x thin films. These CN^{\cdot} radicals when in contact with the Si substrate at the deposition temperature, form bonds with the Si surface to form Si-N-C layer. The crystallinity of the film deposited then depends on the way further bonds are created between depositing CN radicals and the Si-N-C layer.

Complimentary study of the plasma by QMS confirms the dissociation of the precursor gases and formation of growth radicals like C and CN within the plasma that contributes to

film deposition. Figure 5.8 shows QMS spectra of the plasma showing formation C, CN and NH species within the plasma. The NH species is not seen in OES, probably because of domination of the broad peaks of N₂ molecules. Formation of CH and NH species helps in the deposition process on the surface of the depositing film. Hydrogen from both the species act as dangling bonds and help in bonding of the incoming species with the atoms on the top surface of the thin films. In the process hydrogen atoms are removed as hydrogen molecules.

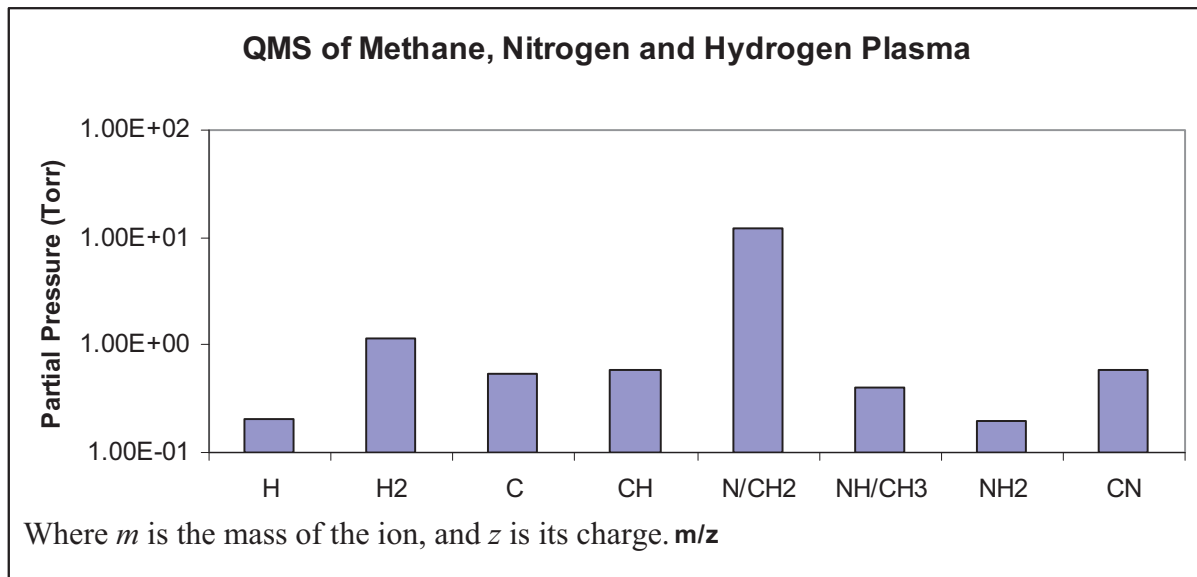


Figure 5.8: Static mode QMS spectra of methane, nitrogen and hydrogen plasma showing different species formed and their partial pressures within the plasma.

It was thought that with longer deposition time thicker films with lower and lower Si diffusion in the films would finally result in almost phase pure β -C₃N₄ thin films. However, no such results were obtained with increased time in this study, and therefore no further research was performed on this topic. We however are the first to report the dependence of the morphology of the deposited Si incorporated CN_x thin films on the sequence of introduction of precursor gases. In a recent paper hardness of Si incorporated carbon nitride was calculated using microscopic model for hardness combined with the first principal calculations [53]. It

was revealed that both α and β - Si-C-N can reach hardness of up to 57-61GPa and are therefore novel super-hard materials. Because of the comparative properties of Si-C-N thin films attention in recent years have shifted from synthesis of CN_x thin films to Si-C-N thin films. Bhattacharya et al. [42] deposited Si-CN thin films by RF magnetron sputtering on industrially important substrate materials such as silicon wafers, borosilicate glasses and stainless steel, and reported a hardness of 17GPa for films deposited on stainless steel substrate. Tomasella et al. [43] deposited amorphous Si-C-N thin films with different nitrogen percent by reactive sputtering. They demonstrated that SiCN can be prepared as a photoelectron material whose band gap can be tailored between 2.9 and 5.0eV by controlling the nitrogen content of the amorphous film.

CHAPTER 6

CONCLUSION AND RECOMMENDATION FOR FUTURE WORK

Conclusions

1. Microwave plasma enhanced chemical vapor deposition technique can be successfully used for deposition of Si incorporated thin films of carbon and nitrogen.
2. Morphology of the Si-incorporated thin films can be effectively controlled in the MPECVD system by controlling the deposition temperature, deposition pressure and the sequence of introduction of the precursor gases.
3. Dependence of the type of film on the sequence of introduction of precursor gases is reported for the first time. Agglomerates of graphitic C-Si-N needles are formed when CH₄ is used as the first precursor gas, while micron size N-C-Si hexagonal crystals are formed when N₂ is added as the first precursor gas in the deposition chamber.

Recommendation for Future Work

1. Research on thin films of N-C-Si rod like crystal, should be continued with the emphasis on growing uniform thin films of the crystals in order to explore interesting properties that the material may offer.
2. Nitrogen precursor gas as the first gas to be introduced in the deposition chamber should be used under high pressure and power conditions. This will help in

establishing a good Silicon nitride interfacial layer for the deposition of well crystallized N-C-Si thin films.

PART III:
DEPOSITION OF CUBIC BORON NITRIDE THIN FILMS BY MPECVD

CHAPTER 1
INTRODUCTION

Boron-Carbon-Nitrogen ternary system consists of another interesting material that rivals the properties of diamond. This zinc-blend crystal structure made of equal atoms of boron and nitrogen is called cubic boron nitride (*c*-BN). It is the second hardest material after diamond, is optically transparent over a large spectral range from UV to visible [29], has wide band gap (6.1 – 6.4eV), can be more easily doped with both n- and p-type [43-45] impurities than diamond, and is stable in contact with Fe, C, and Ni in air at elevated temperatures. These properties make *c*-BN the most promising material for laser optics, high temperature high speed electronic and for applications in machining of ferrous and nickel based materials.

Like diamond and carbon nitride, boron nitride exists in more than one type of bonding configuration. The allotropes of BN include hexagonal boron nitride (*h*-BN), rhombohedral boron nitride (*r*-BN), wurtzitic boron nitride (*w*-BN), turbo-static boron nitride (*t*-BN) and cubic boron nitride (*c*-BN). While *r*-BN is basically *h*-BN with a slight variation in stacking of individual layers, *w*-BN is distorted *c*-BN and, *t*-BN, which is mostly observed in low pressure synthesized BN thin films, is a preferentially oriented BN layer that forms below the *c*-BN layer.

Synthesis of Cubic Boron Nitride (*c*-BN) thin films has been a challenge since the successful synthesis of bulk *c*-BN by Wentroff, using high temperature high pressure technique in the presence of a suitable catalyst, in 1957 [44], [54-58]. MPCVD, Pulsed Laser Deposition and Magnetron Sputtering are few of the thin film deposition techniques that have shown some success in *c*-BN thin film deposition over the last few years [3, 42, 59-66]. Unlike diamond and beta-carbon nitride, *c*-BN is not a metastable material. It is thermodynamically more stable than hexagonal BN (*h*-BN). However, in all the thin film synthesis techniques *h*-BN gets synthesized first and more easily than *c*-BN. Thus the techniques adopted to deposit *c*-BN mainly involved converting *h*-BN into *c*-BN by using high energy ion-bombardment. Use of high energy ion-bombardment resulted in high stress in the deposited thin film that restrict the thickness of the films to less than a micron with thicker films peeling off under the influence of high stress.

Klass et al. [45] discovered that fluorine can etch *h*-BN faster than *c*-BN in a plasma environment. Deposition of thick *c*-BN thin films aided by Fluorine is reported by only a few authors in the recent years [62, 65-70] and therefore the field of exploration of structure and properties of *c*-BN thin films deposited under different conditions is still wide open. In this part of the dissertation, attempt is made to synthesize *c*-BN thin films on Si and diamond coated Si substrates by MPECVD. Both normal mode (10 – 100Torr) and electron-cyclotron resonance mode (10^{-3} Torr) of the system, discussed in Part I, were used to investigate the possibility of *c*-BN thin film synthesis by our MPECVD system.

The synthesized thin films were characterized using SEM, FTIR, and Raman spectroscopy. The results obtained were correlated with the deposition conditions to optimize the deposition parameters. OES and QMS were used to analyze the deposition plasma.

CHAPTER 2

LITERATURE REVIEW

2.1 Structure of Boron Nitride

Boron nitride is a synthetic polymorphic material with stable and metastable allotropes. The stable forms of BN include amorphous (*a*-BN), turbostratic (*t*-BN), hexagonal (*h*-BN) and cubic boron nitride (*c*-BN), while the metastable kinds include wurtzitic (*w*-BN) and rhombohedral boron nitride (*r*-BN). Amorphous boron nitride is a phase with no set long range order with hexagonal layers of BN placed randomly over each other. In *t*-BN while the two-dimensional in-plane order of the hexagonal basal plane is maintained over long range, the planes are stacked in random sequences with varied rotations about the *c*-axis. The *t*-BN structure also shows extensive lattice curvature and has 15% higher inter-planar spacing than *h*-BN [44].

The four main forms of BN are shown in Figure 2.1. Hexagonal BN is very similar to graphite with sp^2 bonded structure consisting of two-dimensional hexagonal (0002) rings with alternate boron and nitrogen atoms stacked in an A \bar{A} A \bar{A} ... sequence. The only difference between the graphite and *h*-BN structure is that the basal planes of *h*-BN are rotated by 180° between alternate layers, such that the nitrogen atom from one basal plane connects with B atom of the next basal plane stacked directly over/below the nitrogen atom [46].

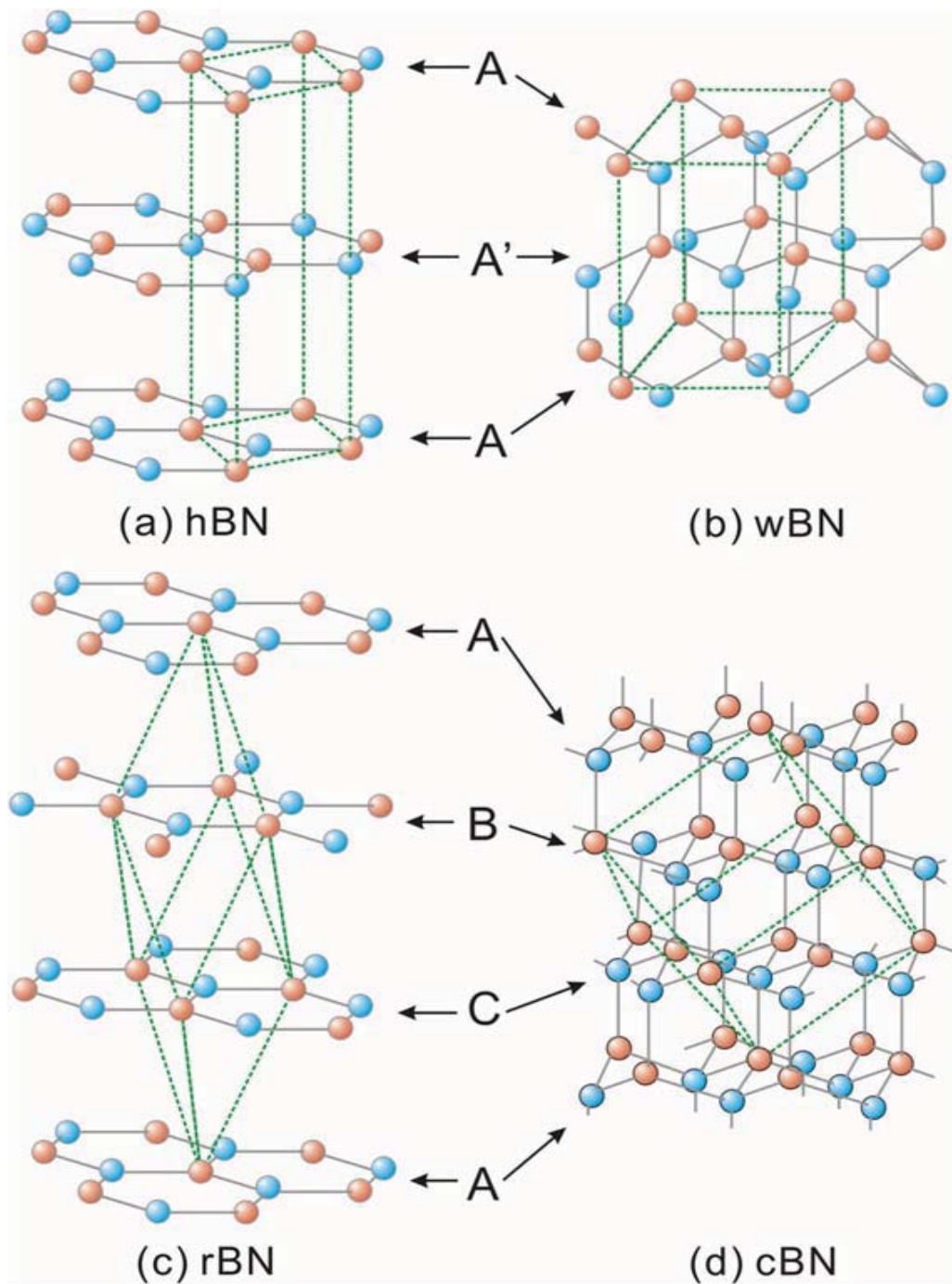


Figure 2.1 Structure of various allotropes of BN: (a) hexagonal (*h*-BN), (b) wurtzitic (*w*-BN), (c) rombohedral (*r*-BN) and, (d) cubic (*c*-BN)

In *r*-BN the stacked basal planes are oriented in the same rotation direction but stacked along the *c*-axis in an ABCABC.... sequence. Cubic-BN's sp^3 bonded structure can be considered as two face centered cubic (FCC) sub-lattices, each with only one type of atom,

interpenetrating into each other and shifted over $\frac{1}{4}$ of the lattice in the diagonal direction. The *c*-BN structure follows the stacking sequence of *r*-BN and results in B-N distance of 0.157nm [44]. The metastable sp^3 bonded *w*-BN is hexagonal, similar to hexagonal diamond (Lonsdaleite) and maintains a stacking sequence similar to *h*-BN [47].

2.2 Properties and Applications of Cubic Boron Nitride

Some of the properties of *c*-BN in comparison with diamond and other semiconductors are summarized in the Table 2.1 below.

Table 2.1: Comparison of various properties of BN with those of other semiconductors [48]

Parameters	<i>c</i> -BN	<i>h</i> -BN	Diamond	3C-SiC	GaAs	Si	GaN
Lattice Constant (Å)	3.615	A=2.504 C=6.661	3.567	4.358	5.65	5.43	A=3.189 C=5.185
Thermal Expansion Coefficient ($\times 10^{-6} \text{ }^\circ\text{C}^{-1}$)	3.5	2.7, 3.7	1.1	4.7	5.9	2.6	4.52
Density (gm/cm ³)	3.487	2.28	3.515	3.216	–	2.328	–
Melting point (°C)	>2973	–	3800	2540	1238	1420	600
Energy bandgap (eV)	6.4	5.2	5.45	3.00	1.43	1.12	3.39
Electron mobility (cm ² /Vs)	–	–	2200	400	8500	1500	3000
Hole Mobility (cm ² /Vs)	–	–	1600	50	400	600	~20
Dielectric Constant	7.1	5.06	5.5	9.7	12.5	11.8	9.5
Breakdown ($\times 10^5 \text{ Vcm}^{-1}$)	~80	~80	100	40	60	3	~80
Resistivity (Ωcm)	10^{16}	10^{10}	10^{13}	150	10^8	10^3	10^{19} - 10^{12}
Thermal Conductivity (W/cm K)	13	–	20	5	0.46	1.5	1.3
Absorption edge (μm)	0.205	0.212	0.20	0.40	–	1.40	0.35
Refractive index	2.117	1.700	2.42	2.65	3.4	3.5	2.33
Hardness (Kg/mm ²), $T = 300\text{K}$	3 - 6000	–	10,000	3500	600	1000	1080

The small lattice constant and the cubic zinc blend structure gives *c*-BN exceptionally high bulk modulus 369 GPa [12], making it the second hardest material after diamond with a

hardness of 30-60 GPa [44]. Cubic-BN is stable at high temperatures of about 1300°C at pressures of up to 1 bar. Because of these properties *c*-BN is an ideal candidate for machining hard and difficult to machine superalloys. Unlike diamond tools which undergo chemical reactions with ferrous metals, *c*-BN is resistant to chemical attack in presence of ferrous metals and Ni alloys at a temperature up to 1200 – 1300°C [48], and therefore *c*-BN powders are already being used as industrial abrasives. Thin films of *c*-BN can also be used to reduce wear and tear of compact discs and other surface sensitive surfaces.

Cubic-BN can be easily doped with n-type of impurity using Si, and p-type using Be and Mg. Microchips made from *c*-BN can operate at high temperatures in acoustic environments, and under high power conditions [44]. Because of its wide energy band gap *c*-BN can be used for ultraviolet (UV) detectors and UV light emitting diodes for optical communications in the deep UV regime [29]. The wide band gap is also useful for applications in high power microwaves as field-effect transistors. Heat sinks of *c*-BN thin films deposited on integrated circuits can greatly help improve the performance of the circuits by dissipating the heat generated by them.

2.3 Synthesis of *c*-BN

Bulk *c*-BN crystals synthesized by high pressure high temperature technique from *h*-BN are commercially available these days. The synthesis of bulk *c*-BN is therefore not covered in this literature review. In the field of thin films of *c*-BN a lot of different physical and chemical vapor deposition techniques combined with a large range of substrate and precursor materials have been attempted. Some of the relatively successful techniques are explained below.

2.3.1 Physical Vapor Deposition (PVD)

2.3.1.1 Magnetron sputter deposition

Sputtering involves ejecting material from a target using mostly an inert ionized gas and depositing the material on a substrate. In a magnetron sputtering unit electrons are trapped around the target material using strong magnets that also lengthen the path of electrons by causing them to take a helical path which results in better ionization of the sputtering gas that removes material from the target. While sputtering can normally be done by using either direct current (DC) or radio frequency (RF) alternating current, DC is used for conducting materials and RF is more suitable for insulating materials. Since both *h*-BN and *c*-BN are insulating materials most of the magnetron sputtering work is done with RF.

Thin films of *c*-BN have been deposited on Si [49] and glass [50] using different types of magnetron sputtering units [42, 75-80]. Radio frequency magnetron sputtering of *h*-BN in Ar resulted in a two layer structure with a sp^2 bonded layer of BN forming between Si substrate and the top *c*-BN thin film [49]. Otano-Rivera et al. [51] investigated the threshold bias voltage for nucleation of *c*-BN in films with high percentages of *c*-BN and associated the bias voltage with chamber pressure and the thickness of sheath that formed between the plasma and the substrate. The dependence of the bias on pressure was explained by the mean free path of the particles bombarding on the growing films. In a related study Le et al. [52] demonstrated that BN thin films deposited in pure Ar plasma were N deficient and that up-to 10%N in the plasma was needed to achieve stoichiometry in the thin films deposited by Magnetron Sputtering of *h*-BN target.

Investigation into the effect of bias on nucleation and growth of *c*-BN by RF magnetron sputtering technique revealed that while a higher bias voltage is required for nucleation of *c*-

BN on the substrate, a reduction of the applied bias during growth helps in achieving higher purity of *c*-BN in the films. The reduction in bias during growth not only reduces the re-sputtering effect that normally results in destabilizing the *c*-BN phase but also reduces stress in the films that prevents it from peeling off from the substrate.

Although cubic boron nitride was successfully deposited using sputtering techniques the thin films however were not phase pure cubic boron nitride. Hexagonal-BN was observed not only in between the substrate and the cubic boron nitride layer but also along with *c*-BN in the upper layers of the film. Another problem with the films was that the *c*-BN in the thin films was not crystalline enough to show good Raman peak.

2.3.1.2 Pulsed Laser Deposition (PLD)

In pulsed laser deposition technique a target material is vaporized in a vacuum chamber using pulsed laser. The vapor is then deposited on a substrate facing the target. The deposition is either done in vacuum, inert atmosphere, gas atmosphere or plasma which reacts with the vapor to deposit a product of the target material and the chamber gas, for e.g. oxide coatings of the pure target materials is obtained by evaporating the target in an oxygen environment to fully oxidize the vapor before the metal oxide gets deposited on the substrate. In PLD the ion/vapor source, the ion flux, the substrate and the substrate temperature can be controlled easily which helps in achieving controlled growth rates.

2.3.1.3 Chemical Vapor Deposition (CVD)

A large variety of chemical vapor deposition (CVD) techniques were explored over the past years for the synthesis of *c*-BN thin films. Some of the CVD techniques used include Microwave Plasma Enhanced CVD (MPECVD) [61, 62, 66] [a,d,q], Electron Cyclotron Resonance MPECVD (ECR-MPECVD) [71, 81-84], Inductively Coupled Radio Frequency Plasma CVD (ICP-CVD) [82, 85-88], Capacitively Coupled Plasma CVD [53], Direct Current Jet Plasma CVD (DC JP-CVD) [62-66], and Magnetically Enhanced ICP-CVD [54].

While Silicon [58-64] has been most extensively explored as substrate material to make use of its excellent properties and applications in the semiconductor industry, Nickel and diamond (diamond thin films on Si substrate) [55, 56] have been explored for their close lattice match with *c*-BN. Substrates of Cobalt containing Tungsten Carbide [54] and Iron [57] have been explored for exploiting the extreme hardness and chemical inertness in cutting tool applications.

Different sources of boron include Sodium Borohydride (NaBH₄) [58], Borazine (B₃N₃H₆) [59], Trimethylborazine (C₃H₁₂B₃N₃) [57], Diborane (B₂H₆) [67, 74, 76, 78], dimethylamine borane ((CH₃)₂NH-BH₃) [60], Borane-Ammonia (BH₃-NH₃) [60, 61], Boron Dichloride (BCl₂) [62], and Boron Trifluoride (BF₃) [69, 71, 84, 86, 88, 92]. Some of the precursors or Nitrogen include Ammonia (NH₃) [82, 88, 90], Trimethylborazine (C₃H₁₂B₃N₃) [57], dimethylamine borane ((CH₃)₂NH-BH₃) [60], Borane-Ammonia (BH₃-NH₃) [60, 61], and Nitrogen (N₂) [53, 54, 56, 61-71]. Hydrogen [62-71, 73-75, 78, 79] was mainly used as a catalyst, while Argon [66, 68, 69, 71, 83, 84, 86-88, 90-92], Krypton [59] and Helium [69, 84, 85, 87] were mainly used as plasma or ionizing gas. The two most successful CVD techniques,

DC Jet Plasma CVD and Microwave plasma CVD, both with ECR and without ECR, are discussed below.

Plasma Jet chemical vapor deposition technique is inherently a technique with high plasma density. The high ion/atom ratio is obtained as a consequence of the high energy involved in the generation of the plasma. This high density plasma technique is already in use for deposition of high quality, thick and rapid-growth diamond thin films [72]. The high density plasma in conjunction with DC bias to the substrate provides an atmosphere where high density of ions bombard the substrate material with high energy creating a condition suitable for *c*-BN nucleation and growth. Using Ar + BF₃ + N₂ + H₂ gas mixture it was demonstrated that *c*-BN content in the films grown on Si wafers, scratched with diamond powder, increased with increasing negative DC bias [62]. A critical bias of -85V was observed to be the optimum bias, above 85V the *c*-BN in films decreased because of re-sputtering effect. Interfacial layers of amorphous (*a*-BN) and *h*-BN were observed between the Si substrate and the *c*-BN film [62]. The columnar growth of *c*-BN observed was associated with the high density of the plasma generated by the DC Jet and the selective etching of *h*-BN by fluorine [62, 63, 65, 66]. It was realized that films deposited in the absence of fluorine, and in the presence of fluorine but without DC bias do not produce any *c*-BN. Only when DC bias and fluorine are both present simultaneously is *c*-BN deposited [65]. *c*-BN deposited with very high DC bias, in the absence of fluorine is mostly very little and highly stressed causing delamination of the as deposited film. Large crystals (0.2 – 0.5µm) with good adhesion and low stress, 1 – 2.3GPa depending on the deposition conditions, were deposited using both fluorine and negative DC bias. Compressive stress between 4 – 20 GPa are normally observed for films deposited with bias and without fluorine [73, 74].

In a two step process where nucleation and growth of *c*-BN were performed under different deposition conditions [65], nucleation of *c*-BN was expedited using higher H₂ flow rates than those used in the growth process. In the growth process the H₂ flow rate was reduced to decrease the growth rate. Simultaneously temperature of the substrate was increased to improve crystallinity and decrease residual stress in the films. It was observed that the crystallinity of the films increased with increasing substrate temperature and the residual stress decreased due to the annealing effect of the increased temperature of deposition [65, 66].

Till date DC Jet Plasma CVD process is one of the most successful technique for the synthesis of *c*-BN thin films. However, till date 100% phase pure *c*-BN thin films without the interfacial *a*-BN and *h*-BN layers is still a challenge. Moreover the films often get contaminated by the electrode material [70] employed for generating the high density plasma.

2.4 Microwave Plasma Enhanced Chemical Vapor Deposition

Initial experiments with MPCVD for synthesis of *c*-BN involved use of various kinds of precursors for Boron and Nitrogen. Experiments with Borazine based plasma resulted mostly in amorphous and *h*-BN even on diamond particles smeared on Si substrate. Solid Sodium hexaboride (NaBH₆) used in a low pressure gas mixture with NH₃ and H₂ to deposit BN thin films on Si substrates seeded with sub micron diamond seeds resulted in nanocrystalline *c*-BN in a matrix of *t*-BN and *h*-BN [58]. *c*-BN nucleated at diamond sites on the Si substrate. The nucleation on Di surface can be explained by the low lattice mismatch between Di and *c*-BN (3.5 and 3.6Å, respectively) of 1.3%.

Diamond thin films of various grain sizes, deposited on Si substrate by MPECVD, were used as substrate for deposition of *c*-BN thin films by B₂H₆ + NH₃ + H₂ + Ar gas mixture in a

MPECVD. BN film deposited showed higher percentage of *c*-BN phase, up to 85%, on films deposited on nano-crystalline diamond as compared with those on micro-crystalline diamond [55]. It was demonstrated that a repetitive multilayer of diamond and *c*-BN can help increase the purity of *c*-BN up to 95%. The percent *c*-BN in the films depended on the deposition pressure with highest quality of *c*-BN film deposited at 0.5 Torr pressure. The deposition at the low pressure was aided with a negative DC bias of 100V. It was observed that at higher pressures the *c*-BN content in the films decreased drastically. The low plasma density at higher pressures is the reason for the decrease in the *c*-BN content. The *c*-BN deposited by MPCVD using high energy ion bombardment however, were mostly nano-crystalline with high internal stresses that lead to rapid delamination of films. Even addition of Fluorine, that helps in etching away *h*-BN in a way equivalent to hydrogen etching graphite in diamond deposition, the highest percent of *c*-BN in the BN thin films was only 70% [70]. The low percent was attributed to the low plasma density of the MPECVD system in comparison with ECR-MPECVD.

In ECR mode of MPECVD the plasma density is increased by enhancement in the absorption of microwave energy achieved by trapping electrons on long cyclotron trajectories induced by the combined effect of the microwave electrical field and external magnetic field. Due to the trapped electrons colliding with ions in the plasma gas, considerably higher ionization, dissociation and excitation is observed [75] [7]. Plasma densities in a microwave discharge in general are limited to a critical density given by $n = 1.2 \times 10^{-2} f^2$, where f is the frequency of excitation [76]. For a 2.45 GHz excitation the plasma density can reach a maximum of $7.2 \times 10^{10}/\text{cm}^3$. The plasma density of an ECR-MPECVD system is almost an order of magnitude greater than this critical plasma density, allowing ionization of the plasma

gases by up to 25% [76, 77]. Additionally, the presence of much higher vacuum, in comparison with MPECVD mode of operation, provides longer mean free path to the plasma gases/ions resulting in fewer collisions of the excited species along their path to the substrate. This greatly increases the ion-to-atom ratio interacting with the growing thin film. The low pressure of operation of ECR and the gyration of the electrons helps in maintaining uniformity of the plasma over a larger area making it possible to deposit uniform thin films over larger areas in comparison with MPECVD and Jet Plasma CVD. Since no electrodes are employed for generating plasma the thin films deposited by ECR-MPECVD are essentially contamination free.

Boron Nitride thin films deposited using Borazine ($B_3N_3H_6$) [59], Trimethyl-borazine and diborane [57], on Si [57, 59] and Fe [53] substrates using ECR-MPECVD were mostly hexagonal in nature. The small fraction of *c*-BN that did get deposited required very high bias of -150V. It was found that although hydrogen in the plasma helps in breaking of the boron and nitrogen source and formation of B-N radicals, that are the building blocks of BN thin films, H is not selective in etching *h*-BN over *c*-BN, as it is in etching graphite over diamond. Even substrate bias that helps in increasing the *c*-BN content of the films doesn't help in etching of the *h*-BN that gets co-deposited.

As mentioned in the discussions before, Fluorine etches *h*-BN six times faster than *c*-BN. The high density of plasma of the ECR-MPECVD, addition of fluorine to the system and presence of substrate bias fulfills all the requirements for deposition of *c*-BN; i.e. high ion/atom ratio, chemical etching of *h*-BN, and high energy ion bombardment. 100nm crystals of *c*-BN were observed for 1 μ m thick film deposited in a ECR-MPECVD using He + Ar + N₂ + BF₃ + H₂ plasma chemistry [74, 75, 79]. A bias of only -40V, much less than that used for *c*-

BN deposition by Jet Plasma CVD, resulted in lower stress in the films deposited on Si substrates [69]. The thin films however had interfacial layer of *h*-BN/*t*-BN below the *c*-BN layer. BN thin films deposited on diamond thin films, grown using bias enhanced nucleation by MPECVD on Si substrates, showed high quality *c*-BN peaks in their Raman spectra. The high quality of the films was attributed to the low lattice mismatch between diamond and *c*-BN of only 1.34%, and the low substrate bias of only -20V employed for the deposition. TEM investigation of the films revealed that the *c*-BN grew directly on the diamond facets, while at areas where Si was exposed a thin layer of *t*-BN was deposited first, before *c*-BN nucleation and growth. The reduction in bias was attributed to the high plasma density achieved by the use of higher microwave power of 1000W at the low pressure of 2×10^{-3} Torr [56]. The role of the small negative bias was only to break the B-F bonds on the growing film facilitating the N bonding necessary for further growth [56]. Thus with Fluorine chemistry, low bias voltage, high plasma density, high density of ion-to-atom ratio approaching the substrate, no contamination source and the ease of control of parameters makes the ECR-MPECVD the most ideal technique for deposition of *c*-BN thin films till date.

CHAPTER 3

OBJECTIVE AND RESEARCH PLAN

The main objective of this part of the research is to attempt synthesis of *c*-BN thin film on Si and diamond coated Si substrate by MPECVD and ECR-MPECVD. The approach was divided into three parts:

1. Synthesize *h*-BN thin films using B₂H₆ and NH₃ as precursors by MPECVD
2. Study the effect of negative DC bias on BN thin films deposited using the optimized conditions for deposition of *h*-BN
3. Synthesize BN thin films using BF₃ and N₂ as precursor gases under both MPECVD and ECR-MPECVD

CHAPTER 4

EXPERIMENTAL

The ASTEX microwave plasma enhanced chemical vapor deposition system described in Part I was used for the synthesis of boron nitride thin films. Diborane (B_2H_6) (5% in Hydrogen) and Boron-Trifluoride (BF_3) (10% in Ar) were used as precursors for Boron, while Ammonia (NH_3) and Nitrogen (N_2) gas were used as precursors for Nitrogen. H_2 (99.999%), Ar (99.9%) and He were used as plasma gases for various experiments. Si (100) wafers of 0.5mm thickness, and diamond thin films deposited by MPECVD on Si wafers were used as substrates.

Along with the normal mode of operation of MPECVD system, the electron cyclotron resonance (ECR) mode of the MPECVD system was also employed for the synthesis of BN thin films. Two modifications were made to the MPECVD system. The first one was a quartz feed-through designed to introduce B_2H_6 , separate from other gases, directly above the plasma. This was necessary to prevent the decomposition of B_2H_6 into metallic boron and hydrogen at temperatures near $100^\circ C$ in the presence of hydrogen gas. The second modification was an indigenously built bias used for providing negative bias to the substrates for *c*-BN synthesis. The modifications made to the MPECVD system required for the synthesis of boron nitride thin films are explained in the proceeding sub-section.

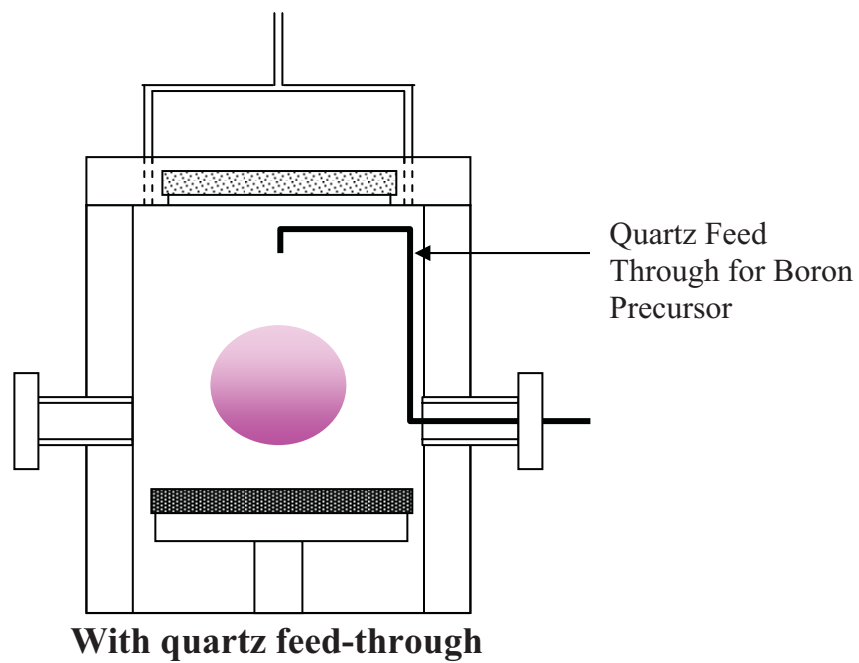
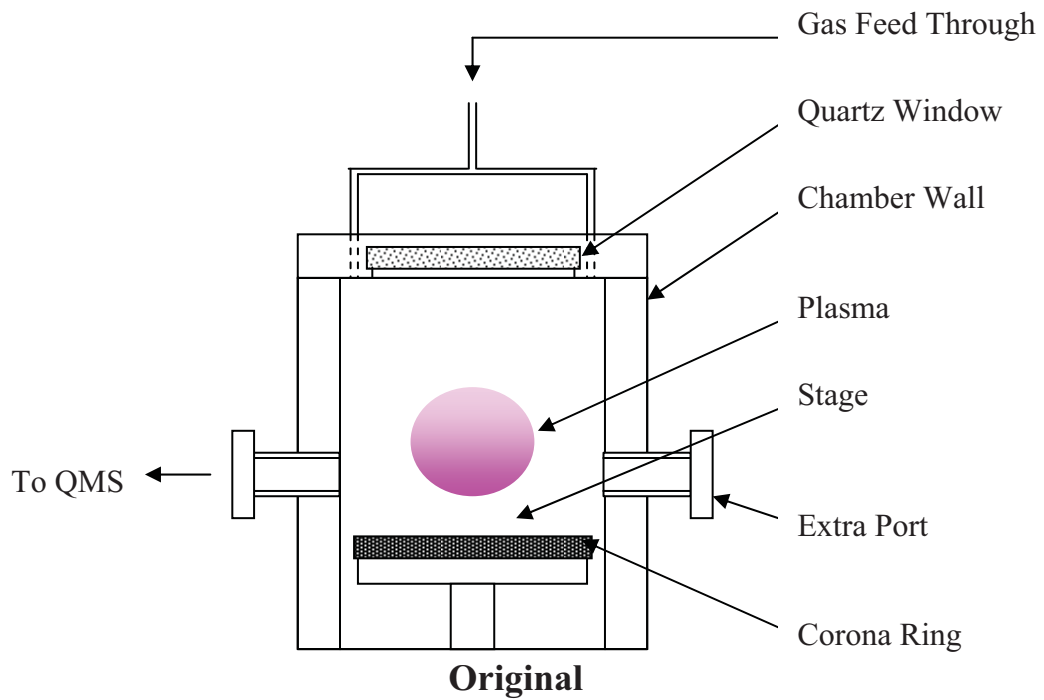


Figure 4.1: Schematic of original and modified MPECVD deposition chamber with quartz feed through

4.1 The Deposition System

MPECVD system described in Part I was used for the deposition of BN thin films. In the synthesis of boron nitride, often boron from the boron precursor gets reduced to metallic boron powder in the presence of hydrogen at little above room temperature, for e.g. when diborane is added along side with hydrogen metallic boron powder is produced by the following reaction and the powder gets deposited on the gas inlets and chamber walls:



Therefore it is recommended to add the two gases separately. In our MPECVD system we used quartz feed-through to add boron precursor separate from other gases and directly above the plasma. Figure 4.1 shows the original and modified gas feed-through employed for BN thin film deposition.

Synthesis of *c*-BN thin films requires high energy ion bombardment of the depositing ions. This is achieved by applying negative DC bias to the substrate. An indigenously prepared flexible bias built using thermocouple (K-type) wire, glass fiber threads and household aluminum foil, as shown in Figure 4.2 was used to supply –ve DC current directly to the substrate.

The flexible DC bias was hooked to a negative DC power supply unit: Advanced Energy MDX 500, capable of delivering negative power up-to 1 KW, with either voltage or current control. Figure 4.3 shows the schematic of the flexible DC bias in use for the two modes of our MPECVD system.

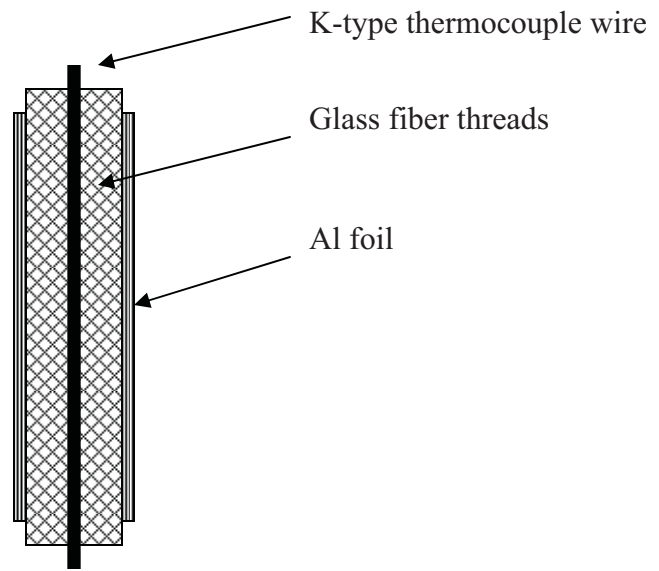


Figure 4.2: Bias cable constructed with K-type thermocouple wire, glass fiber threads and domestic Aluminum foil.

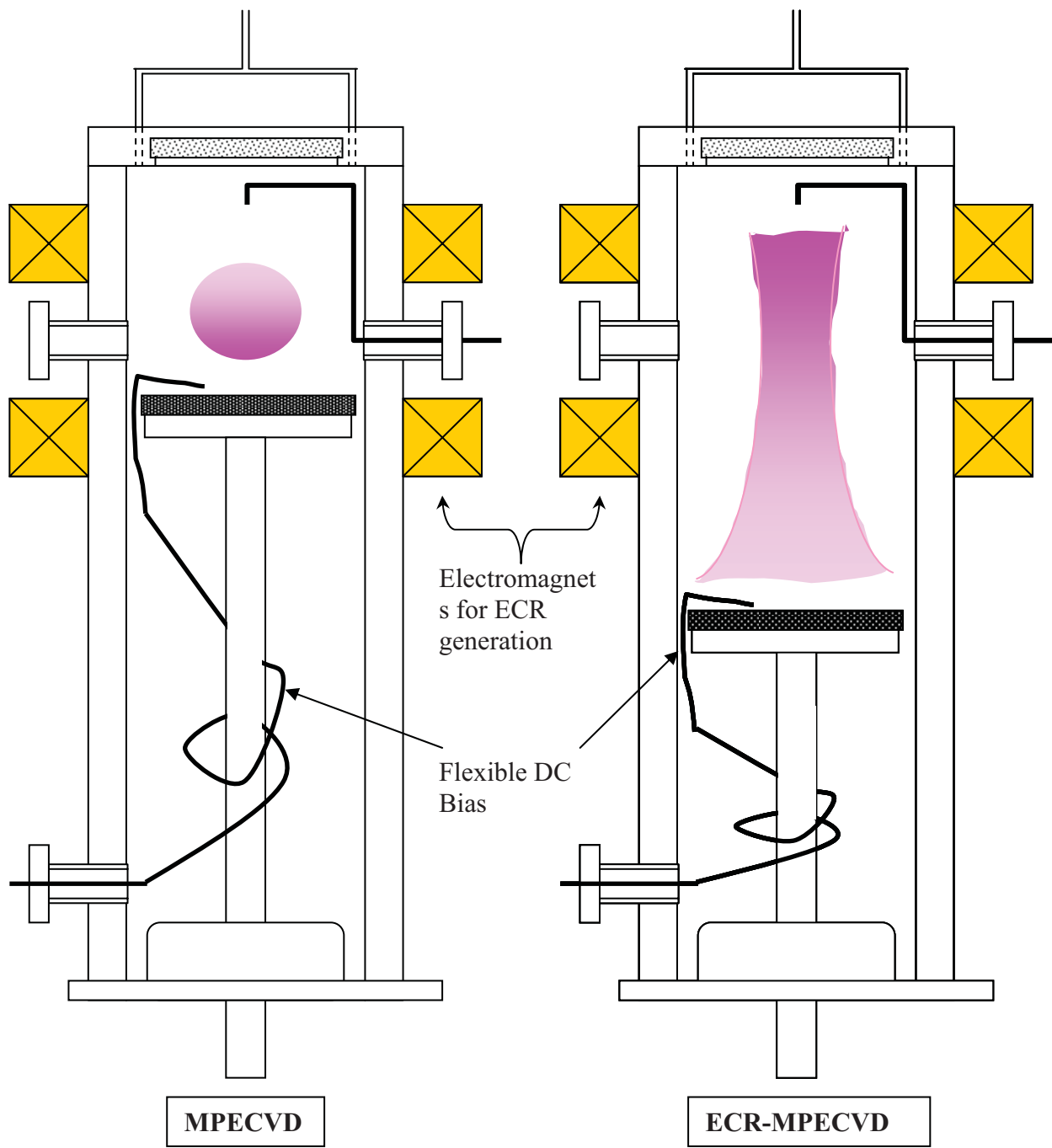


Figure 4.3: Schematic of the flexible DC bias in use for the two modes of MPECVD system.

4.2 Substrate Preparation

Si (100) wafers were cut into 10mm x 10mm squares pieces so that 4 such pieces could be placed below the plasma. The plasma ball varies in size from 1 inch to 2 inches depending on the deposition conditions being used. Using 10mm x 10mm square pieces establishes uniform coverage of the substrates by the plasma and helps in simultaneous deposition of thin films on substrates with different pre-treatments. Si (100) substrates were first cleaned with Acetone to remove oil and other carbohydrates if present on the surface. The substrates were then cleaned with Ethyl alcohol and di-ionized water to remove any acetone remains from the surface. After cleaning with DI water the substrates were immersed in 2% HF solution for 5 minutes to etch native oxygen layer from the surface. For experiments in which diamond coated Si wafers were used as substrate, the diamond films were cleaned only with acetone and alcohol; the HF treatment was not given to the diamond films.

The cleaned and HF treated Si substrates were immediately transferred to an ultrasonic bath containing 20-40 μ m diamond slurry or 20-40 μ m *c*-BN slurry and activated for 2 hours. All substrates after pre-treatment were cleaned with ethyl alcohol and DI water, and dried with dry Nitrogen. The substrates were then immediately transferred to the plasma chamber where they were placed on a 1 mm thick Molybdenum disc that seated directly on the inductively heated hot stage. Before starting each experiment the substrates were given H₂ plasma treatment for 10 minutes to remove any native oxide layer that might have formed between the time the substrate was cleaned and the plasma started.

4.3 Deposition conditions

After substrate pretreatment and loading of substrates, the system is pre-evacuated to 10^{-6} Torr at 350°C. Hydrogen is then introduced in the chamber and a pressure of 10 Torr stabilized using throttle valve. Microwave power of around 350W is then employed to start the plasma. Once stable plasma is established and the initial hydrogen treatment completed, the precursor gases and other parameters are set as per the deposition conditions.

As the first step towards synthesis of *c*-BN, *h*-BN thin films were synthesized using B₂H₆ and NH₃ as precursor gases in H₂ + Ar plasma. The normal high pressure mode of the MPECVD system was employed for this set of experiments. The experiments were performed in two sub-sets. In the first sub-set the experiments were performed with B₂H₆ as the first precursor gas to be introduced in the plasma chamber after H₂ etching, in the second sub-set N₂ was used as the first precursor gas. Table 4.1 gives the deposition parameters for synthesis of *h*-BN thin films on Si substrate.

Table 4.1: Deposition conditions for synthesis of *h*-BN thin films

Substrate	Si (100)
B ₂ H ₆ (sccm)	6
NH ₃ (sccm)	25
Ar (sccm)	25
H ₂ (sccm)	5
Substrate Temp. (°C)	850
Pressure (Torr)	12 – 35
Growth Time (hrs)	5

Experiments on synthesis of cubic boron nitride were performed in the two modes of the MPECVD system and with two different precursor gases for both boron and nitrogen. At first synthesis of *c*-BN thin film was attempted using B₂H₆ and NH₃ as precursor gases by adding negative DC bias to the deposition conditions optimized for *h*-BN thin film synthesis. Effect of increasing DC bias was studied with respect to the percentage of *c*-BN in the thin films. Table 4.2 gives the deposition conditions. In the second set of experiments BF₃ and N₂ were used as precursor gases in the electron-cyclotron-resonance (ECR) mode of the deposition system. Helium (He) gas was added to the system to increase the plasma density. Effect of variation of different parameters was investigated with respect to the percent *c*-BN in the thin films. Table 4.3 gives the experimental conditions used:

Table 4.2: Deposition conditions for the study of effect of D.C. bias

Substrate	Si (100)
B ₂ H ₆ (sccm)	8
NH ₃ (sccm)	50
Ar (sccm)	20
H ₂ (sccm)	10
Substrate Temp. (°C)	925
Pressure (Torr)	60
Bias Current (mAmps)	0 - 300

Table 4.3: Deposition parameters for synthesis of *c*-BN using BF₃ and N₂ by ECR-MPECVD

Substrate	Si (100), Diamond on Si
10 % BF ₃ in Ar (sccm)	0.375 – 13.5
N ₂ (sccm)	4 – 7.5
H ₂ (sccm)	0.7 – 6
Ar (sccm)	2 – 3
He (sccm)	11 – 37
Pressure (Torr)	40 – 68
Power (W)	950
Substrate Temp. (°C)	950
Growth Time (hrs)	0.5
Bias Voltage (V)	
Nucleation	60 – 150
Growth	30 – 50
Bias Current (mAmps)	
Nucleation	30 – 57
Growth	17 – 70

4.4 Characterization Techniques

Thin films of *h*-BN and *c*-BN were characterized using SEM, FTIR spectroscopy, and Raman spectroscopy. Since Raman spectroscopy is a very sensitive technique and depends greatly on the quality of the crystal in the thin films, FTIR was used as the main technique for qualitative and quantitative analysis of our thin films. Table 4.4 gives characteristic peaks of *h*-BN and *c*-BN thin films observed in FTIR and Raman Spectroscopy.

Table 4.4: Characteristic FTIR and Raman shifts peaks for *c*-BN and *h*-BN

	FTIR (wavenumber cm^{-1})	Raman (Raman shift cm^{-1})
<i>c</i> -BN	1065	1300
		1365
<i>h</i> -BN	1080	1380
	1380	

CHAPTER 5

RESULTS AND DISCUSSION OF BORON NITRIDE THIN FILMS DEPOSITED BY MPECVD

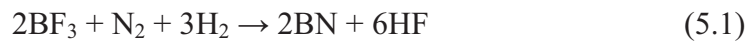
In CVD techniques it was thought that *c*-BN films could be grown under conditions similar to diamond thin films where hydrogen ions would selectively etch sp^2 bonded hexagonal boron nitride (*h*-BN) thus allowing the growth of sp^3 bonded *c*-BN. However it was realized that hydrogen has no preference in etching different forms of BN. It etches both *h*-BN and *c*-BN at the same rate and therefore doesn't assist in deposition of *c*-BN. Physical impact instead of chemical, in the form of high energy ion bombardment was therefore needed to deposit the BN radicals from the plasma in the form of *c*-BN instead of *h*-BN. *c*-BN films deposited using H_2 [54, 55, 58, 60, 78, 79] as the main plasma gas and $B_2H_6 + NH_3$ [55, 78], $B_2H_6 + N_2$ [54, 79], $BH_3 + NH_3$ [78] or $NaBH_4 + NH_3$ [60] as precursor gases using high energy ion bombardment had high induced compressive stresses. The high compressive stresses in the range of 2 – 8 GPa resulted in peeling/cracking of the films, thus restricting the film thickness to less than 1.0 μ m. Also, the films deposited are mostly nanocrystalline in morphology [55] with *h*-BN/tubostratic-BN interfacial layer between the substrate and the *c*-BN film. Till date, using H_2 as the main plasma gas, a maximum of 95% purity *c*-BN film with nanocrystalline morphology and 1 μ thickness has been claimed in the literature [55]. However, for both electrical [80] and mechanical applications film with better crystallinity, purity, and adhesion are needed.

By exposing *c*-BN and *h*-BN powders to BF_3 atmosphere in a CVD system and measuring weight loss after etching, W. Kalss et al. [45] reported that *h*-BN is etched by BF_3

six times faster than *c*-BN. With fluorine etching sp^2 bonded *h*-BN faster than the sp^3 bonded *c*-BN the deposition conditions of CVD *c*-BN became similar to deposition conditions for CVD diamond. High quality 20 μ m thick *c*-BN films were deposited on Si (100) substrate in DC-bias-assisted DC jet CVD system in an Ar + N₂ + BF₃ + H₂ system at 50 Torr pressure and -85 V bias [80].

It was proposed that for the deposition of *c*-BN by BF₃+N₂+H₂+Ar+He in a MPECVD environment:

(a) Hydrogen helps in the formation of BN by the reaction [48, 83]:



Since HF is highly stable BN deposits on the substrate.

(b) Under the influence of a critical substrate bias some of the BN deposits as *c*-BN [44]. This critical substrate bias depends on the operating pressure.

(c) *c*-BN and *h*-BN deposited on the substrate react with highly reactive fluorine ions and molecules to form B-F and B-N bonds, and either stabilize sp^3 bonds on the surface or etch them back to the gas phase [63].

(d) *h*-BN is more rapidly etched than *c*-BN by BF₃ [45], thus leaving only *c*-BN on the substrate. Since H₂ helps in formation of BN and also consumes some F in the plasma chamber, the H₂/F ratio should be carefully maintained such that there is only enough F in the plasma to just etch *h*-BN [62].

(e) Substrate bias helps in activating the chemisorbed species on the *c*-BN nuclei (that survived fluorine etching) and the arriving ions (N₂⁺, BF_x⁺, etc.) for further growth [63].

(f) Ar (and He) maintains plasma and plasma density.

FTIR and Raman spectroscopy were used for characterization of the *c*-BN thin films. In FTIR the characteristic transverse optic (TO) phonon mode of *c*-BN appears at $\sim 1065\text{cm}^{-1}$ while out-of-plane B–N–B bending vibrations and the in-plane B–N stretching modes characteristic of *h*-BN appear at ~ 770 and $\sim 1380\text{cm}^{-1}$, respectively. In Raman spectroscopy *c*-BN's characteristic scattering of TO phonon mode and longitudinal optical (LO) phonon mode is observed at 1050 and 1300 cm^{-1} , respectively, while the phonon mode for *h*-BN is observed at 1370 cm^{-1} [63].

The present work on synthesis of *c*-BN by MPECVD technique is divided into two parts. In the first part 10% B_2H_6 in H_2 and NH_3 were used as boron and nitrogen sources respectively in H_2 plasma for the deposition of *h*-BN thin films. Once suitable conditions were established for *h*-BN synthesis, negative DC bias was used to increase energy of the bombarding ions needed for the formation of *c*-BN. In the second part, 10% BF_3 in Ar as boron source, and N_2 as nitrogen source were used as precursor gases while H_2 was used in small quantities as a catalyst. Ar and He were used as plasma gases. Most of the BF_3 work was performed with negative DC bias in the electron cyclotron resonance (ECR) plasma mode of the MPECVD system as per literature [70-72].

5.1 Hexagonal Boron Nitride Thin Films

Hexagonal thin films were deposited in two sets. In the first set, Boron precursor gas was added first to the H_2 plasma. In the second set, Nitrogen precursor was introduced first. The films deposited were characterized using micro-Raman spectroscopy and the results were analyzed with respect to the deposition pressure and the effect of sequence of introduction of precursor gases.

For both set of experiments the quality of *h*-BN thin films improves with increasing deposition pressure. This is evident from the decreasing full-width at half-maximum of the *h*-BN peak (observed around 1370cm^{-1}). It is also evident from the Raman spectra of the two sets of experiments that the films grown with NH_3 as the first precursor gas are of better quality.

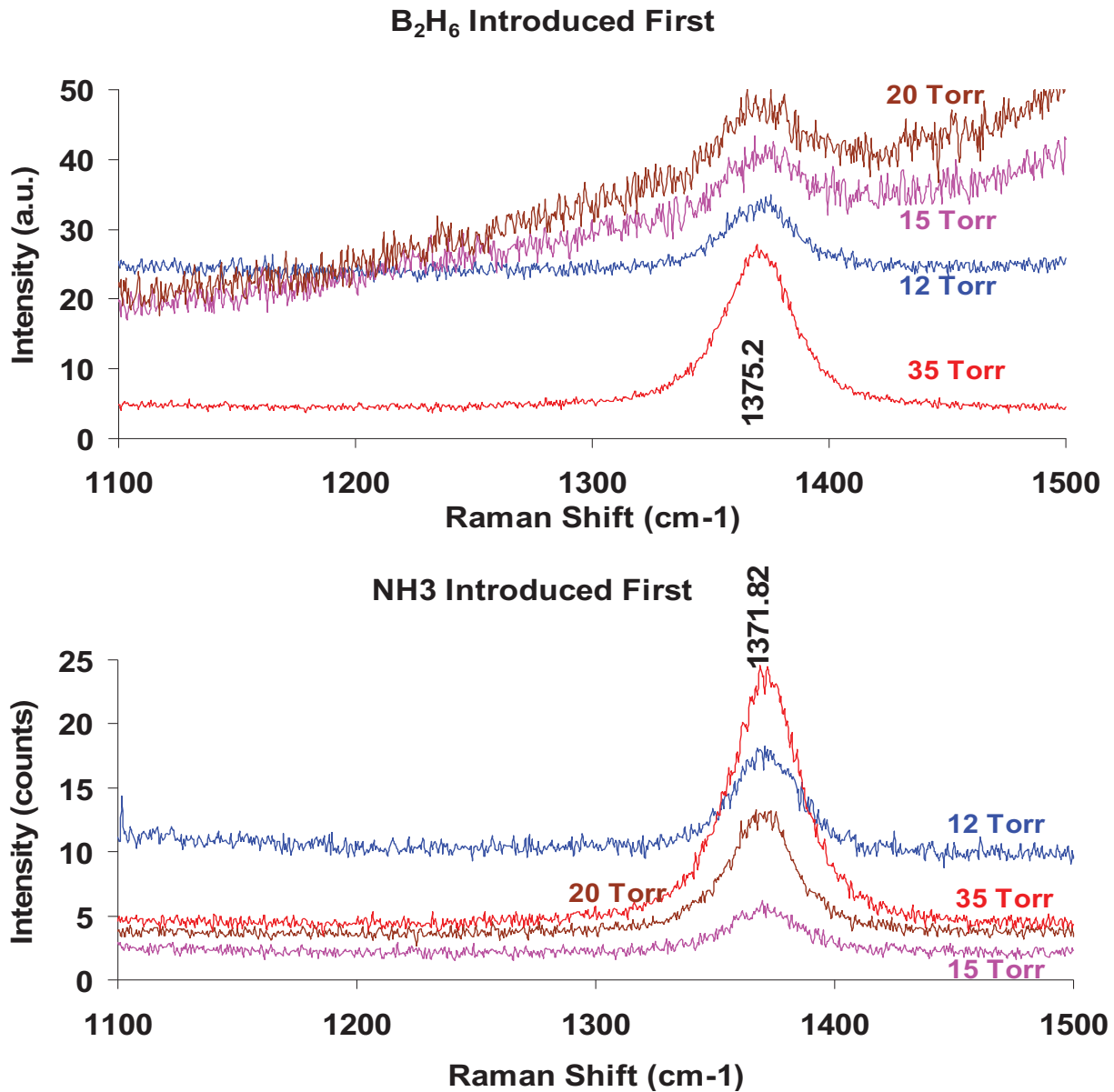


Figure 5.1: Raman spectra for *h*-BN thin films deposited at different pressures. (a) films deposited with B_2H_6 gas as the first precursor gas to be introduced in the deposition chamber, (b) films deposited with NH_3 gas as the first precursor gas to be introduced in the deposition chamber

With N source as the first precursor gas, fresh Si substrate after been etched by Hydrogen plasma, removing any native oxide layer, is exposed first to nitrogen at the high temperature of deposition. Since Si and N from Si-N bonds very easily because of their difference in electronegativity, a layer of N atom forms on the Si substrate. Some silicon nitride may also get synthesized. When Boron source is added to the plasma BN radicals that result from the chemical reaction between B^+ and N^+ ions in the plasma settle on the Nitrogen layer, instead of Si. Boron from BN then bonds with the N on the Si to form B-N bond, while the N either combines with other N or H ions in the gas just above the substrate and escapes as N_2 or NH_3 or combines with adjacent B radical to form another B-N bond on the substrate.

When B_2H_6 is introduced as the first precursor gas, the boron ions from the plasma settling on the Si substrate do not form covalent bonds with Si, resulting in deposition of amorphous boron powder. When NH_3 is introduced N from ammonia under low pressure conditions reacts with B on the substrate to form a covalent short range B-N bond, thus forming amorphous BN. Some of the BN formed in the plasma settles on the amorphous BN thin film as *h*-BN. With increased pressure the density of BN in the plasma increases resulting in higher percentage of *h*-BN in the thin film. However, since the initial interfacial layer of *a*-BN is formed before the *h*-BN is deposited on the substrate, the improvement in quality of the films with pressure is less for thin films deposited with B_2H_6 as the first precursor gas in comparison with thin films deposited with NH_3 as the first precursor gas. Therefore, deposition conditions with higher pressure and NH_3 as the first precursor gases were used for the bias-assisted deposition experimentation.

5.2 Cubic Boron Nitride Thin Films

Negative DC bias was used for all experiments on synthesis of *c*-BN thin films. As mentioned before two sets of precursor gas mixtures were used in two different modes of the CVD system. The films were deposited using conditions mentioned in Table 5.2 and Table 5.3. FTIR spectroscopy was used as the main characterization technique for qualitative and quantitative assessment of *c*-BN in the deposited thin films.

Raman Effect is a very small fraction, about 1 in 10^7 , of the incident phonons, and therefore high intensity laser beams are used to observe the effect clearly. When a well defined structure is probed by an incident laser beam, energy exchange between the incident beam and the electrons causes a change in polarization of the bonds within the material. The change in polarization is characteristic of the material and depends on the vibrational state of the bonds. The amount of energy utilized to cause the change in polarization is observed as a shift, known as Raman shift, in the wavelength of the reflected beam. The observed Raman shift thus represents the vibration state of the bonds and provides information on the internal properties of the material under investigation. The intensity of the peaks/shifts observed depends on the number of vibrating bonds contributing to the shift. In a well-defined Raman active structure a large volume of bonds contribute to the Raman shift and a high intensity sharp peak is observed. With defects and non-uniformity in the structure the number of bonds contributing to the Raman shift decrease significantly and result in broadening and lowering of intensity of the characteristic peak/Raman shift. Additionally, fluorescence, photons released when atoms, molecules or nanostructures relax to their ground state after being excited, becomes dominant in Raman spectra in the presence of nano-crystalline and amorphous material.

BN Thin films deposited with DC bias showed high fluorescence spectra with no *c*-BN peak. Suggesting that the BN films were highly defective, amorphous or nano-crystalline and any *c*-BN in the films was either nano-crystalline or highly defective [44]. Since no appreciable information about the amount or quality of *c*-BN in our films could be obtained from Raman spectroscopy the structure sensitive spectroscopy was not used for characterizing our films.

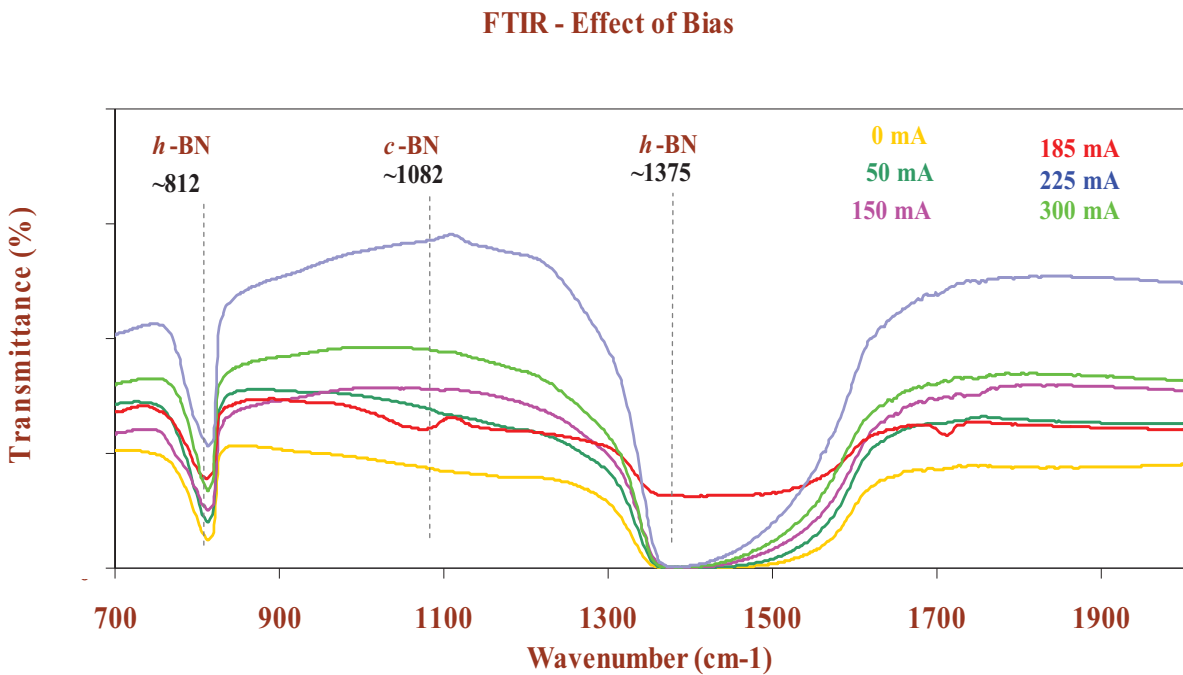


Figure 5.2: FTIR transmission spectra of BN thin films synthesized with increasing negative DC bias

5.2.1. Cubic BN Thin Films Deposited by MPECVD Using B_2H_6 and NH_3

DC bias was added to *h*-BN deposition conditions with the intention of increasing ion bombardment of the precursor gas radicals to convert *h*-BN to *c*-BN [54]. Negative DC bias applied to the experiments was used in the current control mode, which means a constant current was maintained during the experiment while voltage was allowed to vary in order to control the current. Since the current observed corresponds to the density of ions bombarding

the substrate, maintaining current as constant relates to maintaining a constant density of ion bombardment.

In FTIR transmission mode the absorbance of wavelength in the IR region of the electromagnetic spectrum, by the out-of-plane vibration mode of *c*-BN is can be very easily detected very clearly at approximately 1080cm^{-1} . Therefore, FTIR was used as the main characterization technique for the thin films in this research. Figure 5.3 shows transmittance mode FTIR of the films synthesized under different bias conditions. Characteristic vibration peaks of out-of-plane vibration and in-plane vibration modes of *h*-BN are seen at 800 and 1380cm^{-1} , respectively, for all the samples. The characteristic peak of *c*-BN observed near 1080cm^{-1} , was detected only for film deposited with 185mA of DC bias. Since further increase in DC bias didn't increase the *c*-BN content of the films, probably due of re-sputtering effect, bias around 185mA was used for further optimization of the deposition parameters.

Experiments with variation in pressure, power, substrate temperature and precursor gases didn't give any appreciable improvement in *c*-BN content in our films. It was realized that in our system under the most optimum conditions a large quantity of *h*-BN is produced along with some *c*-BN when using B_2H_6 and NH_3 are used as precursor gases. Preferential plasma etching of *h*-BN in the growing film is therefore needed for synthesis of thin films with higher percentages of *c*-BN.

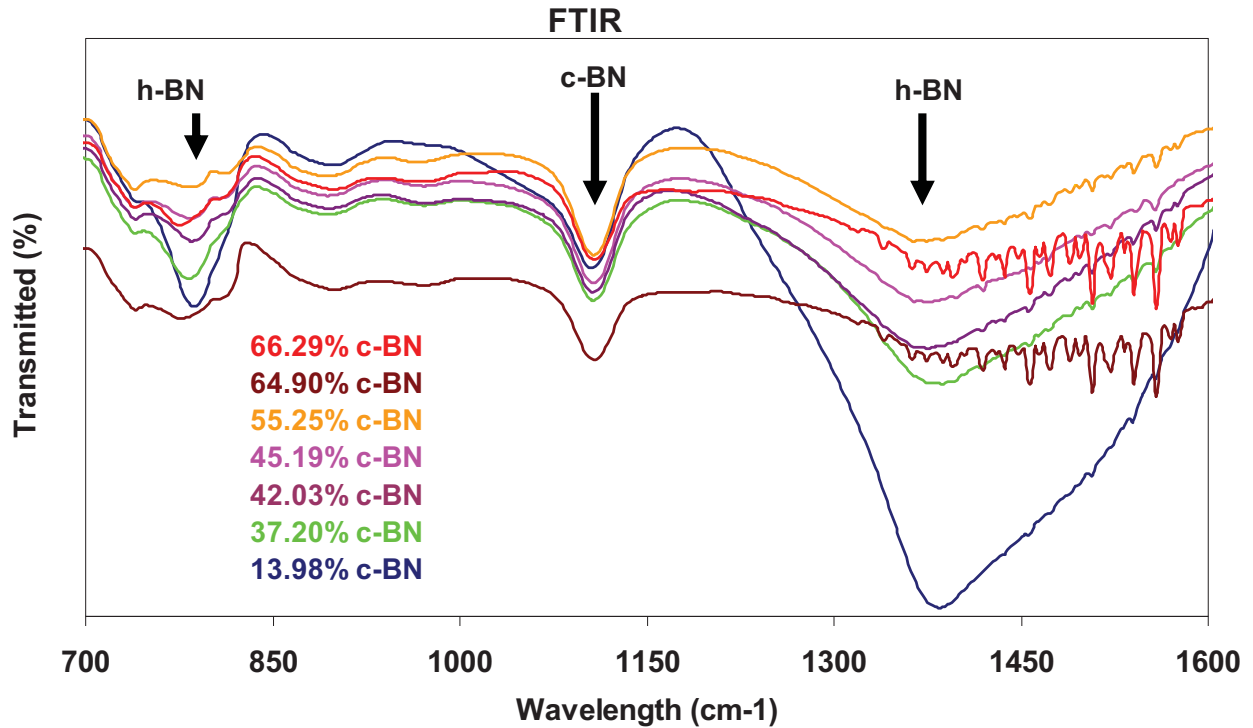


Figure 5.3: Transmission FTIR spectra of BN thin films with varying %*c*-BN. A maximum of 66 percent *c*-BN was achieved in the films

5.2.2. Cubic BN Thin Films Deposited by ECR-MPECVD using BF_3 and N_2

Experiments using 10% BF_3 in Ar were performed in the ECR-MPECVD mode with negative DC bias. According to literature [64, 82] in the ECR mode minimal negative bias is sufficient for nucleation of cubic phase of boron nitride. Hexagonal-BN formed along side is etched by fluorine from BF_3 and thus higher percentages of *c*-BN can be obtained in the thin films [48, 84]. Deposition conditions mentioned in Table 4.3 were used for this set of experiments. A large variation of deposition conditions were tried to optimize the deposition parameters. DC bias was used in the voltage mode for these experiments as per literature [58, 67, 92]. Along with Si substrate diamond thin films were used as substrate material because of the low lattice mismatch (1.34%) between diamond and *c*-BN. Thin films deposited were characterized using FTIR spectroscopy.

Figure 5.3 shows the FTIR spectra of films with varying percent of *c*-BN deposited using conditions mentioned in Table 4.3. A clear peak for *c*-BN is seen around 1080 cm^{-1} along with peaks for *h*-BN at 800 and 1380 cm^{-1} . Percent *c*-BN in the films was calculated from their FTIR spectra by converting % Transmittance to Absorbance and then fitting the *c*-BN and *h*-

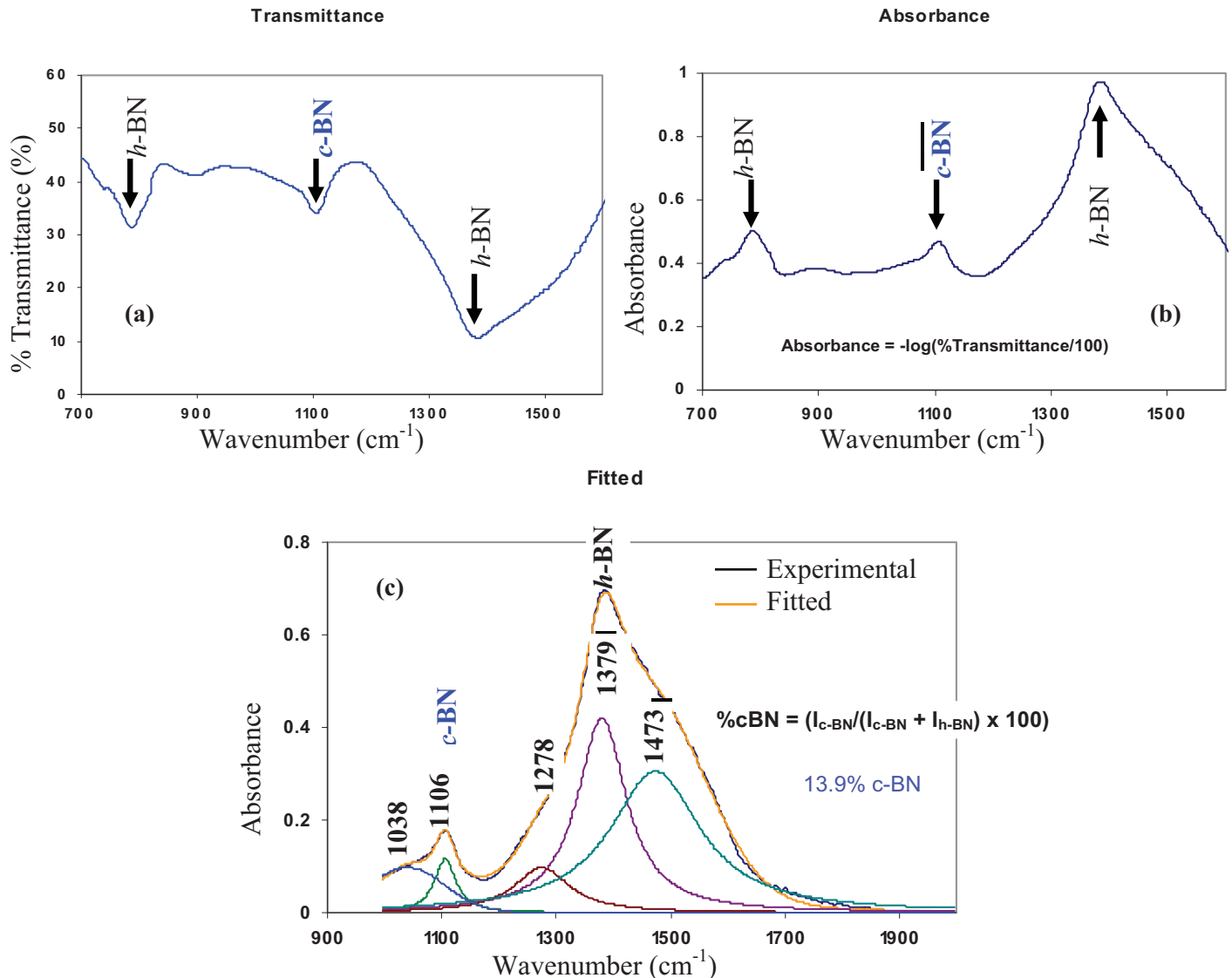
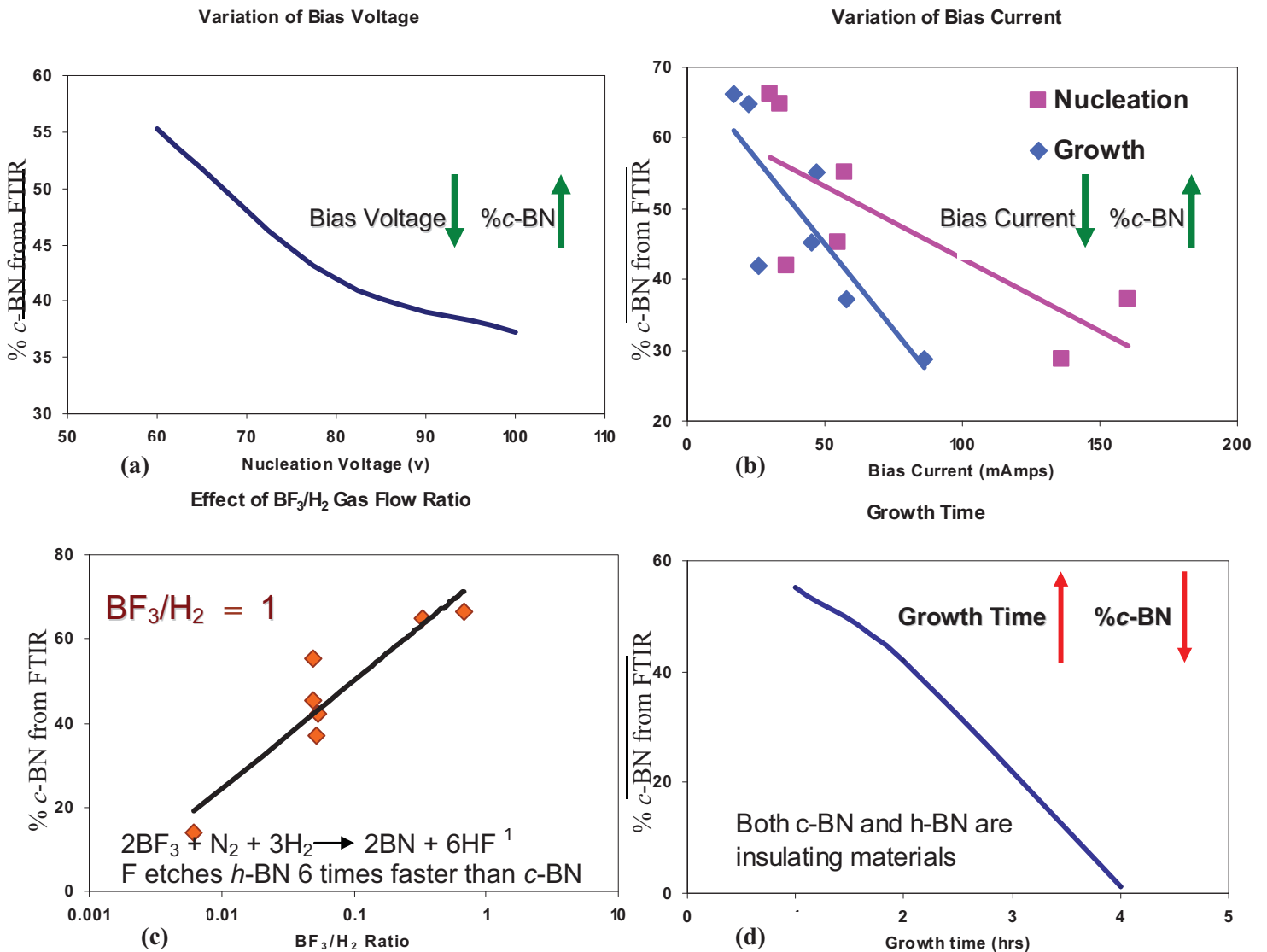


Figure 5.4: (a) Transmission FTIR spectra of BN thin film showing both *h*-BN and *c*-BN peaks. (b) Transmission FTIR spectra from (a) converted to Absorbance spectra using the equation in the Figure, and (c) Deconvoluted and fitted spectra of the Absorbance FTIR spectrum in (b). Equation in (c) is used to calculate %*c*-BN in the film using the *c*-BN and *h*-BN deconvoluted peaks. Using the equation %*c*-BN in the spectrum shown above is 13.9%

BN peaks around 1080 and 1380cm^{-1} , respectively, by Gaussian functions using Peak Fit software. %*c*-BN is calculated from the equation shown in Figure 10c. Up to 66% *c*-BN was observed for the films.



¹ W. Kalss, R. Haubner, B. Lux, *Diamond and Related Materials*, 7 (1998) 369

Figure 5.5: Correlation between process parameters and the %*c*-BN observed in the films by FTIR. (a) Effect of increasing nucleation voltage on %*c*-BN in the thin films, (b) Effect of nucleation and growth currents on %*c*-BN in the thin films, (c) effect of variation in BF_3/H_2 ratio on %*c*-BN in the thin films, and (d) variation of %*c*-BN in the thin films with growth time.

Process parameters used during deposition were correlated with the percentage of *c*-BN observed from FTIR; Figure 5.5 shows the trends observed. It was observed that increase in nucleation voltage has adverse affect on the quantity of *c*-BN in the thin films. Lower nucleation voltages gave higher percentages of *c*-BN. This is in agreement with the literature [54] and is attributed to resputtering of the depositing film under higher bias conditions. Nucleation current and growth current have similar affects as the nucleation voltage. However much lower currents are needed during growth since growth of the *c*-BN nuclei requires only minimum ion bombardment, thus higher bias during growth only causes etching/re-sputtering of *c*-BN nuclei reducing *c*-BN content in the films. This is evident from Figure 5.5(b) which shows that the *c*-BN content decreases sharply with increase in current during growth.

BF_3/H_2 ratio is of utmost importance. H_2 helps in formation of BN in the plasma [81], which deposits as both *h*-BN and *c*-BN under the influence of bias; F from BF_3 does the job of etching *h*-BN and *c*-BN from the depositing film. Since BF_3 etches *h*-BN six times faster than *c*-BN [45], the ratio BF_3/H_2 should be such that only *h*-BN is etched by F. From Figure 5.5(c) it is evident that this ratio should be around 1, which matches closely with the literature [82].

Figure 5.5(d) shows that the %*c*-BN in the films is inversely dependent on the deposition time. This is because BN radicals formed in the plasma deposit as *c*-BN with the aid of negative bias, and since both *h*-BN and *c*-BN are insulating in nature with increasing time the influence of negative bias decreases. As only very small amount of bias is needed in the growth process the growth of *c*-BN nuclei continues at low bias voltages. However, deposition of new *c*-BN nuclei requires high energy ion bombardment provided by DC bias. Thus increasing deposition time under the influence of decreasing bias, nucleation of new *c*-BN particles decreases. *h*-BN that doesn't require bias thus increases in the thin film with

deposition time. Increasing bias during growth can cause high internal stresses or resputtering of the films. Under these conditions higher F is needed in the plasma to efficiently etch *h*-BN from the thin films.

From the discussion above it can be concluded that for thin films with higher percentage of *c*-BN:

1. Bias voltages lower than 60V volts during nucleation and bias current lower than around 10 mAmps are needed
2. BF_3/H_2 ratio should be close-to 1 and,
3. Higher F is needed during the growth process to efficiently etch *h*-BN under lower bias conditions.

To increase fluorine in the plasma BF_3 flow rates would need to be increased. Since BF_3 is 10% in Ar increasing BF_3 increases the Ar content in the plasma chamber. Also, since the BF_3/H_2 ratio should be close to 1 increasing BF_3 flow rates require increase in H_2 flow rates. A large quantity of N_2 with respect to BF_3 is required for effective nitrogen incorporation in the films and to prevent boron from depositing as boron powder. Therefore, N_2 flow rate needs to be increased as well. Helium gas acts as an ionizing gas and helps in maintaining plasma density. With more gases in the plasma chamber higher He flow rates would be required to maintain high plasma density.

Zhang et al [70], used such high flow rates of gases and demonstrated synthesis of high quality *c*-BN thin film at 2mTorr pressure using ECR-MPECVD. However, in our MPECVD system such high flow rates produce much higher deposition pressures, causing reduction in ion energy and decrease in plasma density. To achieve lower pressures under high flow rate conditions, required for the synthesis of good quality *c*-BN thin film higher capacity

turbomolecular pump is needed. Using the current turbomolecular pump a 30sccm total flow rate results in a minimum pressure of 50mTorr. Zhang et al. [70] reported 2mTorr pressure at 200sccm flow rates. At this point we therefore concluded that under the current deposition conditions a maximum of 66% *c*-BN can be deposited in our ECR-MPCVD system. For further improvement in the quantity of %*c*-BN in our thin films a higher capacity turbomolecular pump is needed.

CHAPTER 6

CONCLUSIONS AND RECOMMENDATION FOR FUTURE WORK

1. The MPECVD system was successfully modified to incorporate indigenously build negative DC bias and quartz feed through. The feed-through was used to introduce boron precursor in the deposition chamber separate from other gases.
2. Boron Nitride thin films with a maximum of 66% cubic phase, estimated from FTIR spectra of the films, were successfully deposited using 10%BF₃ in Ar + N₂ + Ar + H₂ + He gases by ECR-MPECVD.
3. A correlation between the process parameters used for synthesis of the thin films and the %*c*-BN observed in them shows that for further improvement in the quality and quantity of *c*-BN in the thin films a more efficient turbomolecular pump capable of maintaining much lower pressures under higher gas flow rates is needed.
4. Film grown using 10% B₂H₆ in H₂ + NH₃ + H₂ gases were mainly *h*-BN in nature. The quality of *h*-BN in the thin films is related to the deposition pressure and improves with increasing pressure. The quality of *h*-BN showed better improvement with pressure for films deposited with NH₃ as the first precursor gas.

Recommendations for future work

1. Thin films synthesis with 10%BF₃ in Ar + N₂ + Ar + H₂ + He gases in the ECR mode of the MPECVD system upgraded with a higher capacity turbo-molecular pump that can support lower pressures at higher flow rates should be attempted.
2. Diamond thin film on Si should be used as substrate.

3. Higher bias voltage and higher hydrogen flow rates during nucleation can help in rapid nucleation of cubic-BN. Lower bias and hydrogen flow rates should be used during growth which may result in lower growth rates but help in etching *h*-BN efficiently thus increasing the %*c*-BN in the film.

PART IV

**EFFECT OF SUBSTRATE PRE-TREATMENT AND DEPOSITION
TEMPERATURE ON THE STRUCTURE, RESIDUAL STRESSES AND
THERMAL CONDUCTIVITY OF DIAMOND THIN FILMS**

CHAPTER 1

INTRODUCTION

Diamond with its excellent thermal conductivity (22W/cmK) and high electric resistance ($\sim 10^{12}$ ohm cm) is an ideal material for heat sink applications for modern shrinking integrated circuits [83]. The extreme thermal conductivity of 22W/cmK is observed only for type IIa natural diamond, which because of obvious reasons of high cost, small size and limited availability cannot be used for electronic applications. However, with advancements in thin film engineering, it is now possible to grow high quality diamond thin films over large areas with good growth rates that can potentially be used for heat sink applications. The thermal conductivity of most diamond thin films, though lower than natural diamond, can reach up to 12-16 W/cmK [84], which is still very good for heat sink applications.

Diamond thin films deposited by chemical vapor deposition (CVD) possess excellent chemical, mechanical, electrical, thermal and optical properties that can be tailored to specific application requirements by making changes to the deposition parameters [85]. Over the last few years attention in the diamond thin film field has shifted towards nanocrystalline and ultrananocrystalline diamond thin films deposited by CVD [98-104]. The nano-crystalline

diamond thin films are attractive for their applications in the electronic industry as heat spreaders, MEMS/NEMS devices and moving mechanical devices because of their better substrate coverage and smoother surfaces [108, 109].

For applications as heat sink/heat spreader diamond thin films are to be deposited directly on the integrated circuits. The conventional techniques of substrate surface activation, for diamond nucleation and, the deposition temperatures are however not suitable because of their damaging effects. It is therefore important to investigate newer nucleation techniques and study the effect of lower deposition temperatures on the quality of nanocrystalline diamond thin films.

It was demonstrated that by addition of varying percentages of Ar to CH_4+H_2 plasma, morphology of diamond thin films could be changed from microcrystalline to nano-crystalline. A considerable amount of work is being done towards understanding the effect of deposition parameters on the properties of the nanocrystalline diamond thin films deposited with more than 90% Ar [105-107, 109-112]. It was however reported by our group [86] that the best quality of diamond crystals, identified by smallest full-width-half-maximum (FWHM) of the characteristic Raman-shift peak for diamond, are obtained for thin films deposited with 39% H_2 , 60%Ar, and 1% CH_4 plasma chemistry. In another study [87] using the above plasma chemistry we reported the deposition of diamond thin films on Si and SiC substrates in the temperature range of 370 – 530°C.

In the present study, using the same plasma chemistry, diamond thin films were synthesized on Si substrate activated for diamond nucleation by conventional substrate abrasion method and by nano-seeding technique employing diamond sol. The thin films were deposited in the temperature range of 600 – 800°C. The films deposited were characterized for

diamond quality, non-diamond content in the films, residual stress, and thermal conductivity by XRD, SEM, Raman and FTIR.

CHAPTER 2

LITERATURE REVIEW

Thermal conductivity is a phenomenon of phonon transfer for covalently bonded materials [88]. A defect free single crystal diamond is the most densely packed structure with no obstruction to transfer of vibrations/phonons and therefore gives the exceptional thermal conductivity. Presence of faults or defects in the diamond crystal causes excess scattering of phonons resulting in loss of phonons and thus decrease in thermal conductivity. In case of diamond thin films along with defects within the diamond crystal, grain boundaries [104, 115], absorbed hydrogen [96, 106, 113, 114], absorbed nitrogen [103, 115], and non-diamond phase present at grain boundaries, contribute to the excess scattering of phonons and thus decrease thermal conductivity of the films.

Efforts have been concentrated in trying to improve thermal conductivity of diamond thin films by improving their quality. Comparison between deposition techniques revealed that films deposited with microwave plasma CVD technique show better thermal conductivity than those deposited with hot filament CVD and electron assisted CVD [88]. Thin films of diamond are generally deposited using Hydrogen-Methane plasma with high concentration of H_2 in the gas mixture. Studies have shown that 0.5% CH_4 in H_2+CH_4 gas mixture gives diamond thin films with higher thermal conductivity than the films grown with 1-2% CH_4 in the plasma [90, 91]. However, at 0.5% CH_4 the growth rate is very low and only increases with increasing CH_4 flow rates [88] with decrease in diamond quality above 2% CH_4 [89]. With further increase in CH_4 in the plasma, hydrogen content in the diamond films increases exponentially [90].

Amongst diamond films grown using MPECVD technique microcrystalline diamond films have thermal conductivity higher than the nanocrystalline diamond thin films. Local Thermal conductivity of polycrystalline diamond films measured by Graebner et al. [91] showed an increase in conductivity from bottom to top surface. With columnar growth observed for polycrystalline diamond film by CVD, the increase in thermal conductivity is associated with decrease in non-diamond phase, decrease in micro-cavities and decrease in grain boundary as the size of diamond crystallites in the growing film increases.

Since thermal conductivity in diamond thin films is hindered by the presence of grain boundaries and defects within the diamond crystals, efforts have been put in trying to reduce the grain boundary density and to improve the quality of diamond in the thin films. Although synthesis of the single crystal diamond by CVD technique is still very difficult, success has been achieved in growing highly oriented films with (001) and (111) orientations, with (001) oriented diamond films showing better thermal conductivity than the (111) oriented diamond films [92]. Diamond (001) oriented thin films grown by three step process of bias enhanced nucleation, etching by hydrogen with bias, and then growth, resulted in films with high thermal conductivity of 14W/Kcm [90]. The increase in thermal conductivity was attributed to decrease in grain boundaries in the oriented films. Amongst (001) oriented diamond films, films grown epitaxially show higher thermal conductivity than the oriented films with random fiber texture. The increase in thermal conductivity in the epitaxially grown diamond film is credited again to decrease in the grain boundaries [93].

In spite of all the developments in improving the quality and thermal conductivity of diamond thin films the use of the films as heat sink on integrated circuits is restricted by the need to bias the substrate and/or by the conventional substrate activation techniques that results

in abrasion of the surface. Other factors that restrict the use of polycrystalline thin films include: pin-holes observed in thin films of only few micron thickness requiring higher thickness for better film coverage, hydrogen trapped in the thin films, rough surface of the film [89] and the ever decreasing size of the integrated circuits making it difficult for nucleation in the trenches of the ICs.

Nano-seeding techniques have been studied to increase nucleation density and to improve the quality and continuity of very thin films [94-97]. Most of the techniques [112-114], however, are not suitable for treatment of sensitive substrates such as integrated circuits (ICs), owing to the damages they induce on the substrate. A simple technique of using diamond colloidal solution was developed by Makita et al. [97]. The method uses purified 3-6nm diamond particles suspended in methyl alcohol, 0.2% HF and water solution. Seeding of diamond was performed by simple dipping of cleaned Si substrate in the diamond colloidal solution. The technique involved no biasing of the substrate or the nano-particles, nor does it involve any kind of surface scratching with the diamond nano-particles and is therefore very promising.

In this study, diamond sol of 3-6nm diamond particles, was used to seed Si (100) substrates for diamond deposition. For comparison purposes diamond films were also grown on Si (100) substrates pre-treated in the conventional way employing 20-40 μ m diamond slurry and ultrasonic activation. The influence of Si substrate pre-treatment by nano-seeding using 3-6nm diamond sol and by ultrasonic activation using 20-40 μ m diamond slurry is investigated with respect to its effect on crystal structure, morphology, residual stress and thermal conductivity of the thin films. Also studied is the effect of deposition temperature on the crystal structure, residual stress and thermal conductivity of the diamond thin films deposited

on the two types of pre-treated Si substrates. Scanning electron microscopy, grazing angle x-ray diffraction, Fourier transform infrared spectroscopy and Raman spectroscopy were used to investigate the morphology, crystal structure, hydrogen absorption, and residual stresses in the diamond thin films deposited at 600, 700 and 800°C. Thermal conductivity of the diamond thin films was measured using Photothermal Reflectivity method using Ar-ion and He-Ne laser.

CHAPTER 3

OBJECTIVE AND RESEARCH PLAN

The objective of this part of the research is two fold:

1. Study the effect of deposition temperature on the morphology, quality, stress and thermal conductivity of diamond thin films deposited using Ar/H₂/CH₄::60/39/1 plasma chemistry
2. Study the effect of substrate pre-treatment on the morphology, quality, stress and thermal conductivity of the deposited diamond thin films.

The main idea behind this part of research is to compare and contrast the compatibility of substrate pre-treatment by diamond sol with conventional substrate pre-treatment technique of scratching the substrate surface with micron size diamond powder in a ultrasonic bath. Substrate pre-treatment with diamond sol could potentially replace conventional abrasion and bias-enhanced nucleation techniques for applications of diamond thin films in electronic industry as heat sinks. The effect of the substrate pre-treatment on the morphology, stress and thermal conductivity of the deposited diamond thin films is compared with the diamond thin films deposited on Si substrate pre-treated in the conventional method. Also studied in this part of the thesis is the effect of deposition temperature on the morphology, quality, stress and thermal conductivity of the deposited diamond thin films.

Argon rich plasma with 60% Ar, 39% H₂ and 1% CH₄ is used for the diamond deposition to take advantage of the plasma chemistry's ability to grow nano-diamond. With nano-diamond in the thin film, the coverage of the thin film improves significantly reducing

micro-cracks that are normally observed for diamond thin films with thickness less than $1\mu\text{m}$ and deposited using only H_2 and CH_4 plasma.

CHAPTER 4

EXPERIMENTAL

Microwave plasma enhanced chemical vapor deposition (MPECVD) system described in Part I was used for the synthesis of diamond thin films. Si (100) wafers were cleaned in acetone, alcohol and water before treating with 5% HF solution to remove native oxide layer from the top surface. The cleaned Si wafers were then immediately transferred to 3-6 nm diamond sol or 20-40 μ m diamond slurry for surface pre-treatment. Si substrates treated with 3-6nm diamond sol were simply dipped in the sol for 2 hours. Si substrates treated with 20-40 μ m diamond slurry were ultrasonically activated for 2 hours. The substrates were then cleaned with distilled water and dried with dry nitrogen before placing them into the deposition chamber. The samples were placed on a molybdenum disc which was kept directly on top of the graphite heating stage. The deposition chamber was then evacuated to a base pressure of 10^{-6} Torr before adding the precursor gases.

The substrates were exposed to H₂ plasma etching for 10 minutes before starting diamond deposition at 20 Torr pressure and 600W microwave power with substrate temperature set at 600°C. This was done to make sure that any native oxide layer on Si substrate that might have been formed between the time the substrate was cleaned and the plasma started, was removed. Table 4.1 list details of the conditions used during deposition.

Table 4.1: Process parameters used for diamond thin film deposition by MPECVD

Pre-Treatment	3-6 nm Diamond Sol, or 20-40 μm Diamond Slurry
H ₂	39 sccm
Ar	60 sccm
CH ₄	1 sccm
Pressure	85 Torr
Power	900W
Temperature	600 – 800°C
Time	72 – 96 hrs

Experiments were done at substrate temperatures of 600, 700 and 800°C measured by IR pyrometer capable of measuring temperature in a plasma environment. The calibration of the IR pyrometer is explained elsewhere [87]. Surface morphology of the films was studied by environmental scanning electron microscopy (Phillips XL 30 ESEM-FEG). Phillips X'Pert diffractometer with Cu-K α radiation of 1.54Å wavelength was used to obtain X-ray diffraction patterns of the thin films. Raman spectra of the film were obtained using NICOLET ALMEGA Raman spectroscope employing a 532nm frequency doubled Nd:YVO₄ DPSS laser. Fourier transform infrared spectroscopy (FTIR) was used to estimate adsorbed hydrogen in the thin films. A BIO-RAD FTS-40 FTIR spectrometer in transmittance mode was used to collect the data averaged over 128 scans with a resolution of 4cm⁻¹.

CHAPTER 5

RESULTS AND DISCUSSIONS

Diamond thin films deposited using the conditions mentioned in Table 4.1 were investigated with respect to the effect of substrate pre-treatment and deposition temperature on the quality, morphology, residual stress and, thermal conductivity. For applications in the electronic industry, the nano-seeding technique is compared with the conventional ultrasonic activation technique, to establish the difference in quality of the diamond thin films deposited on Si substrates treated with the two methods.

Nano-seeding techniques have been studied to increase nucleation density and to improve the quality and continuity of very thin films [94] [95-97]. Shaik et al. [96] demonstrated that by decreasing the diamond particle size used in dry polishing technique for seeding from 0.1 μm to 4nm increased the nucleation density almost 600 times to $1.5 \times 10^{12} \text{cm}^{-2}$. Although the techniques increase the nucleation density appreciably cannot be used for depositing thin films on integrated circuits (ICs) because of abrasive effects during dry polishing.

Electrostatic seeding technique developed by Malshe et al. [94] used electrostatically charged diamond particles that imping on target substrate which was biased to attract the charged particles. The charged particles adhered to the substrate by electrostatic force and were used as nuclei for deposition of diamond thin films. This technique although fast and versatile with respect to diamond particle size and substrate geometry, can be damaging to the integrated circuits.

Electrophoretic seeding technique reported by Valdes et al. [95] used the substrate material as positive electrode and a gold plated monel disk as negative electrode in dispersion containing 0.2g/l of diamond in 18 Mohm-cm water. With this seeding technique nucleation density could be controlled by controlling the electric field applied and time used for seeding. The technique though promising with respect to control of nucleation density cannot be applied to ICs because of the use of electric field.

A simple technique of using diamond colloidal solution was developed by Makita et al. [97]. The method used purified 3-6nm diamond particles suspended in methyl alcohol, 0.2% HF and water solution. Seeding of diamond was performed by simple dipping of cleaned Si substrate in the diamond colloidal solution. In the study presented, this diamond sol technique was used to seed Si (100) substrates for diamond deposition. For comparison purposes diamond was also grown on Si(100) substrates activated with 20-40 μ m diamond crystals by ultrasonic activation.

For a variety of application of diamond thin films in electronic, electrical, biological and other fields, the substrate materials can get damaged very easily under the conventional deposition temperatures for diamond thin films of around 800°C. It is therefore required to further optimize the deposition techniques for temperature sensitive substrate materials. In an effort towards synthesis and characterization of diamond thin films deposited over a large variation in substrate temperature, we previously [87] reported deposition and characterization of diamond thin films on Si (100) substrates in the temperature range of 370 – 530°C using 1% CH₄, 39% H₂ and 60%Ar plasma chemistry. In this study using the same plasma chemistry, along with the effects of substrate pre-treatment, effect of deposition temperature in the range

of 600 – 800°C is investigated with respect to morphology, quality, residual stresses and, thermal conductivity of the deposited diamond thin films.

5.1 Surface Morphology of Diamond Thin Films

Figure 5.1 shows the SEM micrographs of films deposited under different conditions. In each micrograph in Figure 5.1 on the upper left corner, is the average grain size of the respective film. It is seen that for both types of substrate pretreatment the average grain size decreases with decreasing deposition temperature. Films grown at 800°C on both types of pre-treated Si substrate have smooth faceted crystals structure with an average grain size of 6µm. Films grown at 700 and 600°C have smaller grains (2.9 to 4.7µm) with rough surfaces indicative of grain growth by secondary nucleation. Growth by secondary nucleation refers to the increase in size of grains by constant formation of new nuclei on top of initial/existing nuclei, instead of growth of a single nucleus into a complete grain. At higher deposition temperatures the depositing species have higher mobility on the growth surface that helps the nuclei to coalesce with adjacent nuclei reducing grains boundaries/surface energy resulting in smooth faceted grains. At lower deposition temperatures the mobility of the depositing species on the growth surface is limited by their low thermal energies and therefore the coalescence of the nuclei is also limited resulting in rough surface.

At 800°C deposition temperature, the high density of twins observed for films on both types of pre-treated substrates suggests that the twinning phenomenon is mainly influenced by the deposition temperature and not by the substrate pre-treatment. Steeds et al. [98] did TEM investigation of such twinned structure and concluded that each grain is actually an

agglomerate of multiple grains/crystallites with a small variation in growth direction joined together at twin boundaries.

Carbon C_2 radicals formed in the plasma are the primary growth species for diamond thin film deposition in Ar rich environment [98]. The presence of rough surface, indicative of secondary nucleation for films deposited at 700 and 600°C, in contrast to the absence of rough surfaces for films grown at 800°C suggests that at this temperature the C_2 radicals settling onto the depositing films have sufficient kinetic energy and mobility to form a uniform and smooth surface by fully coalescing with the larger grains. However, at lower deposition temperatures the energy and mobility of the radicals probably decrease below the level needed for complete coalescence of the smaller crystallites with the bigger grains causing incomplete coalescence and rough surface of the films.

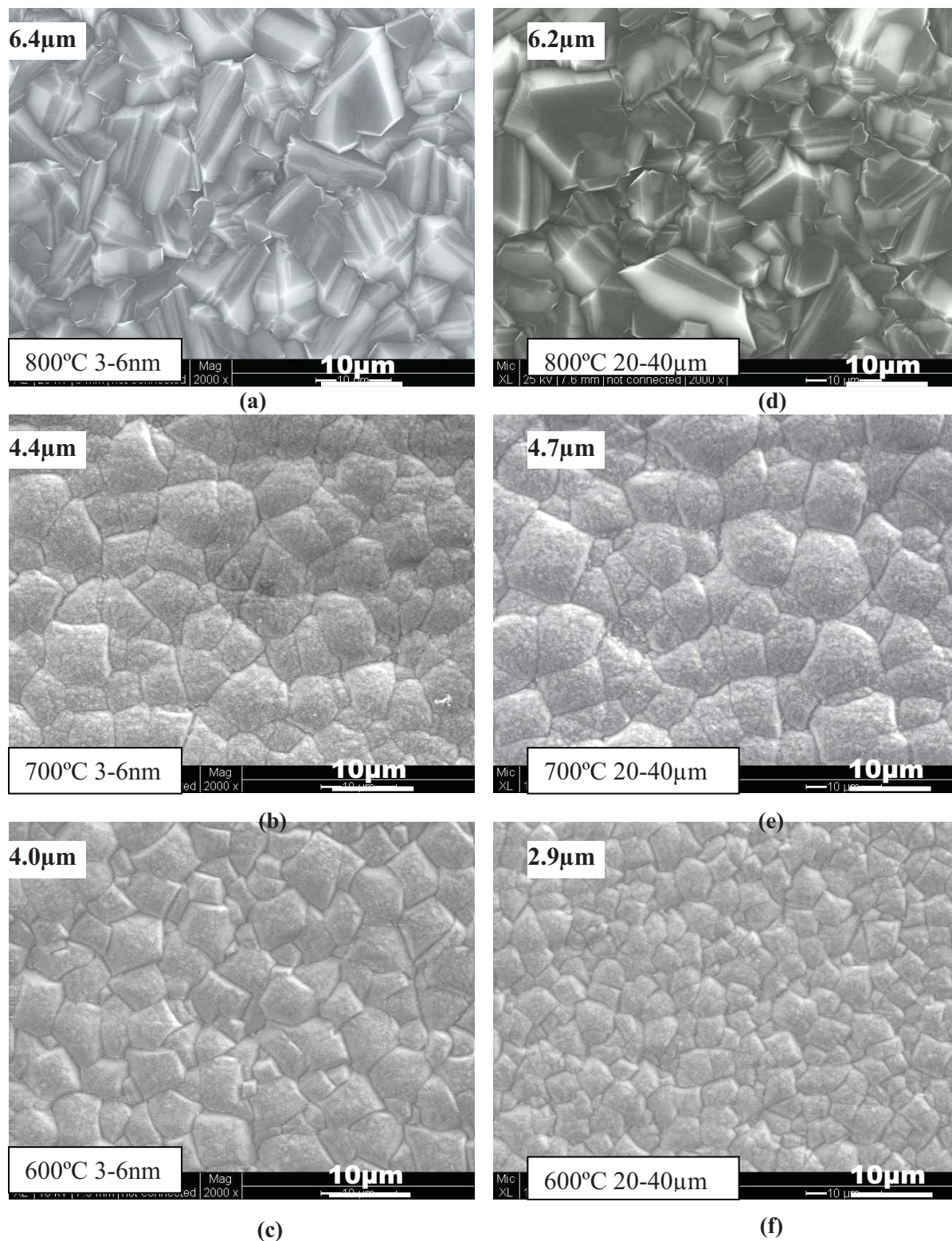


Figure 5.1: SEM micrographs of diamond thin films deposited at 800, 700 and 600°C. (a-c) Diamond thin films on Si substrate pre-treated with 3-6nm diamond sol, and (d-f) diamond thin films on Si substrate pre-treated with 20-40µm diamond slurry. Inset on the left top corner shows the average grain size of the thin films.

5.2 FTIR Spectroscopy for Hydrogen Absorption

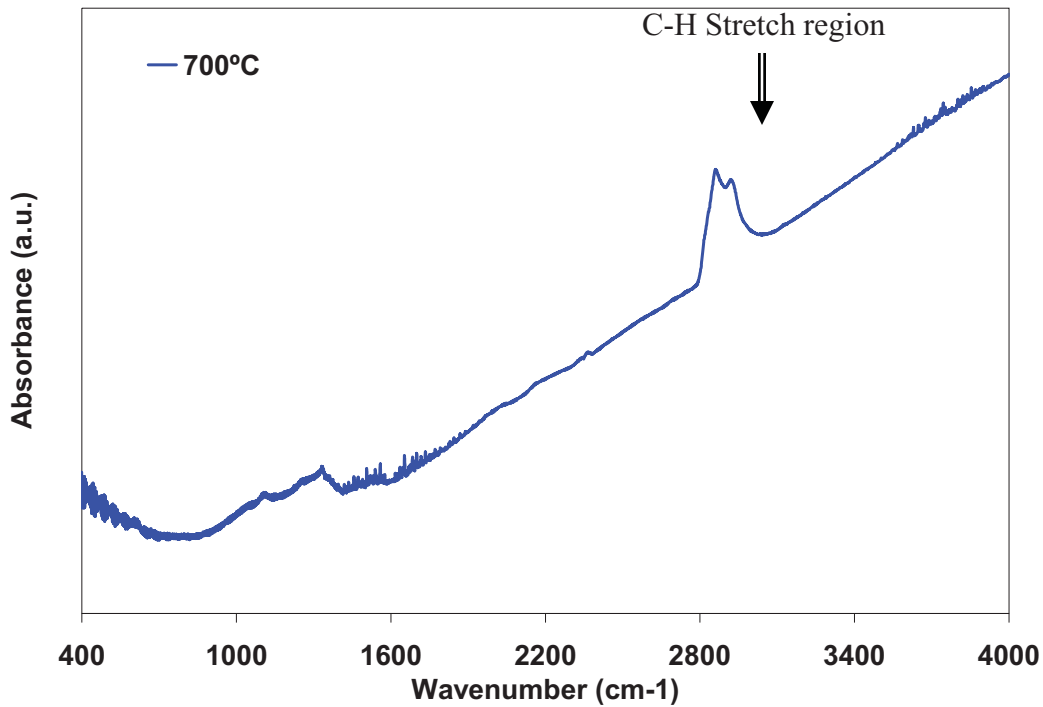


Figure 5.2: Typical FTIR spectrum observed for the diamond thin films deposited at 700°C.

Fourier transform infrared spectroscopy in the transmission mode was used to investigate hydrogen absorption in the films. FTIR spectra were collected over a region of 400 – 4000 cm^{-1} with a resolution of 4 cm^{-1} . Figure 5.2 shows a typical FTIR spectrum observed for the diamond thin film of this study. The C-H stretch region (2700-3300 cm^{-1}), which contains information about hydrogen bonded to carbon is investigated in detail. Slight shifts in the bond vibration frequencies in the C-H stretch region are related to different local environments that are used to distinguish between CH_x groups [99]. The spectra were corrected for the linearly increasing absorption background before deconvoluting by Gaussian functions [99] in the C-H stretch region using Peak Fit software [100] as shown in Figure 5.3. To account for thickness variation of the thin films the FTIR spectra was normalized using the intrinsic two-phonon absorption features for diamond between 1700 and 2650 cm^{-1} [101].

Peaks observed in our films were assigned to specific vibration groups as per literature [5, 126], and are listed in Table 5.1. As can be seen from the table, hydrogen is bonded to both sp^3 and sp^2 bonded carbon, which means that hydrogen is not only trapped at the non-diamond grain boundaries but is also present within the diamond structure as defects.

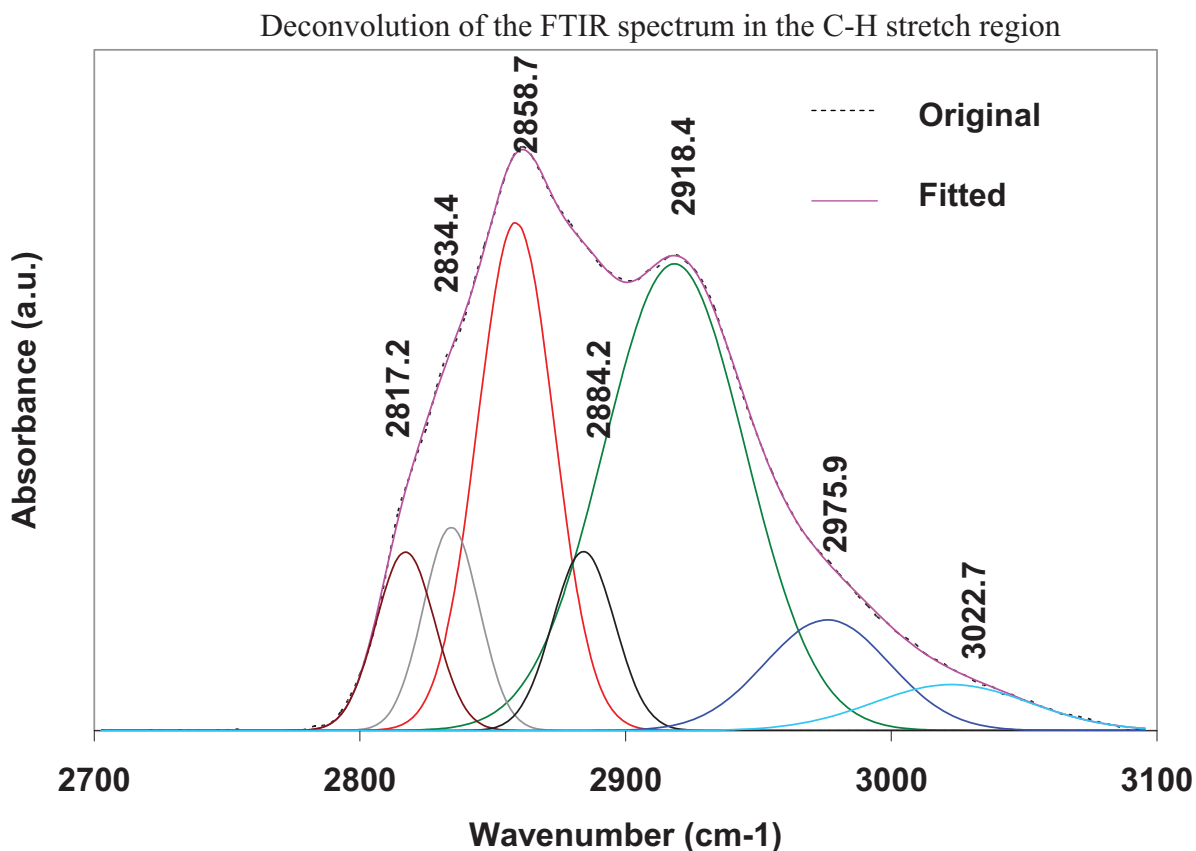


Figure 5.3: C-H stretch region of the FTIR spectrum for diamond thin film grown at 700°C fitted using PeakFit software.

Since the integrated intensity of each deconvoluted peak observed is related to quantity of the C-H bonds for that specific vibration group, the overall integrated intensity of the C-H stretch band from 2800 – 3100 cm^{-1} is proportional to the total amount of hydrogen present in the diamond films. We used the total integrated area under the C-H stretch region to study

Table 5.1: Characteristic vibration frequencies observed in FTIR spectra of the diamond thin films [1, 2].

Wavenumber (cm ⁻¹)	Characteristic group
2819	CVD diamond specific
2833	CVD diamond specific
2850	Symmetric sp^3 CH ₂
2880	Symmetric sp^3 CH ₂
2920	Asymmetric sp^3 CH ₂
2960	Asymmetric sp^3 CH ₂
2980	Symmetric sp^2 CH ₂
3025	Sp^2 CH
3080	Asymmetric sp^2 CH ₂

comparative H₂ incorporation in the diamond thin films with respect to the deposition temperature and substrate pre-treatment.

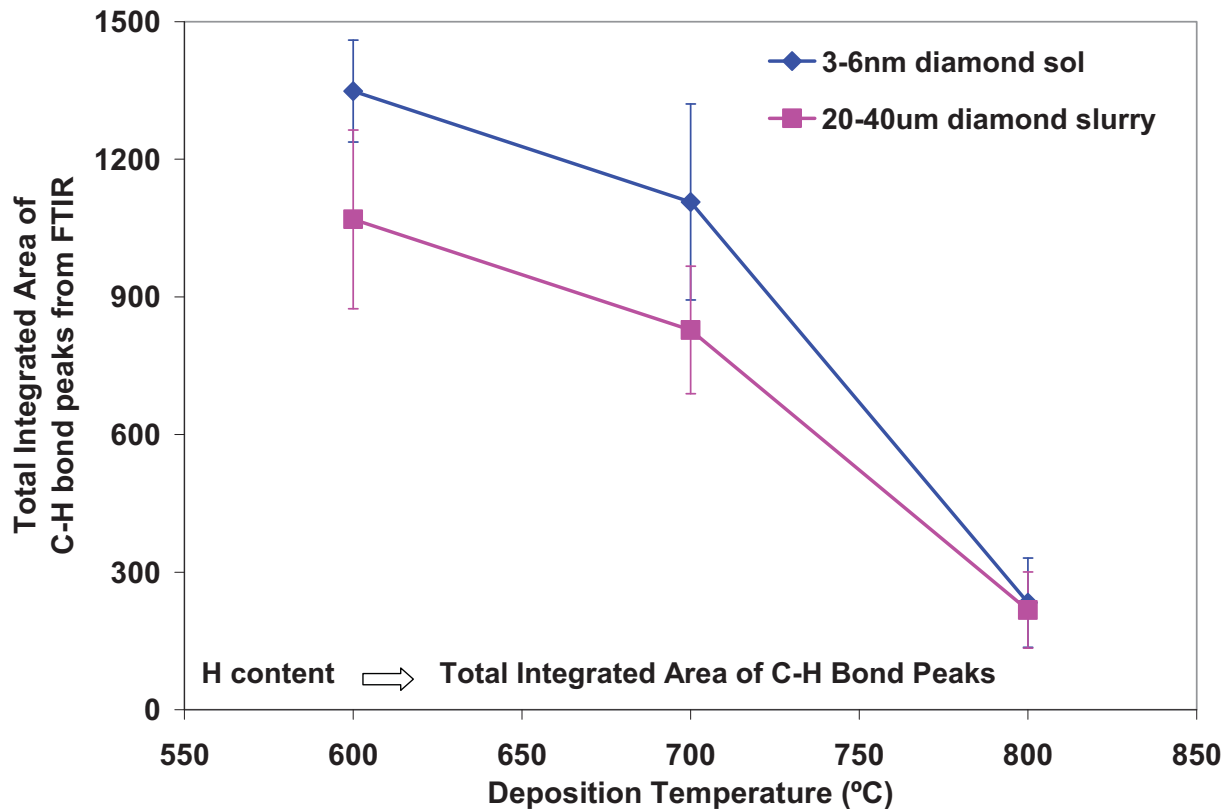


Figure 5.4: Effect of deposition temperature and substrate pre-treatment on the hydrogen absorption in diamond thin films

Figure 5.4 gives the effect of deposition temperature and Si substrate pre-treatment on the hydrogen incorporation into the diamond thin films. The hydrogen trapped in the films decreases with increasing deposition temperature suggesting that at higher deposition temperatures H₂ trapped in the growing film escapes more easily than it does at lower deposition temperatures. Also, with decreasing deposition temperature the efficiency of hydrogen abstraction decreases resulting in increase in trapped hydrogen [102]. Another consequence of decrease in hydrogen abstraction is the increase in non-diamond phase in the thin films as observed by Raman spectroscopy.

At lower temperature the hydrogen trapped in the diamond films is higher for films grown on Si substrate pre-treated with 3-6nm diamond sol than for films deposited on Si pre-treated with 20-40 μ m diamond slurry. This is probably associated with the lower diamond yield (higher non-diamond phase) in the films as observed from Raman spectroscopy.

5.3 Diamond Quality and Yield by Raman Spectroscopy

The diamond thin films were characterized by micro-Raman spectroscopy over the range of 900 to 1800cm⁻¹ with a 532nm frequency doubled Nd:YVO₄ DPSS laser. Figure 5.5 shows the Raman spectra of diamond films deposited at 600, 700 and 800°C on Si substrate pre-treated with 20-40 μ m diamond slurry and 3-6nm diamond sol. Diamond films deposited at 600 and 700°C show the diamond peak around 1332cm⁻¹ followed by a broad hump at around 1500cm⁻¹ associated with non-diamond phases present in the films. Diamond films deposited at 600°C substrate temperature also show a hump around 1200cm⁻¹, which is ascribed to

transpolyacetylene in the thin films [105, 120]. Diamond thin films deposited at 800 °C do not show any hump around 1500cm^{-1} indicative of the near absence of non-diamond phases.

The deconvolution of the Raman spectra for the thin films was done using Peak Fit software [100]. Diamond yield and residual stress in the thin films are calculated from the deconvoluted Raman spectra. The high intensity background observed in films deposited at 600 and 700°C deposition temperatures, is due to fluorescence, which yields a background of increasing intensity with increasing wave number [103]. Before fitting the diamond and non-diamond peaks with Lorentzian and Gaussian functions, respectively, a linear baseline was subtracted from the spectrum. A typical fitted curve after base line correction and the deconvoluted peaks is shown in Figure 5.6 for diamond thin film deposited at 600°C on Si (100) substrate pre-treated with 20-40 μm diamond slurry. Besides sp^3 -bonded diamond and sp^2 -bonded graphite “D” and “G” bands at 1330, 1360 and 1580 cm^{-1} , respectively, several other peaks at 1188, 1301, 1471, 1550 and 1680cm^{-1} are also observed in the fitted spectrum. The peaks at 1188, 1301 and 1471 cm^{-1} are ascribed to transpolyacetylene and amorphous carbon [111, 128, 129], the peak at 1550 cm^{-1} originates from diamond like carbon (DLC), while the peak at 1680cm^{-1} is probably from tetrahedral amorphous carbon (*ta*-C), which is a DLC with the highest sp^3 -carbon content [104].

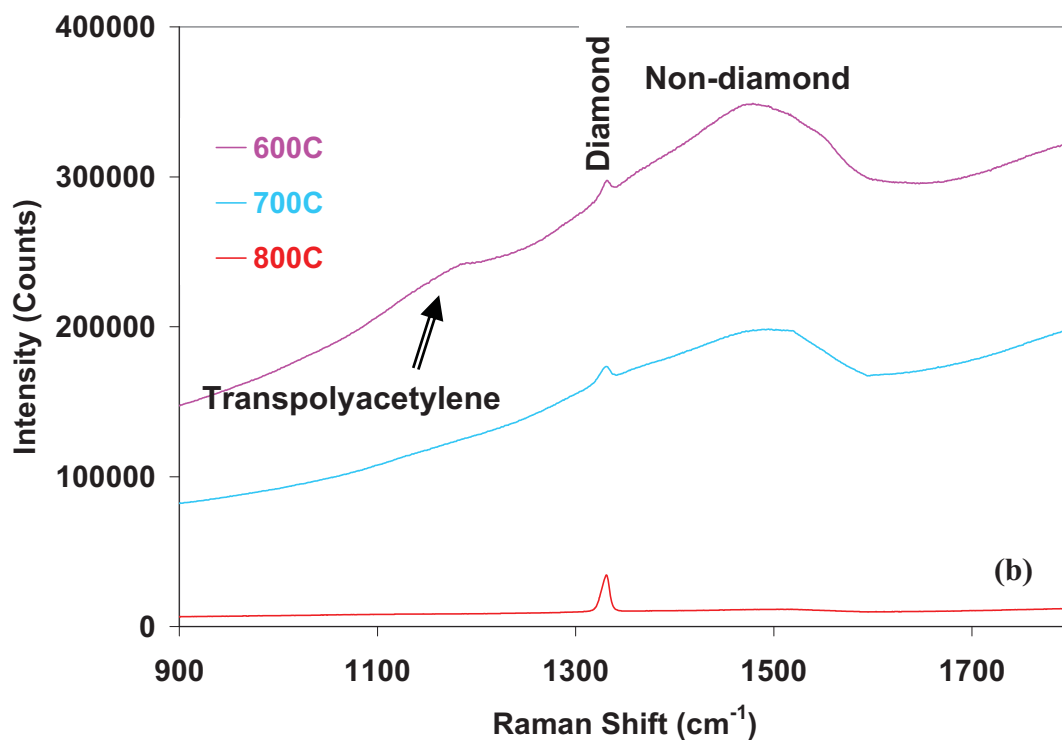
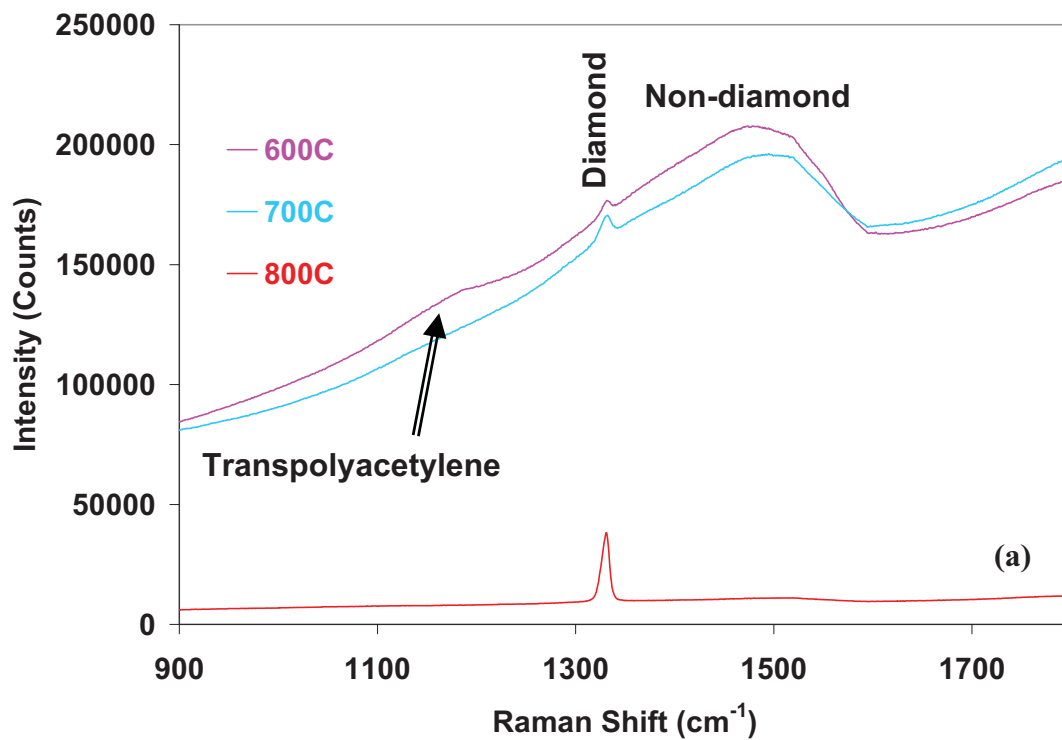


Figure 5.5: Raman spectra of diamond films deposited at different temperatures, from (a) films on Si pre-treated with 20-40 μm diamond slurry, and (b) films on Si pre-treated with 3-6 nm diamond sol

The FWHM (full width half maximum) of the diamond peak for each film was determined from the fitted curves. The FWHM is directly related to the quality of the diamond crystals in the films. The smaller the FWHM the better is the quality of the diamond. Figure 5.7 shows the FWHM of the diamond peak as a function of the deposition temperature. It can be seen that the films deposited at 800°C have the best quality of diamond with the lowest FWHM. Also evident from the plot is that the quality of diamond films grown on Si substrate pre-treated with 3-6nm diamond sol is better than that on Si substrate pre-treated with 20-40 μ m diamond slurry, for all the deposition temperatures studied. The improvement in quality of diamond although not dramatic can be attributed to direct growth of diamond on the 3-6nm diamond particles acting as nuclei avoiding nucleation that often results in formation of *a*-C (amorphous carbon) layer before nucleation occurs [87] and, to the lower residual stress observed for the films.

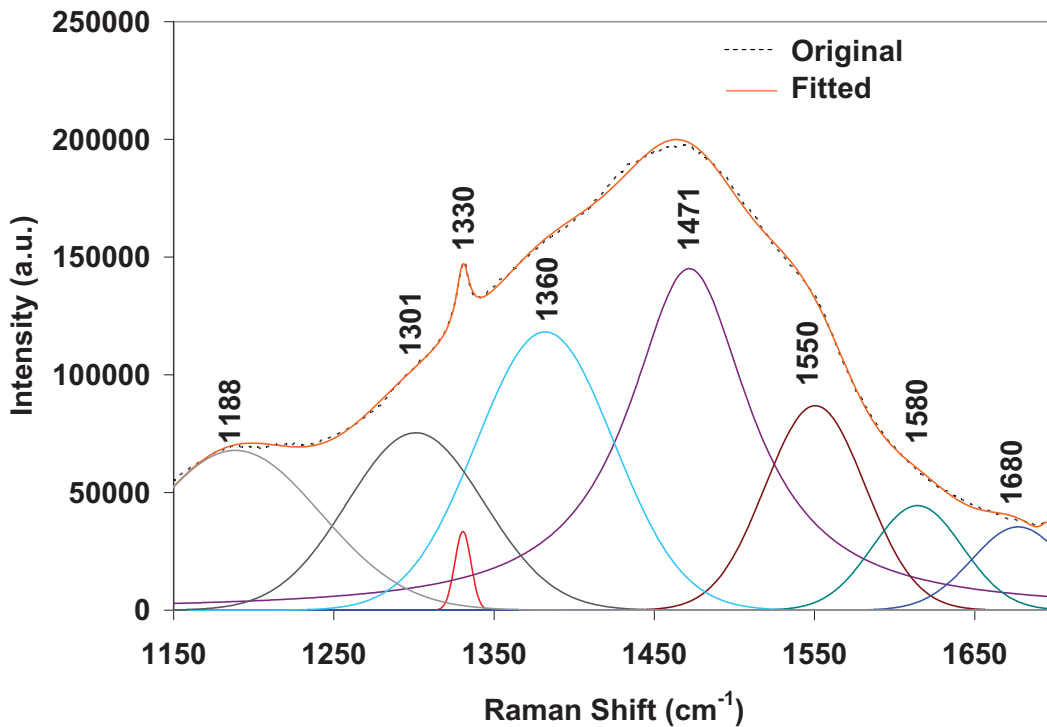


Figure 5.6: Raman spectra for 600°C diamond thin film on Si pre-treated with 20-40 μ m diamond slurry fitted with Peak Fit software.

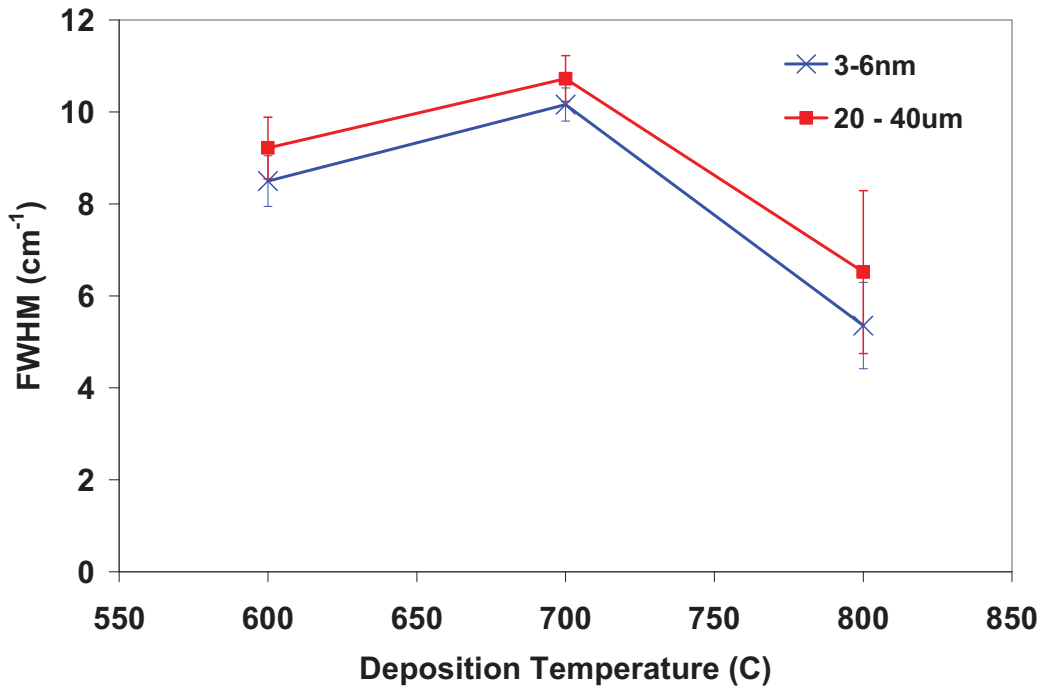


Figure 5.7: Variation of FWHM of diamond peaks from Raman spectroscopy with deposition temperature and substrate pre-treatment.

Diamond yield was calculated from the fitted Raman spectrum using the following formula,

$$Yield(\%) = \frac{A_d}{A_d + \sum_i \left[\frac{A_i}{\chi_i} \right]} \times 100 \quad (5.1)$$

Where A_d is the integrated area under the diamond peak and A_i is the integrated area under the peak for the “ i^{th} ” non-diamond component with scattering cross-section χ_i . The scattering cross section values used for various non-diamond components for calculating diamond yield of the films are reported elsewhere [86, 105]. Diamond yield for the films as shown in Figure 5.8 increases with increasing deposition temperature and reaches almost 100% for films deposited at 800°C. It is evident from the plot that diamond yield for films deposited at higher temperatures is not affected by the substrate pretreatment. However, at lower temperatures

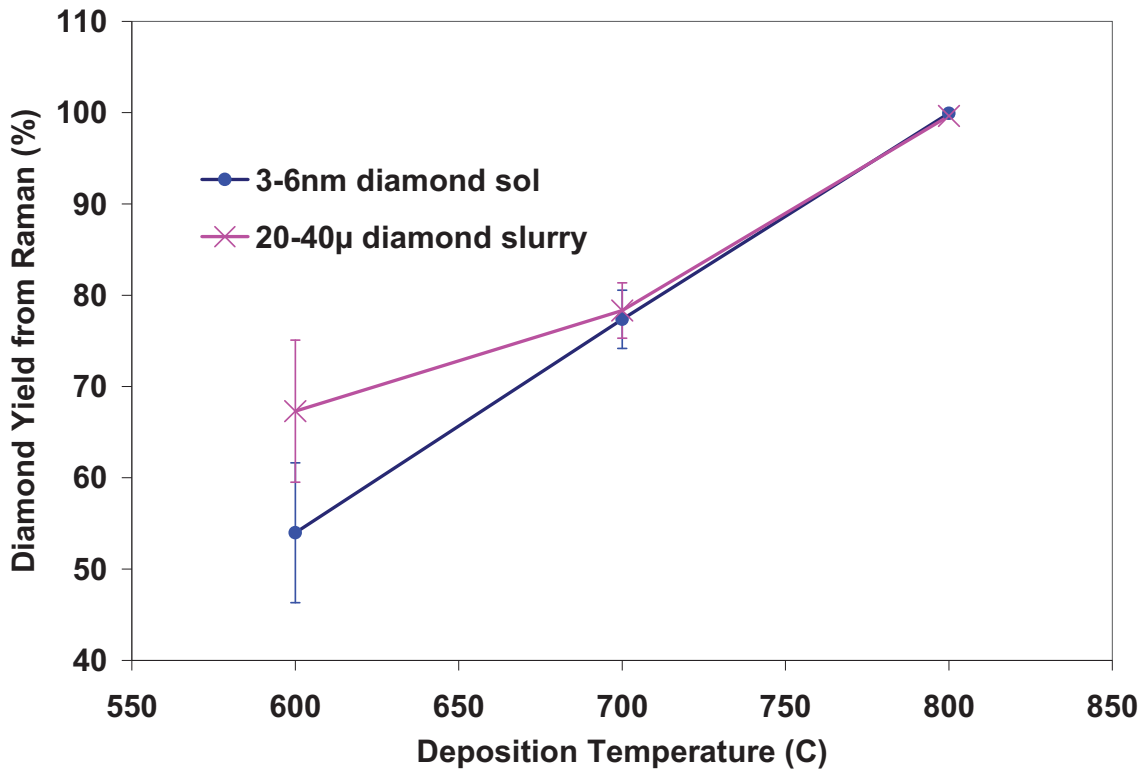


Figure 5.8: Effect of deposition temperature and Si substrate pre-treatment on diamond yield estimated from Raman spectra of the thin films

diamond films on 20-40µm diamond slurry pre-treated Si substrates show higher diamond yield.

The decrease in diamond yield at lower temperatures can be explained by the growth process. As described by Gruen et al. diamond grows by C_2 molecules and C-C dimer interaction in an Ar rich atmosphere [110]. It involves impinging of C_2 molecules and inserting one C atom in the surface of a C-C dimer and then inserting the other C atom into an adjacent C-C dimer bond to form a new surface carbon dimer. According to another study [106] on temperature dependent growth rate of diamond thin films by 99% Ar +1% CH_4 plasma, the % C_2 molecules formed in the plasma utilized for diamond deposition decreases with decreasing temperature. This along with reduced hydrogen abstraction rates at lower

temperatures as evident from FTIR can cause a decrease in diamond yield and increase in non-diamond yield in the films with decrease in deposition temperature.

The relatively higher percent of diamond yield for films on Si substrates pre-treated with 20-40 μ m diamond slurry, in comparison with films on Si substrate pre-treated with 3-6nm diamond sol and deposited at same temperature can be explained from the FTIR results. As mentioned before, with decrease in deposition temperature the efficiency of hydrogen abstraction decreases [102]. The hydrogen abstraction reaction not only removes non-diamond phases from the growing film but also removes the hydrogen attached to the C atoms of the growing film. Therefore with reduced abstraction efficiency at lower deposition temperatures the trapped hydrogen and non-diamond phases in the films increases, decreasing the diamond yield. The comparatively less trapped hydrogen in diamond films on Si substrate pre-treated with 20-40 μ m diamond slurry as observed from FTIR thus indicates relatively better hydrogen abstraction efficiency on the films. Better hydrogen abstraction results in better removal/etching of non-diamond phase from the thin films.

Thus the decrease in diamond yield with decreasing deposition temperature can be ascribed to the two factors mentioned above i.e. decrease in diamond growth rate due to reduced consumption of C₂ molecules and the decrease in hydrogen abstraction efficiency. The difference in the diamond yield at same deposition temperature for the two types of substrate pre-treatments is attributed to the difference in hydrogen abstraction.

5.4 Residual Stress by Raman Spectroscopy

Residual stress present in diamond thin films is calculated from the Raman shift of the diamond peak using the following formula,

$$\sigma_{\text{exp}} = -\frac{\Delta\nu}{\alpha} = \frac{(\nu_0 - \nu)}{\alpha} \quad (5.2)$$

where σ_{exp} is the total stress in the film, α is the pressure coefficient and, ν_0 and ν are the Raman peak positions for unstressed and stressed diamond, respectively. Taking the pressure coefficient, $\alpha = 1.9\text{cm}^{-1}/\text{GPa}$ for the unstressed diamond with $\nu_0 = 1332.3 \text{ cm}^{-1}$ [87] and the Raman shift observed for our diamond peaks, stress calculated for the thin films shows the presence of a tensile stress. Table 5.2 gives the residual stress values calculated using Equation 5.2. For both types of substrate pre-treatments, the residual stress in the films increases with deposition temperature. The residual tensile stress ranges from 0.47 GPa for diamond films on Si substrate pre-treated with 3-6nm diamond sol and deposited at 600°C, to 1.35 GPa for diamond films on Si substrate pre-treated with 20-40 μm diamond slurry and deposited at 800°C. Figure 5.9 shows dependence of the stress on deposition temperature. Comparison of residual stress with diamond yield suggests that the increase in stress is probably directly related to the diamond yield of the films. Higher the diamond yield higher is the stress in the films.

Table 5.2: Residual tensile stresses in diamond thin films on Si substrates pre-treated with 3-6nm diamond sol and 20-40 μ m diamond slurry and deposited at different temperatures.

Deposition Temp. ($^{\circ}$ C)	Residual Stress (GPa)	
	3-6nm Diamond Sol	20-40m Diamond Slurry
600	0.47	0.66
700	0.78	0.75
800	1.1	1.35

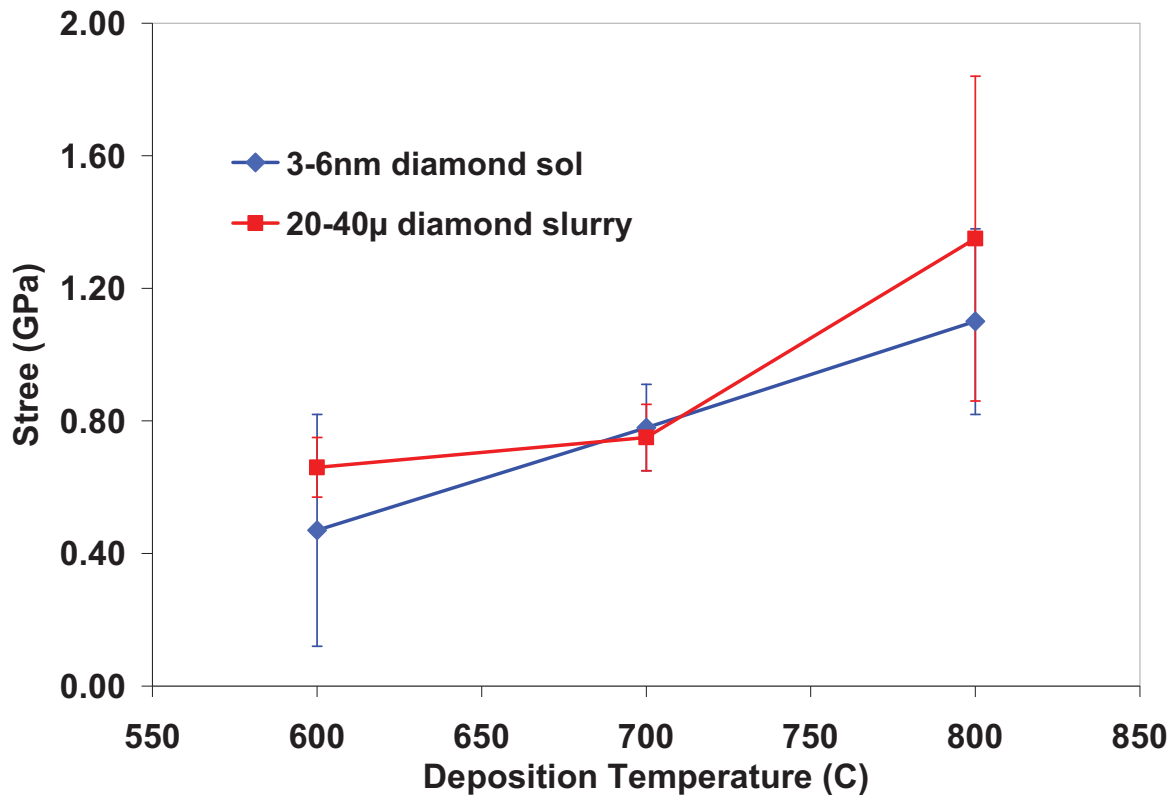


Figure 5.9: Effect of deposition temperature and Si substrate pre-treatment on residual stress in the diamond thin films calculated from the Raman spectra.

5.5 Crystallite Size from X-Ray Diffraction

From SEM micrographs it was observed that the diamond films deposited at 600 and 700 $^{\circ}$ C have agglomerated grain. The exact size of the smaller crystallites that make the agglomerates is however not clear from SEM. X-Ray diffraction patterns were therefore obtained for the films to calculate the average crystallite size using Scherrer's equation.

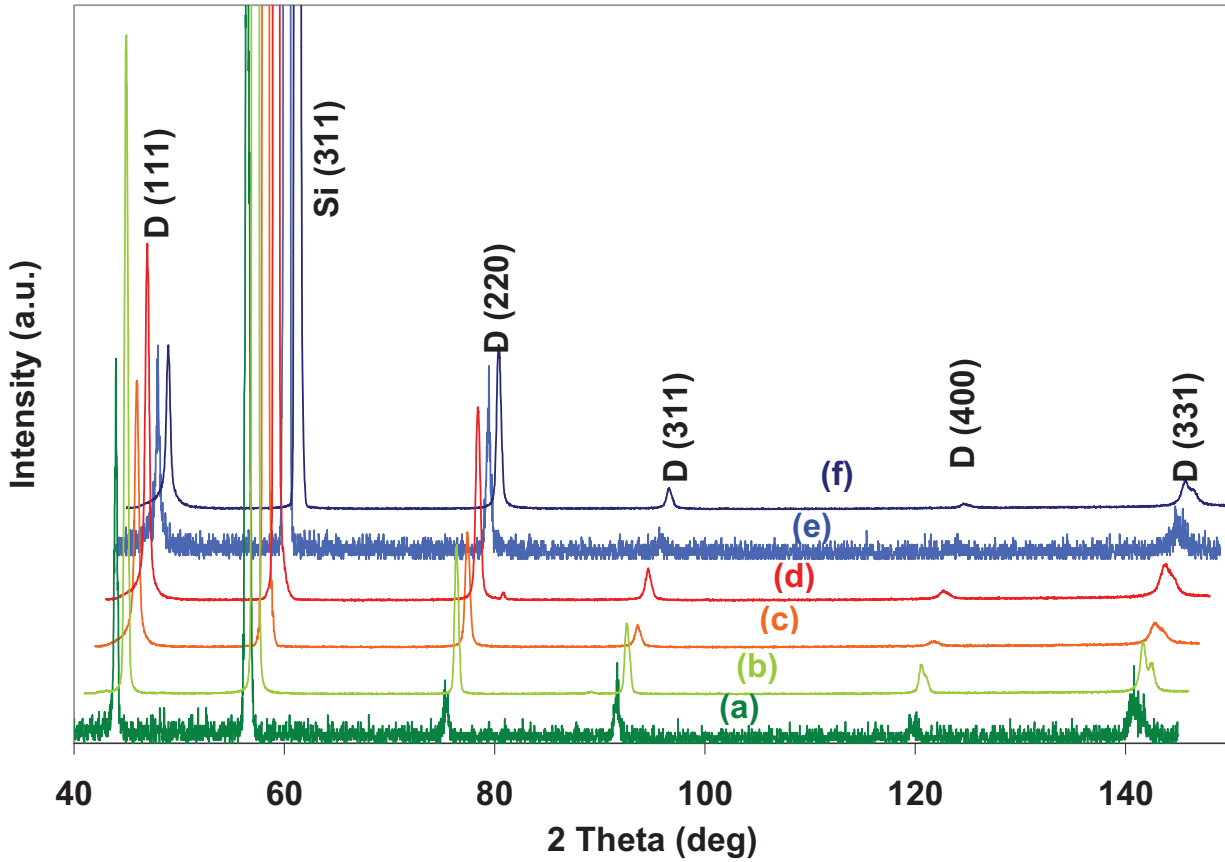


Figure 5.10: Effect of deposition temperature on crystal structure of the diamond thin films. For clarity purposes the patterns are shifted to the right in increments of $1^\circ 2\theta$, and up in increments of 2000 counts. Patterns (a), (c) and (e) represents diamond thin films on Si substrate pre-treated with 20-40 μ diamond slurry and deposited at 800, 700 and 600 $^\circ$ C respectively. Patterns (b), (d) and (f) represent diamond thin films on Si substrate pre-treated with 3-6nm diamond sol and deposited at 800, 700 and 600 $^\circ$ C respectively.

X-ray diffraction from thin films was performed on a Philips X'Pert Pro with Cu – $K\alpha$ radiation of wavelength 1.540598 \AA . A grazing angle XRD technique was used with an incident angle of 3° . Figure 5.10 shows the XRD results. Diffraction peaks of diamond (111), (220), (311), (400) and (331) oriented crystals at 43.98, 75.41, 91.66, 119.73 and 140.23 $^\circ 2\theta$, respectively, are clearly seen for all the samples. It is seen that the Si (311) peak at 56.3 $^\circ 2\theta$ is the dominating peak for all the samples.

The Diamond (220) peak intensity, as seen in Figure 5.10, increases with respect to the Diamond (111) peak with decreasing deposition temperature. Similar observation was

previously reported by our group for diamond thin films deposited at even lower temperatures [87]. The increases of the relative intensity of (220) peak indicates the preferred orientation of the diamond crystals in the [110] direction [108, 132]. Table 5.3 gives the intensity ratio $I_{(220)}/I_{(111)}$ observed for the diamond thin films in comparison with the intensity ratio observed for a standard diamond powder.

Table 5.3: $I_{(220)}/I_{(111)}$ ratio for diamond thin films deposited at different temperatures and substrate pre-treatment in comparison with standard diamond powder.

Deposition temperature (°C)	$I_{(220)}/I_{(111)}$		
	Si pre-treated with 3-6nm diamond sol	Si pre-treated with 20-40 μ m diamond slurry	Diamond powder
600	0.9016	1.0032	0.2883
700	0.4359	0.5519	0.2883
800	0.1272	0.2307	0.2883

It is seen from Table 5.3 that with decreasing deposition temperature the $I_{(220)}/I_{(111)}$ ratio increases, indicating preferential orientation in the [110] direction. Chu et al. [105] in their study on growth kinetics of (100), (110) and (111) homoepitaxial diamond films found that highest growth rates were observed for [110] direction. They attributed the high growth rates to the high density of carbon atoms in the [110] direction. In a complementary study Cheng et al. [107] observed hydrogen plasma etching anisotropy on diamond single crystals using single-pass Brewster-angle transmission spectroscopy of CH stretches on (111), (110) and (100) surfaces. It was discovered that hydrogen etching is highly anisotropic at higher temperatures with preferential formation of <111> oriented facets at the expense of (110) and (100) planes. In light of the above discussions, we can assume that the preferential <110> orientation of the

films deposited at lower temperatures is due to the combined effect of higher growth rate of planes in the [110] direction and the reduced etching of the <110> planes under the low temperature conditions because of low hydrogen abstraction.

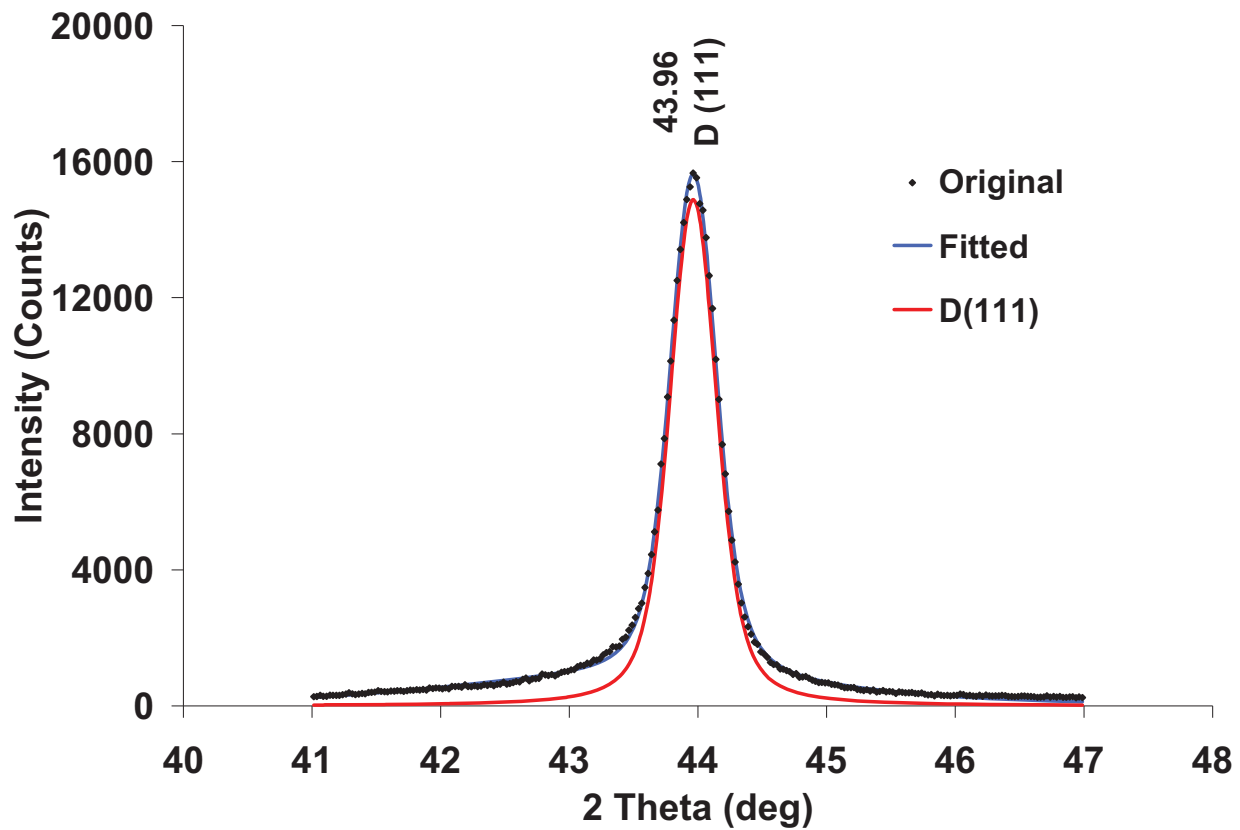


Figure 5.11: Typical diamond (111) diffraction peak, fitted with Voigt Area using Peak Fit Software. The peak in the figure is from XRD pattern of diamond thin film deposited at 700°C on Si substrate pre-treated with 20-40 μ diamond slurry.

The (111) and (110) diffraction peaks of diamond were fitted by Voigt Area [107] using Peak Fit software for films deposited at 600 and 700°C. Figure 5.11 shows a typical fitting profile for D(111) peak. The FWHM of the observed peaks was investigated to calculate the average grain size of the diamond crystallites using Scherrer's equation [108]:

$$D = \frac{0.89\lambda}{B\cos\theta} \quad (5.3)$$

Where D is the crystallite size, λ is the wavelength of the incident Cu-K α radiation of 1.540598Å, B (in radians) is the FWHM of the fitted peak after subtracting the FWHM of the incident beam, and θ (in radians) is the Bragg's angle of diffracted peak. The Scherrer's equation can only be used for very small crystallites sizes generally in the nano-meter range and is therefore not used for grain size calculations for diamond films deposited at 800°C. Table 5.4 gives the crystallite size measured for diamond films deposited at 700 and 600°C on Si substrate pre-treated with the two types of the nucleation treatment. The crystallite size is similar for the two deposition temperatures and substrate pre-treatments and is in the range of 21 – 28nm. The average crystallite size thus measured is used for calculating grain boundary stress in the films.

Table 5.4: Crystallite size measured from XRD patterns of the thin films using Equation 5.3.

Si substrate Pretreatment	Deposition Temperature (°C)	Average D
		Nm
3-6nm diamond sol	600°C	28.15492
	700°C	21.42782
20-40µm diamond slurry	600°C	22.66894
	700°C	22.13907

5.6 Stress Measurement and Analysis

In general, the residual stress in CVD diamond thin films can be ascribed to three different sources i.e., thermal stress (σ_{th}), intrinsic stress (σ_{in}), and stress due to lattice mismatch (σ_{lm}) between Si substrate and diamond thin film. Thermal stress in a film is related

to the coefficient of thermal expansion (CTE) and the difference in CTE of substrate and the film, while intrinsic stress is associated with defects, impurities and grain boundaries. Thus the total theoretical stress (σ_T) in the film can be expressed by,

$$\sigma_T = \sigma_{th} + \sigma_{in} + \sigma_{lm} \quad (5.4)$$

The lattice mismatch between diamond and Si is almost 52%. The stress associated with such a mismatch normally results in a large ($\sim 200\text{cm}^{-1}$) Raman shift of the characteristic diamond peak at 1332cm^{-1} [87]. Also this type of stress is primarily associated with hetero-epitaxial growth. Such a large shift in the diamond peak is not observed for any of our films and therefore the contribution of the lattice mismatch to the overall stress in the films is ignored. Equation (5.4) can thus be reduced to,

$$\sigma_T = \sigma_{th} + \sigma_{in} \quad (5.5)$$

Thermal stress present in the films can be calculated from the following equation:

$$\sigma_{th} = \left[\frac{E_d}{(1-\nu_d)} \right] \int_{T_1}^{T_2} (\alpha_s - \alpha_f) dT \quad (5.6)$$

Where T_1 and T_2 are the deposition temperature and room temperature, respectively, E_d is the Young's modulus of diamond (1210 GPa) and ν_d is the Poisson's ratio (0.1) of diamond, α_s and α_f are the coefficients of thermal expansion of the substrate (Si) and film (diamond),

respectively. The temperature dependent thermal expansion coefficient behaviors for Si and diamond reported in reference [104, 134] were used for the calculation of thermal stress in this study. Compressive stresses in the range of 0.522 to 0.551 GPa were calculated.

In diamond thin films, the intrinsic stress related to impurities, defects and, grain boundaries is mostly dominated by stress due to grain boundaries [109]. For our calculations we therefore assume that the grain boundary stresses are dominant in our films and therefore σ_{in} can be replaced by σ_{gb} (grain boundary stress).

The origin of the grain boundary stress is associated with grain growth. During growth as the grains come within a few atomic distances of each other, they exert an attractive force towards each other in an attempt to reduce their combined surface energy by forming a grain boundary that has a much lower surface energy [134-136]. The individual grains, however, are bonded to substrate and/or with other grains, and therefore resist the movement of grains due to attraction between them. Formation of grain boundary under this condition is then achieved by stretching of the grains towards each other. The mechanism, known as constrained relaxation, thus introduces tensile stress in the growing film by causing tensile strain in the individual grains [110] which is inversely proportional to the average grain diameter as,

$$\sigma_{gb} = \left[\frac{E}{(1-\nu)} \right] \frac{\delta}{d} \quad (5.7)$$

where δ is the constrained relaxation of the lattice constant of diamond and is found to be 0.077nm [109], and d is the average grain diameter of the diamond film. The average grain diameter measured by SEM micrographs (800°C data) and calculated from XRD patterns (700 and 600°C data) were used as d in Equation (7) for diamond films. The calculated grain

boundary tensile stress varies from 0.016 GPa for films deposited at 800°C to 4.8 GPa for films deposited at 700°C.

Table 5.5 summarizes the calculated thermal and grain boundary stresses along with the observed residual stresses in diamond thin films. The tensile stress due to constrained relaxation observed at the grain boundaries is multiplied by diamond yield observed from Raman spectroscopy to calculate the stress contribution of the diamond grain boundaries (σ_{dgb}). It is observed from the table that the calculated diamond grain boundary stress is much higher than the observed residual stresses measured by Raman spectroscopy. The difference in the observed residual stress and the total calculated stresses ($\sigma_{dgb} + \sigma_{th}$), the excess intrinsic stress ($\Delta\sigma$), is compressive for diamond thin films deposited at 600 and 700°C and tensile for diamond thin films deposited at 800°C, as given in Table 5.5.

Table 5.5: A summary of calculated and experimental residual stresses for diamond thin film on Si substrates pre-treated with 3-6nm diamond sol or 20-40 μ m diamond slurry and deposited at different temperature.

Si Substrate Pretreatment	Dep. Temp. (°C)	σ_{th} (GPa)	σ_{gb} (GPa)	D yield (%)	σ_{dgb} (GPa)	σ_{exp} (Gpa)	$\Delta\sigma = \sigma_{exp} - \sigma_{dgb} - \sigma_{th}$ (Gpa)
3-6nm Diamond Sol	600	-0.551	3.67	54	1.98	0.47	-0.959
	700	-0.546	4.83	77.4	3.74	0.78	-2.414
	800	-0.522	0.016	99	0.016	1.1	1.606
20-40 μ m Diamond Slurry	600	-0.551	4.56	67.3	3.07	0.66	-1.859
	700	-0.546	4.67	78.3	3.66	0.75	-2.364
	800	-0.522	0.017	99	0.017	1.35	1.855

$$\sigma_{dgb}^* = \sigma_{gb} \times \text{volume fraction of diamond in the thin films}$$

The excess intrinsic compressive stress for diamond thin films deposited at 600 and 700°C can be attributed to the large amounts of non-diamond carbon, such as graphite and to

trapped hydrogen in films as observed by Raman and FTIR spectroscopy. According to Windischmann [111] the specific volume of sp^2 bonded carbon i.e. graphite is 1.5 times larger than that of diamond. During deposition the simultaneous growth of graphite and diamond results in graphite pushing against the adjacent diamond particles and generating a compressive stresses in the growing thin films. In addition hydrogen trapped in the interstitial sites in diamond thin films, accumulates at the crevices and micropores in the films [111]. The accumulation causes increase in volume of hydrogen at the local sites. The increased volume of hydrogen in the crevices and micropores exerts pressure on adjacent particles generating compressive stresses in the film. Thus the high excess intrinsic stress in the thin films deposited at 600 and 700°C can be attributed to the large amounts of non-diamond carbon and trapped hydrogen in the thin film.

The difference in stress observed for the thin films on Si pretreated with 3-6nm diamond sol and 20-40 μ m diamond slurry can be attributed to diamond nucleation on the two types of pre-treated substrates. On Si pre-treated with 3-6nm diamond sol, diamond nanoparticles from the sol adhere to the Si surface by electrostatic force and act as nuclei for diamond growth. Diamond thin films deposited on these nuclei are not directly bonded to the Si substrate and therefore stress associated with expansion mismatch between substrate and film is probably at its minimal. In case of Si pre-treated with 20-40 μ m diamond slurry diamond nuclei are chemically bonded to Si by a thin interfacial layer of Si-C [42]. Additionally, nuclei form in the crevices and sharp edges of the scratches, caused by ultrasonic activation, on the Si surface that provides the nuclei additional mechanical bonding. Diamond thin films on these nuclei are therefore strongly bonded with the surface and hence the stress associated with

expansion mismatch between substrate and film is higher than that observed for Diamond on Si pre-treated with 3-6nm diamond sol.

Films deposited at 800°C as observed from SEM are highly twinned with grain size of approximately 6µm. From XRD data we find that the intensity ratio $I_{(220)}/I_{(111)}$ for diamond thin films deposited at 800°C (Table 5.3) is smaller than that for standard diamond powder suggesting some $\langle 111 \rangle$ texturing in the film. Wit [110] explained the formation of partial disclinations at the twin boundaries when two (111) planes growing parallel to the growth direction merge to form a twin. Growth by secondary nucleation, as is the case in an Ar rich plasma environment, often results in nuclei oriented almost parallel to each other that grow to join at the twin boundaries. When three or more twin planes merge together, wedge/star disclinations are created that induce strain in the growing crystal [110]. Steeds [98] used TEM to show that each large grain, such as those observed for 800°C diamond thin films in this study, consists of a number of individual smaller grains that are related to each other by common twinning operations consistent with the common growth direction. These smaller grains connected to each other by two, three, four or five-fold junctions form wedge/star disclinations. Wit calculated the radial and circumferential stresses associated with partial disclinations for an infinitely long isotropic cylinder as:

$$\sigma_{rr} = \frac{0.026G}{2\pi(1-\nu)} \ln\left(\frac{r}{R}\right) \quad (8)$$

$$\sigma_{\phi\phi} = \frac{0.026G}{2\pi(1-\nu)} \left(\ln\left(\frac{r}{R}\right) + 1 \right) \quad (9)$$

Where σ_{rr} is the radial stress, $\sigma_{\phi\phi}$ is the circumferential stress, r is the distance from the center of the disclination, R is its outer radius, G the shear modulus and ν is the Poisson's ratio. While

the radial stress associated with twinning due to disclination remains compressive, according to Steeds [98] stresses within the grains increase as R increases, with the result that the circumferential stress becomes tensile for bigger grains.

Michler et al. [112] did micro-Raman stress measurements on less strained $\langle 001 \rangle$ planes and correlated the results with TEM investigation of the same areas. They observed inhomogeneous stress distribution within a single grain. Within a grain, areas that had twins or dislocations, tensile stress was observed, while areas away from the dislocations/twins and free of any defects showed compressive stresses. This confirms the argument of Wit and Steeds that twinning, which is a type of dislocation, results in the generation of tensile stresses in the diamond thin film during growth. Since the diamond thin films deposited at 800°C in this study have (111) texture and have a very high density of twins as observed from SEM, we can construe, as per the discussion above, that the residual tensile stress in the films is due to stresses associated with twin formation during growth. Also worth noting is the near absence of non-diamond carbon and trapped hydrogen that contribute to compressive stresses in diamond thin films.

5.7 Thermal Conductivity measurement by Photothermal Reflectivity Method

Thermal conductivity of the diamond thin films was measured using Photothermal Reflectivity method explained below. Before thermal conductivity measurements, the samples were polished to mirror finish and coated with a very thin, 50 nm layer of nickel to improve reflectivity of the samples.

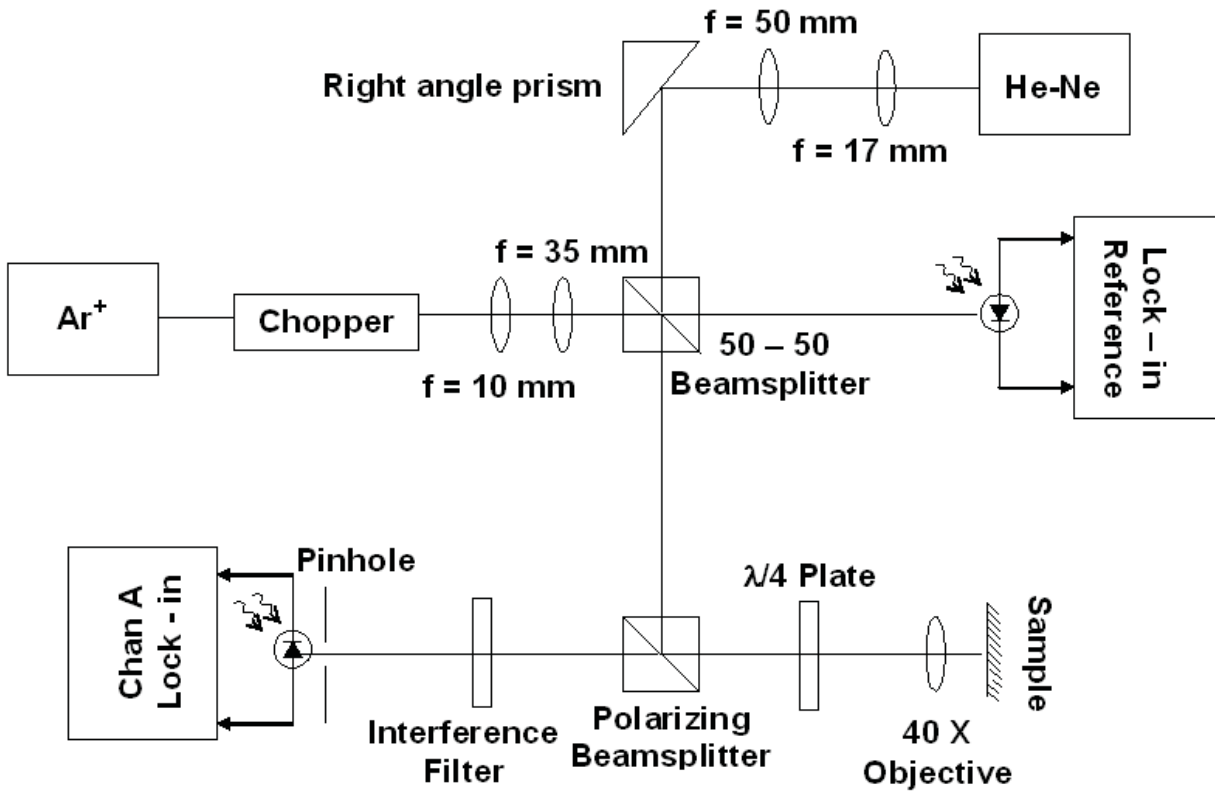


Figure 5.12 Schematic of the Photothermal Reflectivity system used for measurement of thermal conductivity of diamond thin films.

Figure 5.12 gives a schematic of the Photothermal Reflectivity system used for thermal conductivity measurements. It consists of two lasers, He-Ne (5 mW) probe laser and Ar-ion (Ar^+ ; 100 mW) pump laser. The argon-ion laser was used as a continuous square-wave with intensity modulated by a mechanical chopper with a chopping frequency of up to 20kHz. Both the lasers, argon-ion and He-Ne, are linearly polarized at the source and are combined together by a 50 – 50 beam-splitter. The combined beams are then passed through a polarizing beam-splitter, a $\lambda/4$ – wave plate and a microscope objective before focusing on the sample surface. The polarizing beam-splitters reflects light in a particular plane of polarization and transmits light that is orthogonally polarized. The plane of polarization of the reflected light from the sample gets rotated by ninety degrees after passing through the $\lambda/4$ – wave plate the second

time, and results in beam getting transmitted through the polarizing beam-splitter instead of being reflected back towards the 50 – 50 beam-splitter. The interface filter then eliminates the Ar^+ beam from the combined reflected beam, after which the reflected H-Ne laser is incident on a photodiode.

The high power intensity modulated Ar^+ laser when focused on the sample generates oscillatory heat flux of frequency corresponding to the mechanical chopper, and thus acts as the “pump” beam. The oscillatory heat flux causes thermal waves, or temperature oscillations, in the sample. These temperature oscillations are at the same frequency as the heat flux but phase shifted along the direction of heat flow. This phase shift in the thermal waves depends on the physical properties of the material (diamond) and its thermal conductivity. The temperature oscillations caused by the thermal wave results in corresponding change in the surface reflectivity, since surface reflectivity is directly proportional to the temperature of the sample. These changes in reflectivity are measured as phase shift of the low-intensity He-Ne laser, the probe laser. The He-Ne laser to be used as the probe laser is initially coincident with the Ar^+ laser and is then translated to measure the phase shift as a function of distance. The lock-in amplifier then measures the phase shift of the reflected light with respect to the chopping frequency.

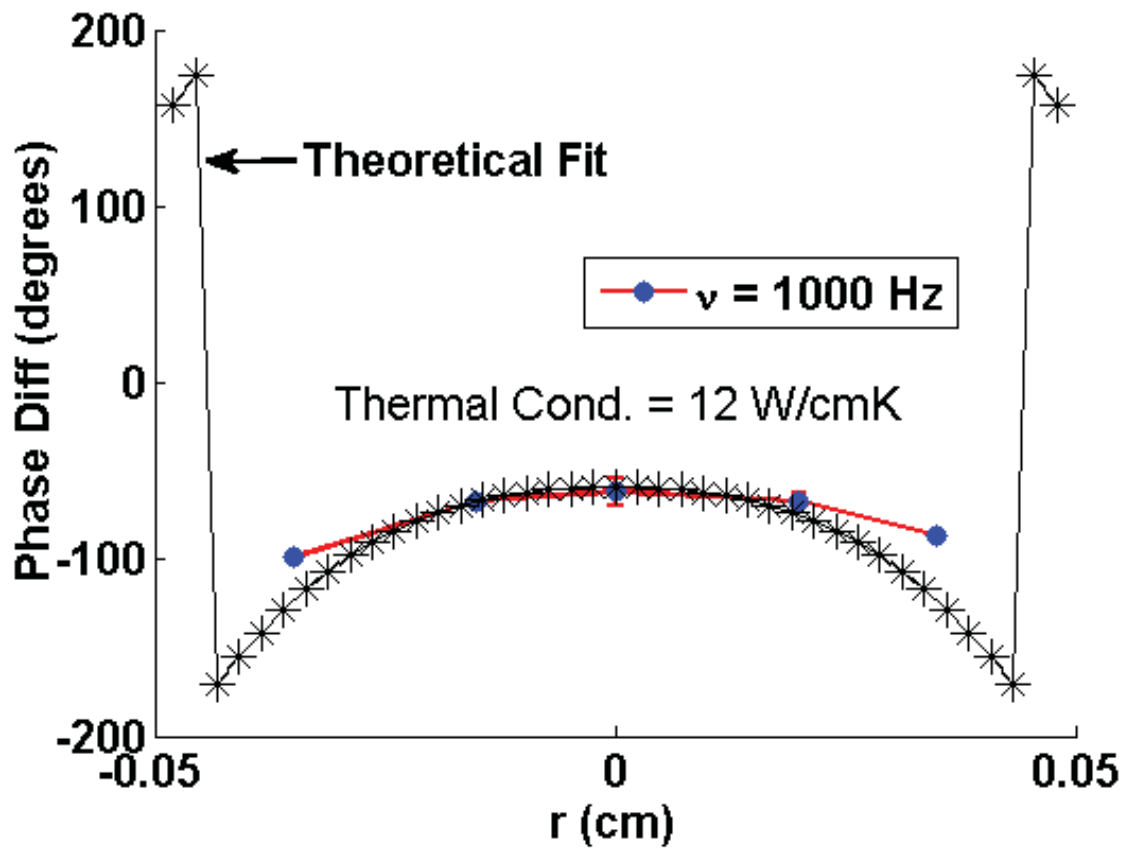


Figure 5.13: Phase profile plot of a 20 μm thick diamond film on silicon.

Thermal conductivity measurements on glass and SiC performed using the system described above showed values of 0.01 W/cmK and 3.5 W/cmK respectively, that compare well with the published values [113, 114]. Initial results on thermal conductivity measurements on diamond thin films deposited in this study match well with the literature. Thin films deposited at 800°C on Si substrates pre-treated with the two types of pretreatment show similar thermal conductivity values of 12W/cmK. For films deposited at 600°C the thermal conductivity dropped to 0.01W/cmK.

The high thermal conductivity of diamond thin films deposited at 800°C suggests that the transfer of phonons within the thin films is not obstructed by discontinuities and defects

within the thin film. The constant thermal conductivity for the diamond thin films deposited at 800°C on the two types of pre-treated substrates suggests that at the deposition temperature substrate pre-treatment doesn't affect the thermal conductivity of diamond thin films. Nano-seeding technique explored in this research can therefore be used to replace the conventional seeding technique for applications in the semiconductor industry as heat sinks where the substrates are allowed to reach high temperatures. The good thermal conductivity of diamond thin films deposited at 800°C can be attributed to the high diamond yield, large grain size and low hydrogen and non-diamond contamination in the thin films,

The low thermal conductivity for nano-crystalline diamond thin films deposited at 600°C is an indication of the excess scattering and loss of phonons at defects, grain boundaries, and inclusions in the films. The high density of grain boundaries, lower diamond yield and large quantity of trapped hydrogen in the thin films contribute to the excess scattering and loss of phonons resulting in the low thermal conductivity of the thin films.

CHAPTER 6

CONCLUSIONS

Diamond thin films deposited at different temperatures using 60% Ar, 39% H₂ and 1% CH₄, show a large variation in grain size and crystal orientation. With decrease in deposition temperature from 800 to 700°C the grain size decreases from around 6µm to 28nm, respectively. Further decrease in deposition temperature does not seem to have any effect on the grain size. Diamond thin films deposited at 700 and 600°C show preferred orientation in the <110> direction due mainly to the lower etching rates of the <110> planes at the deposition temperatures and the lower hydrogen abstraction efficiency at the deposition temperature. Films deposited at 800°C show some preference in the <111> direction. The changes in morphology and crystal orientation, however, are not affected by the type of substrate pre-treatment. The quality of diamond in the films decreases with deposition temperature. It is, however, comparatively better for all films deposited on Si substrate pre-treated with 3-6nm diamond sol as is evident from the lower FWHM for the films. These conclusions suggest that nano-seeding technique can be used to replace ultrasonic activation for applications in the electronic industry.

Residual stress observed for diamond thin films in this study was tensile in nature and increased with increasing deposition temperature. For films deposited at 600 and 700°C the residual tensile stress is attributed to high intrinsic tensile stresses at the grain boundaries generated by constrained relaxation and reduced by compressive stresses due to the high volume of non-diamond carbon and trapped hydrogen in the films. For films deposited at

800°C the intrinsic tensile stress is attributed to the high density of twins formed during the growth process and the near absence of non-diamond phases and trapped hydrogen.

Si substrate pre-treatment has a very small effect on residual stresses of the films studies. For films deposited on Si substrate pre-treated with 20-40 μ m diamond slurry the slight higher stress in comparison with films on Si substrate pre-treated with 3-6nm diamond sol was attributed to the mechanical and chemical bonding between the growing film and the substrate. This suggests that stress in diamond thin film can be reduced to a certain level by employing nano-seeding technique, like the one used in this paper, for substrate activation.

Part V

CONCLUSIONS AND RECOMMENDATION FOR FUTURE WORK

CONCLUSIONS

Thin films in the boron-carbon-nitrogen system were successfully deposited using electron cyclotron resonance equipped microwave plasma enhanced chemical vapor deposition system. The capability of the technique to provide stable deposition conditions under large variations in pressure, power and temperature and the flexibility of using a variety of precursors can be attributed to the success of the MPECVD technique. While silicon incorporated carbon nitride, hexagonal boron nitride and diamond thin films were deposited under the normal operating mode (10 – 100Torr) of the CVD system, thin films of cubic boron nitride require the low vacuum (10^{-3} Torr) conditions of the ECR mode. Thin films of diamond deposited under different deposition temperatures were possible because of the stability of the microwave plasma.

The pure hypothetical β -C₃N₄ could not be deposited because of the strong repulsion between nitrogen lone pairs caused by the very structure of the hypothetical carbon nitride that makes the structure unstable and difficult to synthesize. However, thin films of silicon incorporated carbon nitride with two different morphologies were successfully deposited. It was discovered that under the deposition conditions the morphology of these Si-C-N thin films could be controlled by controlling the sequence of introduction of the precursor gases. Well crystallized hexagonal Si-C-N crystals of size ranging up to 100 μ m (depending on the deposition pressure) are deposited when nitrogen precursor is introduced as the first precursor

gas in the deposition chamber after stabilizing the other deposition parameters. Agglomerated nano-crystals of C-Si-N with graphitic structure are deposited when carbon precursor is introduced as the first precursor gas in the deposition chamber after stabilizing the other deposition parameters. The influence of sequence of introduction of precursor gases is reported for the first time and is attributed to the electronegativity of Si, C and N.

Crystallinity of hexagonal boron nitride thin films deposited in the normal mode of MPECVD increased when ammonia was used as the first precursor gas introduced in the deposition chamber. The quality of the films was also found to be directly related to the deposition pressure.

The ECR-MPECVD system was upgraded with an indigenously built flexible bias. The flexible nature of the bias allowed its use in both the normal (MPECVD) and low pressure (ECR) mode of the system. The negative DC bias along with 10%BF₃ in Ar and, N₂ as precursor gases in the ECR mode was successfully employed to deposit thin films with 66% *c*-BN phase. It was realized that although adding negative DC bias and Fluorine helped in deposition of cubic phase of boron nitride, to deposit 100% *c*-BN phase much lower deposition pressures than can be achieved in our MPECVD system are required. However with the current lowest pressure of 50 mTorr a maximum of 66% *c*-BN with remainder *h*-BN could be deposited successfully.

MPECVD is a well know technique for the synthesis of diamond thin films. The technique was used here to study the effect of deposition temperature and substrate pre-treatment on the thermal conductivity and residual stress in diamond thin films for application as heat sink in the electronic industry.

RECOMMENDATIONS FOR FUTURE WORK

- Using MPECVD synthesize Si-C-N thin films with varying composition of C and N to explore their physical, optical and electronic properties.
- Thin films of C-Si-N can also be explored for their properties.
- Up-grade the MPECVD system with new turbo-molecular pump to deposit thin films of ~100% *c*-BN on Si and Diamond thin films on Si substrates.
- Once optimized, *c*-BN thin films can be deposited on other industrially important materials like WC, Ni, glass, diamond on WC, etc.
- Using MPECVD and nano-seeding techniques diamond thin films deposited with different gas chemistries deposited at low deposition temperatures should be explored to find the plasma chemistry that provides best thermal conductivity at the low deposition temperatures.

References:

- [1] V. Jayaseelan, in *Materials Science and Engineering*, Masters in Materials Science and Engineering, University of Cincinnati, Cincinnati **2000**.
- [2] D. A. Glocker, E. K. R. Laboratories, I. S. Shah, E. I. d. P. d. N. Co, *Handbook of Thin Film Process Technology*, Institute of Physics Publishing Bristol and Philadelphia, **1995**.
- [3] S. M. Rossnagel, J. J. Cuomo, W. D. Westwood, Eds., *Handbook of Plasma Processing Technology: Fundamentals, Etching, Deposition, and Surface Interactions*, **1990**.
- [4] B. Dischler, C. Wild, *Springer* **1998**.
- [5] Lin, Dandy, *Diamond Chemical Vapor Deposition, Nucleation and Early Growth*, Noyes Publications, **1995**.
- [6] Pan, Kania, *Diamond: Electronic Properties and Applications*, Boston: Kluwer Academic, **1995**.
- [7] I. Applied Science and Technology, Woburn **1991**.
- [8] M. f. o. e. spectroscopy.
- [9] K. Byrappa, T. Ohachi, *Crystal Growth Technology*, William Andrew Inc., Norwich, New York, **2003**.
- [10] F. Rouessac, A. Rouessac, *Chemical Analysis: Modern Instrumentation Methods and Techniques*, John Wiley & Sons Ltd., **2007**.
- [11] P. H. Dawson, *Quadrupole Mass Spectrometry And Its Applications*, American Institute of Physics, **1995**.
- [12] A. Y. Liu, M. L. Cohen, *Science* **1989**, 245.
- [13] S. Xu, S. Kumar, Y. A. Li, N. Jiang, S. Lee, *Journal of Physics: Condensed Matter* **2000**, 12, L121.
- [14] H. Ling, J. D. Wu, J. Sun, W. Shi, Z. F. Ying, N. Xu, W. J. Pan, X. M. Ding, *Diamond and Related Materials* **2002**, 11, 1584.
- [15] W. Shi, J. D. Wu, J. Sun, H. Ling, Z. F. Ying, X. M. Ding, Z. Y. Zhou, F. M. Li, *Applied Physics A* **2001**, 73, 605.
- [16] T.-Y. Yen, Chou, Pin-Chang, *Applied Physics Letters* **1995**, 67.
- [17] V. N. Khabashasku, J. L. Margrave, K. Waters, J. A. Schultz, *Thin Solid Films* **2001**, 381, 62.
- [18] A. Y. Liu, R. M. Wntzcvitch, *Physical Review B* **1994**, 50, 10362.

- [19] J. Bulir, M. P. Delplancke-Ogletree, J. Lancok, M. Jelinek, C. Popov, A. Klett, W. Kulisch, *Diamond and Related Materials* **2001**, *10*, 1901.
- [20] A. Badzian, T. Badzian, *Diamond and Related Materials* **1996**, *5*, 1051.
- [21] L. Jiang, A. G. Fitzgerald, M. J. Rose, A. Lousa, S. Gimeno, *Surface and Interface Analysis* **2002**, *34*, 732.
- [22] C. Peijiang, *Material Chemistry and Physics* **2001**, *72*, 93.
- [23] Z. Zhor, L. Xia, *Journal of Physics D: Applied Physics* **2002**, *35*, 1991.
- [24] A. J. Steven, *Journal of American Chemical Society* **1996**, *118*, 10900.
- [25] R. Jeanloz, *Annual Review of Physical Chemistry* **1989**, *40*.
- [26] C. B. Agee, *Journal of Geophysics* **1995**, *100*.
- [27] Y. P. Zhang, Y. S. Gu, X. R. Chang, Z. Z. Tian, D. X. Xhi, X. F. Zhang, *Material Science and Engineering B* **2000**, *78*, 11.
- [28] D. X. Shi, X. F. Zhang, L. Yuan, Y. S. Gu, Y. P. Zhang, Z. J. Duan, X. R. Chang, Z. Z. Tian, N. X. Chen, *Applied Surface Science* **1999**, *148*, 50.
- [29] L. Vel, G. Demazeau, J. Etoumeau, *Material Science and Engineering B* **1991**, *10*, 149.
- [30] J. Y. Wu, C.-T. Kuo, P.-J. Yang, *Material Chemistry and Physics* **2001**, *72*, 245.
- [31] Y. S. Gu, Y. P. Zhang, Z. J. Duan, X. R. XChang, Z. Z. Tian, N. X. Chen, *Journal of Material Science* **1999**, *34*, 3117.
- [32] Z. J. Zhang, *Applied Physics Letters* **1995**, *66*, 3582.
- [33] D. J. Johnson, Y. Chen, Y. He, R. H. Prince, *Diamond and Related Materials* **1997**, *6*, 1799.
- [34] Z. J. Zhang, J. Huang, S. Fan, C. M. Lieber, *Material Science and Engineering A* **1996**, *209*, 5.
- [35] M. B. Huang, *Nuclear Instruments and Methods in Physics Research B* **2002**, *196*, 75.
- [36] D. Y. Lee, Y. H. Kim, I. K. Kiwn, H. K. Baik, *Thin Solid Films* **1999**, *355-356*, 239.
- [37] Y. S. Gu, Y. P. Zhang, Z. J. Duan, X. R. Chang, Z. Z. Tian, D. X. Shi, L. D. Ma, X. F. Zhang, L. Yuan, *Material Science and Engineering A* **1999**, *271*, 206.
- [38] L. C. Chen, C. K. Chen, S. L. Wei, D. M. Bhusari, K. H. Che, Y. F. Chen, Y. C. Jong, Y. S. Huang, *Applied Physics Letters* **1998**, *72*, 2643.

- [39] S. Bhattacharya, O. Auciello, J. Birrel, J. A. Carlisle, L. A. Curtiss, A. N. Goyette, *Applied Physics Letters* **2001**, 79, 1441.
- [40] Y. Sakamoto, M. Takaya, *Surface and Coatings Technology* **2003**, 160-170, 321.
- [41] Y. Fu, C. Q. Sun, H. Du, B. Yan, *Surface and Coatings Technology* **2002**, 160, 165.
- [42] R. N. Singh, D. Das, *International Materials Reviews* **2007**, 52, 29.
- [43] E. Tomasella, F. Rebib, M. Dubois, J. Cellier, M. Jacquet, "Structural and optical properties studies of sputtered a-SiCN thin films", **2008**.
- [44] C. B. Samantaray, R. N. Singh, *International Materials Reviews* **2005**, 50, 313.
- [45] W. Kalss, R. Haubner, B. Lus, *Diamond and Related Materials* **1998**, 7, 369.
- [46] P. B. Mirkarimi, D. L. Medlin, K. F. McCarty, D. C. Dibble, W. M. Clift, J. A. Knapp, J. C. Barbour, *Journal of Applied Physics* **1997**, 34, 732.
- [47] W. J. Zhang, Y. M. Chong, I. Bello, S. T. Lee, *Journal of Physics D: Applied Physics* **2007**, 40, 6159.
- [48] M. Z. Karim, D. C. Cameron, M. S. J. Hashmi, *Surface & coatings technology* **1993**, 60, 502.
- [49] K. Bewilogua, J. Buth, H. Hübsch, M. Grischke, *Diamond and Related Materials* **1993**, 2, 1206.
- [50] S. Gimeno, J. L. Andu'jar, E. Bertran, A. Lousa, *Diamond and Related Materials* **1996**, 5, 535.
- [51] W. Otaño-Rivera, L. J. Piliore, R. Messier, *Applied Physics Letters* **1998**, 72, 2523.
- [52] Y. K. Le, H. Oechsner, *Applied Physics A: Materials Science & Processing* **2004**, 78, 681.
- [53] M. N. P. Carreño, J. P. Bottecchia, I. Pereyra, *Thin Solid Films* **1997**, 308-309, 219.
- [54] K. K. Chattopadhyay, A. N. Banerjee, S. Kundoo, *Materials Letters* **2003**, 57, 1459.
- [55] T. S. Yang, Y. P. Cheng, C. L. Cheng, M. S. Wong, *Thin Solid Films* **2004**, 447-448, 136.
- [56] I. Bello, W. Zhang, Y. Lifshitz, K. M. Chan, X. Meng, Y. Wu, C. Y. Chan, S. T. Lee, *Advanced Materails* **2004**, 16, 1405.
- [57] F. Kiel, M. Cotarelo, M. P. Delplancke, R. Winand, *Thin Solid Films* **1995**, 270, 118.
- [58] H. Saitoh, W. A. Yerbough, *applied Physics Letters* **1991**, 58, 2228.

- [59] S. M. Gorbatkin, R. F. Burgie, W. C. Oliver, J. C. Barbour, T. M. Mayer, M. L. Thomas, *Journal of Vacuum Science and Technology A* **1993**, *11*, 1863.
- [60] I. Konyashin, J. Loeffler, J. Bill, F. Aldinger, *Thin Solid Films* **1997**, *308-309*.
- [61] M. P. Chowdhury, A. K. Pal, *Journal of Physics D: Applied Physics* **2004**, *37*, 261.
- [62] W. J. Zhang, S. Matsumoto, *Applied Physics A* **2000**, *71*, 469.
- [63] S. Matsumoto, W. J. Zhang, *Diamond and Related Materials* **2001**, *10*, 1868.
- [64] J. Vilcarromero, M. N. P. Carreño, I. Pereyra, *Thin Solid Films* **2000**, *373*, 273.
- [65] W. J. Zhang, X. Jiang, S. Matsumoto, *Applied Physics Letters* **2001**, *79*, 4530.
- [66] W. XZhang, S. Matsumoto, Q. Li, I. Bello, S.-T. Lee, *Advanced Functional Materials* **2002**, *12*, 250.
- [67] J. Yu, S. Matsumoto, *Diamond and Related Materials*, *12*, 1903.
- [68] J. Yu, S. Matsumoto, *Journal of Materials Research* **2004**, *19*, 1408.
- [69] C. Y. Chan, W. J. Zhang, X. M. Meng, K. M. Chan, I. Bello, Y. Lifshitz, S. T. Lee, *Diamond & Related Materials* **2003**, *12*, 1162.
- [70] W. J. Zhang, C. Y. Chan, K. M. Chan, I. Bello, Y. Lifshitz, S. T. Lee, *Applied Physics A: Materials Science & Processing* **2003**, *76*, 953.
- [71] H. Yamamoto, S. Matsumoto, K. Ohada, J. Yu, K. Hirakuri, *Diamond & Related Materials* **2006**, *15*, 1351.
- [72] C. Li, H. Li, D. Niu, F. Lu, W. Tang, G. Chen, H. Zhou, F. Chen, *Surface and Coatings Technology* **2007**, *201*, 6553.
- [73] T. Yoshida, *Diamond and Related Materials* **1996**, *5*, 501.
- [74] P. B. Mirkarimi, K. F. McCarty, D. L. Medlin, *Materials Science & Engineering R* **1997**, *21*, 47.
- [75] A. Sherman, *Chemical vapor deposition for microelectronics: principles, technology, and applications*, William Andrew Publishing, **1987**.
- [76] J. Asmussen, *Journal of Vacuum Science and Technology A* **1989**, *7*, 883.
- [77] O. A. Popov, *Journal of Vacuum Science and Technology A* **1989**, *7*, 894.
- [78] X. Ma, J. Yang, D. He, G. Chen, *Thin Solid Films* **1998**, *322*, 37.
- [79] H. Yang, C. Iwamoto, T. Yoshida, *Thin Solid Films* **2002**, *407*, 67.

- [80] K. J. Liao, W. L. Wang, C. Y. Kong, *Surface and Coatings Technology* **2001**, *141*, 216.
- [81] W. J. Zhang, S. Matsumoto, *Chemical Physics Letters* **2000**, *330*, 243.
- [82] Q. He, C. Li, C. Franke, L. Pilione, B. Drawl, F. Lu, R. Messier, *Thin Solid Films* **2005**, *474*, 96.
- [83] W. D. Brown, R. A. Beera, H. A. Naseem, A. P. Malshe, *Surface & coatings technology* **1996**, *86*, 698.
- [84] W. L. Liu, M. Shamsa, I. Calizo, A. A. Balandin, V. Ralchenko, A. Popovich, A. Saveliev, *Applied Physics Letters* **2006**, *89*.
- [85] P. W. May, *Philosophical Transactions: Mathematical, Physical and Engineering Sciences* **2000**, *358*, 473.
- [86] R. Ramamurti, V. Shanov, R. N. Singh, S. Mamedov, P. Boolchand, *Journal of Vacuum Science and Technology A: Vacuum, Surfaces and Films* **2006**, *24*, 179.
- [87] D. Das, V. Jayaseelan, R. Ramamurti, R. S. Kukreja, L. Guo, R. N. Singh, *Diamond and Related Materials* **2006**, *15*, 1336.
- [88] C. Gu, Z. Jin, X. Lu, G. Zou, J. Zhang, R. Fang, *Thin Solid Films* **1997**, *311*, 124.
- [89] H. Yoshikawa, C. Morel, Y. Koga, *Diamond and Related Materials* **2001**, *10*, 1588.
- [90] K. Baba, Y. Aikawa, N. Shohata, *Journal of Applied Physics* **1991**, *69*, 7313.
- [91] J. E. Graebner, S. Jin, G. W. Kammlott, J. A. Herb, C. F. Gardinier, *Applied Physics Letters* **1992**, *60*, 1576.
- [92] C. Gu, X. Jiang, Z. Jin, *Diamond and Related Materials* **1999**, *8*, 262.
- [93] S. D. Wolter, D. A. Borca-Tasciuc, G. Chen, N. Govindaraju, R. Collazo, F. Okuzumi, J. T. Prater, Z. Sitar, *Diamond and Related Materials* **2003**, *12*, 61.
- [94] A. P. Malshe, R. A. Beera, A. A. Khanolkar, W. D. Brown, H. A. Naseem, *Diamond and Related Materials* **1997**, *6*, 430.
- [95] J. L. Valdes, J. W. Mitchel, J. A. Mucha, L. Seibles, H. Huggins, *Journal of the Electrochemical Society* **1991**, *138*, 635.
- [96] A. A. Shaik, M. A. Khan, H. A. Naseem, W. D. Brown, *Thin Solid Films* **1999**, *355*, 139.
- [97] H. Makita, K. Nishimura, N. Jiang, A. Hatta, T. Ito, A. Hiraki, *Thin Solid Films* **1996**, *281-282*, 279.

- [98] J. W. Steeds, A. E. Mora, S. J. Charles, D. J. F. Evans, J. E. Butler, *Materials Chemistry and Physics* **2003**, *81*, 281.
- [99] K. M. McNamara, B. E. Williams, K. K. Gleason, B. E. Scruggs, *Journal of Applied Physics* **1994**, *76*, 2466.
- [100] AISN Software, SPSS Inc, Chicago, IL, **1997**.
- [101] C. J. Tang, A. J. Neves, M. C. Carmo, *Applied Physics Letters* **2005**, *86*, 1.
- [102] X. Xiao, B. W. Sheldon, Y. Qi, A. K. Kothari, *Applied Physics Letters* **2008**, *92*.
- [103] A. C. Ferrari, J. Robertson, *Physical Review B - Condensed Matter and Materials Physics* **2001**, *63*, 1214051.
- [104] S. Yang, Z. He, Q. Li, D. Zhu, J. Gong, *Diamond and Related Materials* **2008**, *17*, 2075.
- [105] C. J. Chu, R. H. Hauge, J. L. Margrave, M. P. D'Evelyn, *Applied Physics Letters* **1992**, *61*, 1393.
- [106] P. Joeris, C. Benndorf, S. Bohr, *Journal of Applied Physics* **1992**, *71*, 4638.
- [107] C. L. Cheng, H. C. Chang, J. C. Lin, K. J. Song, J. K. Wang, *Physical Review Letters* **1997**, *78*, 3713.
- [108] A. Heiman, E. Lakin, E. Zolotoyabko, A. Hoffman, *Diamond and Related Materials* **2002**, *11*, 601.
- [109] B. W. Sheldon, A. Rajamani, A. Bhandari, E. Chason, S. K. Hong, R. Beresford, *Journal of Applied Physics* **2005**, *98*, 1.
- [110] R. De Wit, *Journal of Physics C: Solid State Physics* **1972**, *5*, 529.
- [111] H. Windischmann, G. F. Epps, Y. Cong, R. W. Collins, *Journal of Applied Physics* **1991**, *69*, 2231.
- [112] J. Michler, K. Von, J. Stiegler, E. Blank, *Journal of Applied Physics* **1998**, *83*, 187.
- [113] M. E. Levinshte n, S. L. Rumyantsev, M. Shur, *Properties of Advanced Semiconductor Materials: GaN, AlN, InN, BN, SiC, SiGe*, Wiley-Interscience, **2001**.
- [114] V. V. Kondrashev, S. L. Yampol'skii, Y. V. Kalyazin, A. S. Verteletskaya, *Chemical and Petroleum Engineering* **1987**, *22*, 502.